UNIVERSITÉ DE NANTES
UFR MEDECINE

———

ÉCOLE DOCTORALE DE BIOLOGIE-SANTE

Année 2014

N° attribué par la bibliothèque

								0	4

Microenvironnement osseux et ostéolyse: application au descellement aseptique des implants orthopédiques

———————

THÈSE DE DOCTORAT

Discipline : Biologie – Médecine – Santé

Spécialité : Aspects Moléculaires et Cellulaires de la Biologie

Présentée
et soutenue publiquement par

Luis CORDOVA JARA

Le 17 juin 2014, devant le jury ci-dessous

Président :

M. LAQUERRIERE Patrice Professeur des Universités, CNRS-Strasbourg

Rapporteurs :

M. MAINARD Didier Professeur des Universités - Praticien Hospitalier CHU- Nancy
M. HAMADOUCHE Moussa Professeur des Universités - Praticien Hospitalier CHU Cochin-Paris

Examinateurs :

M. LAQUERRIERE Patrice Professeur des Universités, CNRS-Strasbourg

Mme. TRICHET Valérie Maître de Conférences des Universités, Nantes

M. HEYMANN Dominique Professeur des Universités - Praticien Hospitalier, CHU - Nantes

Directeur de thèse :

M. PASSUTI Norbert Professeur des Universités - Praticien Hospitalier, CHU – Nantes

Microenvironnement osseux et ostéolyse: application au descellement aseptique des implants orthopédiques

THESE DE DOCTORAT

Ecole Doctorale de BIOLOGIE-SANTE
Biologie – Médecine – Santé
Aspects Moléculaires et Cellulaires de la Biologie

Présentée
et soutenue publiquement par

Luis CORDOVA JARA

Le 17 Juin 2014, devant le jury ci-dessous

Rapporteurs

M. MAINARD Didier Professeur des Universités - Praticien Hospitalier CHU- Nancy
M. HAMADOUCHE Moussa Professeur des Universités - Praticien Hospitalier CHU Cochin-Paris

Examinateurs

M. LAQUERRIERE Patrice Professeur des Universités, CNRS-Strasbourg
Mme. TRICHET Valérie Maître de Conférences des Universités**,** Nantes
M. HEYMANN Dominique Professeur des Universités - Praticien Hospitalier, CHU - Nantes

Directeur de thèse
M. PASSUTI Norbert Professeur des Universités - Praticien Hospitalier, CHU - Nantes

Periprosthetic bone microenvironment: application to aseptic loosening of orthopaedic implants

Ph.D. THESIS

Thesis submitted in fulfillment of the requirements for the degree of

DOCTOR OF PHILOSOPHY

Doctoral School of BIOLOGIE-SANTE
Cell and Molecular Biology

by

Luis CORDOVA JARA

June 17, 2014

Thesis Committee

Rapporteurs
M. MAINARD Didier Professeur des Universités - Praticien Hospitalier CHU- Nancy
M. HAMADOUCHE Moussa Professeur des Universités - Praticien Hospitalier CHU Cochin-Paris

Assessors
M. LAQUERRIERE Patrice Professeur des Universités, CNRS-Strasbourg
Mme. TRICHET Valérie Maître de Conférences des Universités**,** Nantes
M. HEYMANN Dominique Professeur des Universités - Praticien Hospitalier, CHU - Nantes

Supervisor
M. PASSUTI Norbert Professeur des Universités - Praticien Hospitalier, CHU - Nantes

ABSTRACT

Prosthetic joint replacement is one of the most successful procedure performed today, however 10-20% of patients show periprosthetic osteolysis induced by wear particles released from bearing surfaces at 10 years leading to the surgical revision of the prosthesis. In this regard, the long-term survival of joint implants continues to be a major challenge in orthopedic research. Thus, a better understanding of the pathophysiology of periprosthetic osteolysis induced by wear particles is essential for the development of new therapeutic strategies.

This report provides an overview of current concepts of osteoimmunology applied to periprosthetic osteolysis and aseptic loosening of orthopedic implants. In the experimental part, this study aims to deep in the understanding of mechanisms of osteolysis by a) identifying cell populations of human periprosthetic membranes retrieved from surgical revisions, b) reproducing the inflammatory and osteolytic changes in a calvaria mouse model and evaluating the interference of RNA targeting the receptor activator of nuclear factor kappa B (RANK) as a new therapeutic approach for this condition and, finally, c) evaluating the interactions between polyethylene nanoparticles and human $CD14^{+}$ monocyte/macrophages at cellular level.

Luis CORDOVA, DDS
Oral and Maxillofacial Surgeon

PhD student

Born in Traiguén, Chile, September 12, 1973

Professional address:	INSERM UMR 957	Phone: +33 (0)2 40 41 28 45
	Faculty of Medicine	Fax: +33 (0)2 40 41 28 60
	1 Rue Gaston Veil	luis.cordova-jara@univ-nantes.fr
	44035 Nantes cedex 1, France	www.u957.univ-nantes.fr

Publications

2014

Cordova LA, Stresing V, Gobin B, Rosset P, Passuti N, Gouin F, Layrolle P, Trichet V, Heymann D. Aseptic implant loosening: contributions and future challenges of mouse models in translational research, Clinical Science (2014) 127 (Part.5), 277-293 doi: 10.1042/CS20130338, **Published online**).

Cordova LA, Trichet V, Escriou V, Rosset P, Amiaud J, Battaglia S, Charrier C, Gouin F, Passuti N, Heymann D. Inhibition of osteolysis and increase of bone formation after local administration of siRNA-targeting RANK in a polyethylene-particle-induced osteolysis model, ***Submitted for publication.***

Cordova LA, Amiaud J, Piot B, Battaglia S, Charrier C, Heymann D. Zoledronic acid induces bone remodeling disruption in a mouse model of osteonecrosis of the jaws (ONJ), ***In preparation***

Cordova LA, Brulefert K., Corvec S., Amiaud J., Guilbaud F., Passuti N., Heymann D., Heymann MF., Cell characterization of human periprosthetic pseudomembranes, ***In preparation***

2013

L. Cordova, S. Battaglia, C. Charrier, D. Heymann, Alveolar bone changes and the role of osteoclasts in zoledronic acid - treated mice (Abstract of ICOMS 2013), International Journal of Oral and Maxillofacial Surgery, Volume 42, Issue 10, October 2013, Pages 1185-1186, ISSN 0901-5027, http://dx.doi.org/10.1016/j.ijom.2013.07.063

http://www.sciencedirect.com/science/article/pii/S0901502713003561

International Presentations

2013

siRNAs in therapy of experimental particle-induced osteolysis, 88eme Congress of Orthopedic and Traumatology Society (SOFCOT), Paris, France (expected November 12, 2013). **Oral presentation**

Alveolar bone changes and the role of osteoclasts in Zoledronic Acid - treated mice, 21st ICOMS Barcelona, Spain, October 21-24, 2013. **Oral presentation**

Role des cytoquines dans les descellements aséptiques des prothèses articulaires, SORRO Société d'Orthopédie, Rhumatologie et Radiologie de l'Ouest – SORRO, Le Croisic, France, April 21-24, 2013. **Oral presentation**

2012

RNA interference targeting *Rank* has a protective role in a UHMWPE-induced osteolysis mouse model (French version). 15émes Journées Françaises de Biologie des Tissues Minéralisés, 30 May-1 July, Poitiers, France. **Oral presentation**

Mouse models in osteonecrosis of the jaws. Société de Stomatologie et Chirurgie Maxillo-faciale de l'Ouest, November, Saint Nazaire, France. **Oral presentation**

Preliminary report of development of mouse model of osteonecrosis of the jaw (ONJ), **XXI** EACMFS2012 congress, September, Dubrovnik, Croatia. **e-Poster Presentation**

Zoledronic acid in the treatment of particle-induced osteolysis in mice, Encuentros 2012, July, Paris, France. **Oral Presentation**

Intérêt de l'Acide Zolédronique dans le traitement de l'ostéolyse induite pour particules de polyéthylène" (French version). 14émes Journées Françaises de Biologie des Tissues Minéralisés, 29-31 Mai, Bordeaux, France. **Poster Presentation**

Zoledronic Acid has a protective role in UHWMPE particles induced osteolysis in mice (French version). Société Française de Recherche Orthopédique et Traumatologique. Journée du 30 mars 2012. Faculté de Médecine de Paris VII, Hopital Bichat, Paris, France. **Oral Presentation**

2011

Mouse model features in peri-prosthetic osteolysis. Journées scientifiques de l'école doctorale Biologie Sante, L'UNAM, Novembre, Nantes, France. **Oral Presentation**

Bone microenvironment associated to wear debris in TMJ implants: 20th International Conference on Oral and Maxillo-facial Surgery ICOMS November 1-4, 2011, Santiago of Chile. **Oral Presentation**

This work was carried out at the Laboratory of Pathophysiology of Bone Resorption and Therapy of Primary Bone Tumors - INSERM UMR-S 957 by the financial support provided by the Agence Nationale de la Recherche - GRANT Pathophysiology of Human Diseases, Project N°RO7196N, INSERM, University of Nantes and by CONICYT-University of Chile.

Je tiens à remercier tout particulièrement:

Mon épouse Mina pour m'avoir accompagné dans ce projet de famille. Je remercie mes parents (Gladys et Héctor), mes frères (Edgardo et Claudio) et ma belle famille (Mina, Juan, Juan Andrés et Daniel) pour leurs visites et préoccupations constantes.

Monsieur Dominique Heymann pour m'avoir accueilli dans son laboratoire depuis 2007 à travers les différents stages et depuis 2010 a plein temps pour ma thèse. Merci pour la qualité de ses conseils, pour sa confiance et pour avoir accepté de faire parti de mon jury de thèse.

Monsieur Norbert Passuti pour avoir dirigé ce travail pendant 4 années et pour avoir largement faciliter l'échange des connaissances entre la clinique orthopédique et le laboratoire.

Messieurs Didier Mainard, Moussa Hamadouche et Patrice Laquerriere qui me font un grand honneur en acceptant d'être rapporteurs et examinateur de ce travail.

Madame Valérie Trichet pour ces conseils scientifiques lors de la thèse et pour l'enseignement. Et pour avoir accepté de faire partie de mon jury de thèse.

Monsieurs François Gouin et Philipe Rosset pour l'enrichissant support clinique de cette thèse.

Madame Françoise Rédini, pour ses conseils en expérimentation animale, aspect sur lequel repose une grande partie de mes travaux.

Monsieur Pierre Layrolle pour partager ses connaissances en biomatériaux et pour m'avoir fourni le support matériel pour l'expérimentation animale.

Très particulièrement a Martine Berreur, Céline Charrier, Séverine Battaglia, Jérôme Amiaud et Régis Brion pour leur gentillesse, leurs qualités professionnelles et leur disponibilité à répondre aux centaines de questions que j'ai eu pendant ces 4 ans.

Madame Marie Francoise Heymann et mademoiselle Bénédicte Brulin pour leur collaboration et leur qualité professionnelle, qui ont été essentielles au cours de cette dernière année de thèse.

Messieurs Philipe Hulin et Steven Nedellec pour leur aide précieuse a la plateforme micro PICELL-IRS, Nantes.

Verena Stresing pour les bons moments au laboratoire et l'aide précieuse dans la rédaction en anglais.

Les camarades du bureau, Marie et Romain pour leurs dépannages avec divers protocoles scientifiques et informatiques, respectivement. Les barcelonaises Lidia et Marta pour leur bonne humeur constante.

Kevin Brulefert pour avoir propulsé l'équipe «ostéolyse périprothétique» avec son sérieux travail. Pour la bonne humeur, l'intégration a l'ortho-foot hebdomadaire et les mises à jour sur le sport international…je souhaite pour lui une bonne coupe du monde pour la France, un bon avenir familial et une excellente carrière professionnelle.

Tous les membres du laboratoire et de l'unité de thérapie expérimentale pour leur aide, leur soutien et la bonne ambiance quotidienne.

Madame Elena Ishow et monsieur Adrien Faucon (CEISAM) pour son incalculable collaboration scientifique, support d'une des études de cette thèse. Vous m'avez fait découvrir quelques intéressants aspects chimiques des biomatériaux.

Monsieur Guy Louarn (IMN), pour l'aide dans la caractérisation des biomatériaux.

Monsieur Jacques Marie Mercier, pour m'accueillir dans son Service de Stomatologie et Chirurgie Maxillo-faciale du CHU-Nantes et supporter toujours ma carrière professionnelle. Et pour entretenir ce lien étroit depuis 25 ans entre le Services Nantais et Chilien.

Monsieur Pierre Corre, un personnage clé dans cet ambitieux projet et un très bon ami. Je serai toujours reconnaissant de son soutien et je lui souhaite un excellent futur familial, professionnel et scientifique.

Monsieur Jorge Gamonal, doyen de la Faculté d'Odontologie de l'Université du Chili, pour son intérêt pour le développement de la recherche scientifique, pour le soutien financier et pour avoir accepté mon départ.

Monsieur Juan Cortés, mon maitre en Chirurgie Bucalle et Maxillo-faciale et un bon ami, merci pour ses conseils et son soutien moral.

Mme. Susana Encina pour me donner l'opportunité de travailler dans l'académie et développer significativement la spécialité au Chili.

Monsieur Roberto Pantoja, Chef du service de Chirurgie Buccale et Maxillo-faciale de l'hôpital San Borja Arriarán á Santiago du Chili, pour établir le lien entre le service Chilien et Nantais et aussi pour son accord pour mon départ en France.

Monsieur Victor Tirreau, directeur du Département de Chirurgie Buccale et Maxillo-faciale, Université du Chili pour sont accord pour mon départ.

Pamela Agurto, Rodrigo Bravo, Rodrigo Casassus et Marcelo Mardones, les amis qui ont toujours été intéressés par notre parcours.

TABLE OF ABBREVIATIONS

A

ALP
Alkaline phosphatase · 4, 13, 42, 44, 53, 105, 133
ALVAL
Aseptic lymphocyte-dominated vasculitis-associated lesions · 67, 121
AP1
Activator protein 1 · 40
ARMD
Adverse responses associated with metal debris · 66, 67, 121

B

BMI
Body mass index · 92
BMPR-IB
Type I bone morphogenetic protein receptor · 123, 181
BMPs
Bone morphogenetic proteins · 40, 42, 43, 50
BMU
Basic multicellular unit · 4, 1, 38, 39, 56, 57
BRC
Bone-remodeling compartment · 4, 39, 56, 57
BSP
Bone sialoprotein · 4, 39, 40, 42, 44
BSU
Bone structural unit · 36, 37

C

C/EBPS
CCAAT/enhancer- binding proteins · 40
Ca^{+2}
Calcium · 34
CBFA-1
Core-binding factor-1 alpha subunit · 39
CFU-M
Mononuclear precursor called Macrophage-Colony Forming Unit · 47
CGRP
Calcitonin gene related peptide · 84, 175
COLL1
Collagen 1 · 39, 41, 42, 44
COX
Cyclo-oxygenase · 85, 92
Cr-Co
Chrome-Cobalt · 62, 66, 68, 78, 82
CSF-1R
Colony stimulating factor 1 receptor · 72
CTR
Calcitonin receptor absorption inhibitor · 47

D

DAMPs
Endogenous damage-associated molecular-patterns · 6, 27, 75, 76, 122
DLS
Dynamic light scattering · 101, 108, 144
DNA
Deoxyribonucleic acid · 102, 103, 106, 177, 181

E

ERs
Estrogenic receptors · 78

F

FAM-siRNAs
Carboxyfluorescein-labeled siRNAs · 137
FCS
Foetal calf serum · 100
FGF
Fibroblast growth factor · 40, 42, 43, 167

G

GM-MSCF
Granulocyte-macrophage colony-stimulating factor · 92
GNAS1
Stimulatory Gas subunit · 93

H

H&E
Haematoxylin & Eosin · 98
HCl
Chlorhydric acid · 53
HEK 293
Human Embryonic Kidney 293 · 9, 15, 99, 101, 124, 136
HRAs
Hip resurfacing arthroplasties · 66, 92
HSCs
Hematopoietic stem cells · 34, 47

I

IFN- γ
Interferon gamma · 75
IL-1β
Interleukin -1 beta · 6, 50, 71, 75, 78
IL-6
Interleukin -6 · 6, 8, 16, 41, 50, 71, 73, 74, 75, 84, 88, 92, 93, 112, 122, 159, 175
iNOS
Inducible NO synthase · 74

K

K.O.
Knock-out · 83

L

LPS

M

N

O

P

R

S

T

U

V

Z

FIGURES

TABLES

VIDEOS

TABLE OF CONTENTS

FRENCH SUMMARY

L’arthroplastie totale de la hanche est l’une des procédures médicales fréquemment réalisée aujourd'hui et son indication dans la population jeune et active est en augmentation. Les couples de frottement actuellement disponibles ont démontré un grand taux de réussite. Néanmoins, entre 10 et 20% des patients montrent des signes d'ostéolyse aseptique périprothétique induite pour les particules d’usure relarguées de ces couples de frottements. Ces signes apparaissent entre 5 et 10 ans après la pose implantaire et, conduisent à un descellement de l'implant puis à un changement de la prothèse associé parfois à des techniques de reconstruction osseuse (révision chirurgicale). Malheureusement, la révision et le changement de prothèse ne garantissent pas une meilleure durée de vie du nouveau matériel implanté. Les estimations pour 2030 concernant les indications d’arthroplastie totale de hanche et la révision chirurgicale sont en faveur d’une augmentation respectivement de 154% et 137%. Ces données auront un impact économique majeur sur les budgets de santé publique. Pour cette raison, l’amélioration de la durée de vie à long terme des implants articulaires continue de ce fait d'être un défi majeur en chirurgie orthopédique. Une meilleure compréhension de la physiopathologie de l'ostéolyse periprothétique induite par des particules est ainsi essentielle pour le développement des nouvelles stratégies thérapeutiques.

Actuellement, l'ostéolyse induite par des particules est directement en lien avec l'interaction entre les aspects tribologiques (relargage des particules d’usure), biomécaniques de la prothèse et la susceptibilité individuelle de l’hôte (prédispositions génétique ou immunitaire acquise). Des études cliniques ont montré principalement des données rétrospectives concernant le comportement tribologique depuis 1960, cependant, aucun protocole de prévention à long terme n’a été établi à ce jour. Certaines études de suivi à court terme des séries de cas cliniques ont montré que l’amélioration de la qualité des biomatériaux disponibles pour les couples de frottement actuelles, telles que le polyéthylène hautement réticulé ou des nouvelles céramiques, diminuent la production des particules et le taux d’usure (volume d’usure/an) des arthroplasties totales. Ces données font envisager un allongement de la durée de vie des nouveaux implants par rapport aux classiques et permettent d’espérer une amélioration du pronostique des patients. Cependant, seulement quelques études rétrospectives pertinentes ont décrit un suivi à long terme (> 10 ans) des prothèses et leur devenir.

D’après la proposition des particules d’usure et son rôle potentiel comme un activateur du système immunitaire en 2007, le concept classique d'une "réponse inflammatoire et ostéolytique induite pour les particules relarguées d’un système de frottement" devient beaucoup plus complexe. Le concept actuel reconnaît une réponse spécifique en fonction de la structure chimique, la taille et la forme des particules relarguées. Concernant la structure chimique des débris d'usure, par sa pertinence clinique, le polyéthylène a été le plus étudié d’un point de vue expérimental. D’autre part, la taille des particules relarquées apparaît comme un critère majeur dans la réponse biologique. Ainsi, leur taille variable, allant de chaînes polymériques jusquà des particules nanométrique et micrométriques, détermine les modes d'internalization et d'activation des

phagocytes. Ainsi, l'étude des interactions biologiques entre particules et les macrophages est un aspect central dans ce domaine.

Cette thèse donne une vision générale des concepts actuels de l'ostéoimmunologie dans les descellements aseptiques d'implants orthopédiques et décrit les principales approches expérimentales *in vitro* et *in vivo* permettant l'étude des mécanismes biologiques impliquées dans ces descellements. La partie expérimentale est organisée en trois sections : 1) identification des populations cellulaires présentes dans des membranes périprothétiques humaines provenant de révisions chirurgicales, 2) modélisation des descellements de prothèses chez la souris et le développement de nouvelles approches thérapeutiques basées sur l'utilisation d'ARN interférences ciblant le Receptor Activator of NF-KB (RANK) et 3) analyse *in vitro* des interactions précoces entre les nanoparticules de polyéthylène et les macrophages.

Profil cellulaire des membranes périprothétiques humaines

Les principales cellules décrites, composant la niche périprothétique ont été classiquement les macrophages, ostéoclastes et ostéoblastes. Cependant, il existe d'autres types cellulaires moins étudiés comme les fibroblastes, les cellules stromales, les mastocytes, les cellules endothéliales et les cellules effectrices du système immunitaire inné et/ou acquis. La caractérisation des cellules de l'immunité dans les pseudomembranes periprothetiques humaines constitue une opportunité pour approfondir les connaissances sur la physiopathologie de l'ostéolyse périprothétique et pour identifier de nouvelles cibles thérapeutiques. Le but de ce travail a été de réaliser une cartographie cellulaire des tissus periprothetiques en comparaison du tissu synovial humain non pathologique.

L'examen histologique a montré que les pseudo-membranes présentent une couche fibreuse périphérique entourant un stroma central très vascularisé et présentant un inflitrat cellulaire important par rapport à la synovie primaire. L'infiltrat cellulaire est constitué de cellules géantes multinucléées ayant « phagocyté » des particules comme le montre la présence des particules de polyéthylène et métalliques dans le cytoplasme des cellules. Des cellules T ($CD3^+$, $CD4^+$ et $CD8^+$) et B ($CD20^+$) ont été identifiées formant un syncytium péri vasculaire. Les mastocytes ($CD117^+$) ont également été détectés, dispersés aléatoirement dans les pseudomembranes. Dans le cas d'une lésion associée à une couple de frottement métal-sur-métal, nous avons observé une nécrose extensive de la pseudomembrane. Les cellules géantes multinucléées ont été reconnues comme étant $CD68^+$ et $TRAP^-$, confirmant leur phénotype proche de la lignée monocyte/macrophage. En outre, nous avons observé les lymphocytes T ($CD3^+$, $CD4^+$ et $CD8^+$) en contact étroit avec les cellules multinucléées entourant les grosses particules de polyéthylène. Cependant, les lymphocytes n'ont pas été observés en contact avec les cellules multinucléées qui phagocytent les débris métalliques. Un autre rôle important attribué à la lignée monocyte/macrophage est d'agir comme une cellule présentatrice d'antigènes, qui relie la réponse inflammatoire non spécifique à la réponse immunitaire adaptative spécifique. Dans notre étude, nous avons

montré des signes morphologiques du contact étroit entre $CD14^+$ monocytes/macrophages et les lymphocytes T, suggèrant le lien fonctionnel entre ces deux lignées. Nous avons constaté une immunolocalisation plus marquée pour CD3 et CD4 que pour CD8, suggérant l'activation d'une réponse lymphocytaire T auxiliaire plutôt qu'une réponse cytotoxique. D'autre part, un fort immunomarquage des cellules B péri-vasculaires a été également observé. Ces résultats suggèrent le developpement d'une réponse cellulaire et humorale adaptative déclenchée par les macrophages engloutissant les grosses particules de polyethylene.

La nécrose étendue observée dans une pseudomembrane récupérée à partir d'un patient atteint d'une pseudotumeur de la hanche associée à une couple métal-sur-métal suggère une réaction à corps étrangers aux débris métalliques (acronyme anglais: ARMD) ou, éventuellement, une lésion aseptique associée a une vascularite avec prédominance lymphocytaire (acronyme anglais: ALVAL). Cependant, nous n'avons pas pu caractériser ces cellules en raison de la nécrose dans les tissus prélevés.

Notre étude montre que les caractéristiques cellulaires des pseudomembranes periprothetiques des patients porteurs d'une prothèse descellée avec particules d'usure de polyéthylène ou métalliques, sont différentes des membranes synoviales qui proviennent des patients arthrosiques. Ces différences comprennent des éléments histologiques typiques de la réponse immunitaire innée tels qu'une réaction inflammatoire chronique aux particules d'usure qui se caractérise par un stroma fibreux et très vascularisé, un infiltrat cellulaire dense comprenant des monocyte/macrophages $CD68^+$ et $TRAP^-$ et exceptionnellement des mastocytes $CD117^+$. En outre, nous avons observé l'activation des cellules T et B dans le site péri-vasculaire, ce qui suggère l'activation potentielle de la réponse immunitaire acquise.

Inhibition de l'ostéolyse et augmentation de la formation osseuse après administration locale de siRNA ciblant RANK dans un modèle d'ostéolyse induite par des particules de polyéthylène

Le processus d'ostéolyse péri-prothétique induite par des particules d'usure relarguées à partir des surfaces de contact femoro-acetabulaire des implants orthopédiques, est directement en lien à la une réponse inflammatoire locale établie par les macrophages pro-inflammatoires (M1) qui produisent de l'interleukine 1 (IL-1) et du Tumor Necrosis Factor alpha (TNF-α). Les particules de grand taille (> 20 μm) agissent comme des molécules qui induisent une signal de danger ou « danger associated molecular patterns » (DAMPs). Ces signaux sont détectés par les Toll-Like Receptors macrophagiques (TLRs), conduisant à l'activation de la réponse immunitaire innée de type inflammatoire chronique similaire à une «réaction à un corps étranger". Les particules de taille inferieure (<20 μm) et les ions, sont absorbés et activent le NALP3-inflammasome menant vers la réponse immunitaire adaptative. Les deux voies immunitaires activent les facteurs de transcription (NF-KB et NF-IL6), induisent l'augmentation de la synthèse d RANK Ligand (RANKL), et des cytokines pro-inflammatoires (IL-1β, IL-6, TNF-α). Ces cytokines ont été reconnues comme étant les principales molécules

associées au maintien de l'environnement inflammatoire périprothétique et à la stimulation de l'ostéoclastogénèse.

L'inhibition de l'axe RANKL-RANK constitue une approche thérapeutique efficace pour réduire la différenciation et l'activation des ostéoclastes. Les thérapies reposant sur des molécules anti-ostéoclastiques telles que les bisphosphonates et l'anticorps monoclonal anti-RANKL (Dénosumab™), ont été évaluées dans de modèles expérimentaux des pathologies osseuses ostéolytiques. D'autre part, de nouveaux inhibiteurs, tels que des peptides conçus pour cibler une zone spécifique d'interaction de RANK à RANKL sont actuellement en développement pré-cliniques. Aussi, la prévention de la perte osseuse en bloquant l'axe de RANK-RANKL a été décrite dans deux modèles expérimentaux d'ostéolyse induite par des particules en utilisant: a) une protéine recombinante de RANK (RANK: Fc), et b) de l'acide zolédronique. Malgré ces résultats précliniques encourageants, ils n'ont pas encore été transférés à la clinique humaine.

Les siRNA (small interfering RNA) ou petits ARN interférents (pARNi) sont de petits ARN pouvant se lier spécifiquement à une séquence d'ARN messagers. Les siRNAs régulent la synthèse des protéines par un mécanisme d'inactivation d'un gène spécifique. Les approches thérapeutiques basées sur l'utilisation de siRNA apparaissent comme des thérapies spécifiques et biocompatibles ayant démontré un bénéfice thérapeutique dans le cancer, la dégénérescence maculaire liée à l'âge et certaines maladies virales. Il y a deux aspects essentiels qui doivent être pris en compte dans cette stratégie: l'identification de cibles cliniquement pertinentes et l'utilisation de vecteurs efficaces garantissant leur libération. Le ciblage de l'axe RANKL-RANK a été décrite dans des cellules murines *in vitro* par Wang et al (2010 et 2012) et Ma et al (2012) avec une inhibition efficace de l'expression de RANK, de la différenciation des ostéoclastes et une réduction de l'ostéolyse utilisant des siRNA *Rank* et shRNA *Rank*, ciblant le transcrit RANK chez la souris.

L'administration systémique des siRNAs thérapeutiques utilisant des vecteurs biologiques et synthétiques a été utilisée dans différents modèles expérimentaux de pathologies osseuses, comprenant: les métastases osseuses (ciblage de la luciférase et système de libération utilisant l'atélocollagène) et la polyarthrite rhumatoïde (ciblant le TNF-α, IL-1β, IL-6 et IL-18 et système de libération utilisant des liposomes cationiques RPR209120/DOPE). Dans le domaine de l'ostéolyse induite par des particules d'usure, l'utilisation de siRNA ciblant la transcription du récepteur de type IB de la BPM2/4 libérés à l'aide d'un vecteur adénoviral recombinant a été reportée. L'administration locale de siRNA est une stratégie intéressante pour contourner les obstacles anatomiques et l'optimisation de sa biotransformation lors de son trafic. Ainsi, l'administration locale de siRNA RANKL délivrés par le liposome cationique RPR209120/DOPE dans un modèle murin d'ostéosarcome ou la libération locale de lentivirus ciblant β110 une sous-unité de la voie PI3K/AKT dans un modèle d'ostéolyse induite par des particules, ont été décrites. Malgré l'état actuel des connaissances en thérapie expérimentale utilisant la technologie à base de siRNA pour l'ostéolyse induite par particules, aucune donnée ciblant l'axe RANKL-RANK par la libération locale de siRNA à l'aide d'un vecteur synthétique n'est

disponible. Nous nous sommes basés sur l'hypothèse que les siRNA ciblant RANK, délivré localement par un liposome cationique pourrait être une approche efficace pour inhiber localement ostéoclastogenèse *in vivo*. Le but de notre étude a été de démontrer l'effet thérapeutique de trois doses de siRNA ciblant à la fois RANK humain et les transcrits de RANK chez la souris (RANK-811 siRNA) dans un modèle de souris d'ostéolyse induite par des particules de polyéthylène (PE).

Le ciblage des composantes de la triade OPG / RANKL / RANK par siRNA apparaît comme une approche thérapeutique prometteuse. Les études expérimentales du blocage de la signalisation de RANKL-RANK par siRNA ciblant *Rank* (*Mus musculus*) ont déjà été décrites *in vitro*, avec une inhibition efficace de l'expression de *Rank*, de la différenciation des ostéoclastes et de l'ostéolyse. De la même manière, l'efficacité *in vitro* d'un siRNA RANKL- sur des cellules humaines HEK-293 exprimant RANKL et dans un modèle murin d'ostéosarcome a été démontrée. Notre étude présente des données pré-cliniques sur l'efficacité de la répression de RANK en utilisant trois séquences inter-espèces de siRNA dans les cellules humaines HEK 293 exprimant RANK et dans les cellules murines RAW 264.7. Parmi les trois séquences analyées, la séquence RANK-811 a été choisie pour évaluer son effet sur l'ostéolyse dans le modèle animal en raison de sa meilleure efficacité *in vitro* (48,7% d'inhibition d'expression de RANK).

In vivo, nous avons d'abord confirmé la pertinence du modèle utilisée de calvaria de souris et de l'efficacité du siRNA. L'implantation des particules de PE en site calvaria constitue la référence actuelle pour l'évaluation précoce des interactions des tissus – particules. Les particules utilisées, d'origine commerciale, avaient une taille moyenne de 7 µm (données non présentées), et sont considérées comme « phagocytables » selon le concept de "particules de taille critique". Nous avons aussi confirmé la validité du modèle par les différences significatives observées sur tous les paramètres ostéolytiques entre le groupe implanté (PE-siLucF) et le groupe non implanté (Sham). Notre étude a montré pour la première fois une inhibition efficace de l'ostéolyse induite par des particules de PE dans un modèle *in vivo* en utilisant une séquence de siRNA ciblant le récepteur RANK humain. Ces siRNA ont également la capacité de bloquer la séquence murine. Après injection de doses croissantes de siRNA 811 RANK, nous avons observé une réduction importante du nombre de cellules $TRAP^+$ de type ostéoclaste, dans la zone para-sagittale des calvarias implantées. Ces observations nous permettent de suggérer une sensibilité élevée de précurseurs ostéoclastiques pour l'absorption du lipoplexe injecté. Le vecteur synthétique utilisé dans nos expériences (liposome cationique RPR209120/DOPE + plasmide) a également montré son efficacité dans la libération locale de siRNA ciblant *Rankl*, par injection intra-tumorale (osteosarcome) dans des travaux précédents. De même, Khoury *et al*. (2006 et 2008), décrit l'efficacité de l'administration systémique de siRNA ciblant les cytokines pro-inflammatoires (TNF-α, IL-1β, IL-6 et IL-18) en utilisant le même type de formulation dans un modèle de souris de polyarthrite rhumatoïde.

Les doses de 5 et 10 μg de RANK-811 siRNA ont réduit de manière significative l'expression de *Rank* et de la *cathepsine K*, confirmant ainsi l'inhibition de l'ostéoclastogenèse et de l'ostéolyse. Nous avons cependant observé une réponse contradictoire avec la dose de 2,5 μg avec une inhibition significative du nombre des cellules $TRAP^+$ avec une forte expression de la *cathepsine K* et *Rank*. Pour expliquer ce fait, nous proposons un déséquilibre entre la quantité du transcrit de *Rank* et la faible dose de siRNA administrée dans notre expérience (2,5 μg). L'évaluation volumétrique par micro-tomodensitométrie a montré que 10 μg de siRNA RANK-811 prévient la perte osseuse comparée au groupe contrôle (PE-siRNA LucF). Nous avons également observé une efficacité importante du lipoplexe dans la corticale externe plutôt que dans la corticale interne de la voûte crânienne. La diffusion optimale du volume injecté à l'intérieur du cortex pourrait être limitée par l'anatomie locale (surface érodée de l'os trabéculaire et les espaces dans le diploë), la réaction inflammatoire induite par les particules et / ou par la viscosité du lipoplexe.

Nos résultats sont compatibles avec un effet anti-resorptive directe du siRNA RANK-811 comme le démontre les signes d'inhibition de l'ostéoclastogenèse et de l'ostéolyse associée. L'effet protecteur de la perte osseuse observée sur le même modèle suite à l'administration de l'acide zolédronique soutient notre hypothèse. Les modalités d'entrée des siRNA dans les cellules pourraient être liés à leur internalisation comme cela a été démontré par l'utilisation de siRNA marqués à la carboxyfluorescéine (FAM-siRNA) sur les monocytes / macrophages dans un modèle murin de la polyarthrite rhumatoïde. De tels complexes pour détecter son trafic dans le tissu osseux ont également été montrés par Zhang *et al*. (2014) en utilisant des siRNA ciblant la lignée ostéogène et délivrés par des liposomes cationiques attachés à six séquences répétitives d'acides aminés. Le siRNA et le liposome cationique utilisé dans notre étude n'a pas de séquence FAM ajoutée et ne possède pas non plus d'affinité intrinsèque pour le tissu osseux, ce qui contribue probablement à limiter son efficacité. Il pourrait être envisagé de libérer notre siRNA RANK-811, en site osseux, à l'aide des biomatériaux utilisés pour la régénération osseuse, des peptides ciblant les cellules osseuses ou d'un liposome cationique modifiée. D'autres études sont en cours actuellement pour déterminer la (les) cellule (s) cibles du siRNA RANK 811.

En conclusion et suite au traitement local par trois doses différentes de siRNA RANK-811 libérées par le liposome cationique (RPR209120/DOPE) dans un modèle murin d'ostéolyse péri-prothétique induite par les particules PE, le volume osseux a été conservé à la dose de 10 μg. Tandis que 5 μg de siRNA RANK-811 diminue significativement l'ostéoclastogenèse, l'ostéolyse et les paramètres inflammatoires, la dose de 2,5 μg a révélé des effets contradictoires qui pourraient être attribués à un effet immuno-activateur du lipoplexe ou de ces composants. Les données microarchitecturales, histologiques et moléculaires soutiennent l'efficacité de cette approche thérapeutique basée sur les siRNA-ciblant RANK, libérés localement en site osseux, dans la cadre de la prévention de l'ostéolyse induite par des particules d'PE. Des études complémentaires seront nécessaires pour préciser les conditions optimales d'administration du siRNA, la (les) population(s) cellulaire(s) cible(s) et ses effets secondaires potentiels. Cette étude renforce le concept de l'utilité de la thérapie

basée sur l'utilisation de siRNA ciblant RANK, un acteur innovant et pertinent dans la physiopathologie de l'ostéolyse induite par des particules.

Interaction des macrophages et des nanoparticules de polyéthylène en site périprothétique

Les macrophages sont des phagocytes qui internalisent et tuent des agents « externes » de danger en activant la réponse immunitaire innée et adaptative. Ils contribuent à l'homéostasie tissulaire au cours des processus cataboliques. Les phagocytes constituent une cible intéressante pour comprendre ou traiter des pathologies associées une réponse immunitaire exacerbée.

La membrane plasmique est une structure dynamique qui sépare et coordonne l'homéostasie du milieu intra et extracellulaires par l'entrée ou la sortie de molécules. Tandis que les petites molécules (acides aminés, des sucres et des ions) traversent la membrane par le biais de pompes ou de canaux, les macromolécules entrent dans l'espace intracellulaire par la formation des vésicules membranaires ou d'endocytose (invagination de la membrane plasmique). L'endocytose inclus l'internalisation des particules solides et de grande taille (phagocytose) ou des fluides (pinocytose). Quatre mécanismes différents ont été reconnus dans le processus de pinocytose : a) la macropinocytose, b) l'endocytose dépendante de clathrine (CME) ou c) de la cavéoline et d) l'internalisation indépendante de la clathrine ou des cavéolines. Ces voies d'endocytose sont impliquées dans des processus physiologiques comme la transduction du signal induite par les hormones, la surveillance immunitaire, la présentation d'antigène et l'homéostasie cellulaire.

Les particules d'usure relarguées par des couples de frottement métal sur polyéthylène de haut poids moléculaire (PE) constituent un facteur clé dans la réponse inflammatoire et l'ostéolyse à l'interface périprothétique, conduisant à la formation de tissu inflammatoire chronique et l'ostéolyse. Cependant, après 13 ans d'utilisation du polyéthylène hautement réticulé, un polyéthylène amélioré; le relargage des particules d'usure et les taux d'usure semblent avoir significativement diminués. Par ailleurs, la durée de vie des implants et le pronostic des patients après une arthroplastie totale ont également été améliorés. Malgré ce rapport encourageant, le nombre d'études rétrospectives concernant l'évaluation à long terme est encore faible et le niveau de recommandation clinique est bas.

Classiquement, la taille des débris a été corrélée à la capacité de l'internalisation des macrophages. Bien que les grosses particules (> 20 μm) induisent la fusion et multinucléation, les plus petites (entre 1 et 20 μm) seraient internalisées par phagocytose. Cependant, 90% des particules d'usure générées dans les remplacements articulaires sont submicrométriques (à l'échelle nanométrique). Bien qu'elles semblent trop petites pour être phagocytées, l'effet des nanoparticules de polyéthylène reste moins connu. La libération des chaînes courtes de polymères qui vient de la rupture du polyéthylène a été rapportée comme un « challenge » supplémentaire pour

les tissus périprothétiques. Les nanoparticules de polyéthylène semblent donc être de nouveaux acteurs impliqués dans la physiopathologie des descellements aseptiques.

Récemment, le lien entre le système immunitaire et osseux a été proposé dans le descellement aseptique, ouvrant une nouvelle ère dans ce domaine. La connaissance des interactions macrophage-particules dans le domaine de l'ostéolyse périprothétique a été considérablement améliorée au cours des dernières années par l'optimisation des modèles cellulaires *in vitro*. La plupart des rapports se sont concentrés sur la relation entre la nature chimique des particules d'usure, leur taille et la nature de la réponse biologique induite. Cependant ils existent peu de rapports dans la littérature scientifique qui décrivent le processus d'internalisation, le trafic intracellulaire et l'impact des nanoparticules fluorescentes de polyéthylène sur l'activation cellulaire et la survie des macrophages humains. Le but de ce rapport a été d'étudier le processus d'internalisation par les monocytes/macrophages humains $CD14^+$.

Pour évaluer l'effet de la dose des nanoparticules de polyéthylène fluorescents sur l'internalisation par les monocytes/macrophages $CD14^+$ en culture, nous avons dans un premier temps comparé trois ratios de nanoparticules par cellule (8000, 4000 et 2000), à un temps fixé arbitrairement après la stimulation (48 heures). L'intensité de fluorescence (MFI) des nanoparticules de polyéthylène a été détectée par cytométrie en flux et a été utilisé comme indicateur de capture. Les résultats ont été exprimés par le rapport de la MFI des nanoparticules de polyéthylène fluorescentes captées par les macrophages sur la MFI de l'isotype de contrôle. Nous avons constaté une augmentation de la valeur relative du MFI par rapport à une augmentation du ratio nanoparticules/cellules. Ainsi, ce rapport est de 2,2 pour un ratio de 2000, de 3,4 pour un ratio de 4000 et de 5,7 pour un ratio de 8000.

Une cinétique de capture des nanoparticules a ensuite été réalisée. Nous avons donc comparé l'effet des deux ratios de nanoparticules par cellule (4000 et 2000) après 24, 48 et 72 heures de culture. Aucune modification significative de la capture des nanoparticules au ratio de 2000 n'a été observée entre 24 heures (2,3 fois), 48 heures (2,2 fois) et 72 heures (2,3 fois). La capture au ratio de 4000 a démontré une augmentation de la valeur de MFI par rapport au ratio de 2000, néanmoins il a maintenue un schéma similaire d'absorption à 24 heures (3,2 fois), 48 heures (3,4 fois) et 72 heures (3,7 fois).

Nous avons ensuite sélectionné le ratio de 4000 nanoparticules par cellule afin d'évaluer la capture des nanoparticules fluorescentes de polyéthylène pendant les 12 premières heures en utilisant les mêmes méthodes. Nous avons constaté une réponse dépendante du temps avec une augmentation progressive de la valeur relative de MFI à partir de la première heure. Ainsi , nous avons observé une augmentation progressive du signal à 1 heure (1,5 fois), 4 heures (2,3 fois), 8 heures (3,3 fois) et 12 heures (5,1 fois).

Bien que l'augmentation de la MFI observée en cytométrie de flux démontre une interaction *in vitro* entre les nanoparticules fluorescentes de polyéthylène et les monocytes/macrophages $CD14^+$, nous ne pouvons

pas différencier par cette méthode les nanoparticules qui ont été internalisées de celles qui ont adhérées à la surface cellulaire (124). Nous avons donc étudié par microscopie confocale, l'internalisation des nanoparticules au ratio de 4000 particules par cellule après 48 heures de contact. Nous avons observé deux constantes de morphologie cellulaire: a) des cellules adhérentes caractérisées par leur forme allongée et présentant des nanoparticules dans leur cytoplasme et b) des cellules peu adhérentes avec une forme arrondie et un cytoplasme sans particule. Nous avons également pu observer que les nanoparticules fluorescentes de polyéthylène étaient localisées à la fois à l'intérieur et à l'extérieur des cellules. Les images de microscopie confocale permettent de visualiser des particules de polyéthylène, de taille nanometrique variable, dans le cytoplasme des cellules. Certaines particules se localisent en contact des membranes cellulaires et déforment celles-ci, suggérant ainsi un processus d'endo- ou d'exocytose.

Pour évaluer le comportement des monocytes/macrophages $CD14^+$ en présence des nanoparticules fluorescentes de polyéthylène, une étude par vidéomicroscopie time-lapse a été réalisée pendant 72 heures. Nous avons également confirmé la présence de nanoparticules dans le cytoplasme des cellules à 4 heures après la stimulation. Puis, entre 4,5 et 5,5 heures après contact, nous avons observé leur trafic intracellulaire et à 6 heures leur libération dans le milieu extracellulaire. Plus tard, à 10 heures, nous avons constaté que certaines cellules s'arrondissent et deviennent non-adhérentes, suggérant un processus de mort. Au contraire, d'autres restent adhérentes et internalisent les particules puis libèrent brutalement celles-ci après 20 heures. Entre 48 et 72 heures de culture, nous avons constaté une grande mortalité cellulaire, cependant certaines cellules restent très actives venant prendre en charge les débris cellulaires afin de les éliminer, et d'autres venant détruire des cellules vivantes ayant préalablement phagocytées.

Nous avons montré que les nanoparticules fluorescentes de polyéthylène ont été internalisées progressivement par les monocytes/macrophages $CD14^+$ d'une manière dépendante de la dose et du temps. Les trois ratios « particules/cellule » testés à 48 heures ont montré une capture progressive des nanoparticules par les cellules. Nous avons pu constater la présence des nanoparticules fluorescentes à l'intérieur du cytoplasme de cellules dés 4 heures de contact (par vidéo-microscopie) et jusqu'a 24 heures de culture. A partir des 24 heures et jusqu'à 72 heures nous n'avons observé aucun changement dans la capture des particules, marquant une capacité maximale de phagocytose des cellules.

D'autre part, une fois que les nanoparticules sont internalisées, elles semblent perdre de leur intégrité avant d'être libérée dans le milieu extracellulaire à 48 heures. L'internalisation des nanoparticules induit des changements importants de la forme des macrophages et la mort cellulaire.

Nous avons constaté que les nanoparticules, initialement de petite taille et compactes, après internalisation, se « dissociaient » et s'organisaitent dans des corps arrondis de différentes tailles avec une distribution hétérogène dans le cytosol des macrophages. Par ailleurs, un processus de relargage des particules a pu être observé aprés 48 heures de culture. Certains travaux publiés, ne différencient pas les nanoparticules adhérentes à la surface de la cellule et celles internalisées. Néanmoins, d'autres études tentent d'élucider cette différence en utilisant le « right angle scatter » (RAS) qui est corrélé avec la granulométrie de la cellule. D'autres études utilisent l'élimination des nanoparticules adhérentes par refroidissement physico-chimique. Notre étude combinent une approche quantitative par cytométrie en flux et qualitative par microscopie confocale.

Les macrophages constituent la première barrière cellulaire devant les « Pathogen-Associated Molecular Patterns » (PAMPs) et induisent l'activation de la réponse immunitaire innée et/ou acquise. Les particules d'usure relarguées à partir des surfaces orthopédiques agiraient aussi comme des « Danger Associated Molecular Patterns » (DAMPs), induisant l'activation de voies de signalisation macrophagique dépendantes des « Toll like receptors » (TLRs) et de la voie de NALP3-inflammasome, un signal de danger intracellulaire. L'activation de ces voies intracellulaires pourrait induire l'activation du facteur de transcription NF-KB et le clivage des formes immatures de l'interleukine–1 (IL-1β) et de l'interleukine-18 (IL-18) en des formes matures via l'activation de la caspase-1. De nombreuses hypothèses concernant la mort cellulaire programmées ont été décrites. Parmi celles-ci, la pyroptose, une mort cellulaire dépendante de la caspase-1 avec le relargage du contenu inflammatoire cellulaire, constitue un phénomène intéressant qui pourrait expliquer le comportement des phagocytes devant un volume des particules d'usure. Ce processus reste à comparer avec le concept classique d'apoptose.

Nos résultats confirment l'internalisation des nanoparticules fluorescentes de polyéthylène par les macrophages, puis un processus de dissociation et finalement un relargage à partir 20 heures (video-microscopie) et 48 heures (confocale) dans le milieu extracellulaire. Nous avons constaté des changements morphologiques post-relargages des nanoparticules qui suggèrent une induction de mort cellulaire ou un processus d'exocytoses des particules initialement phagocytées. Cependant, nous ne connaissons pas la mécanistique du processus d'internalisation, de l'activation ou de la mort des macrophages dans nos conditions expérimentales. Plusieurs données cliniques et expérimentales confirment la présence de la caspase-1 et la libération d'IL-1β et d'IL-18 dans le modèle d'interaction particules-macrophages, ce qui nous laisse penser qu'un processus de pyroptose pourrait expliquer la mort cellulaire.

Nous pouvons conclure que les nanoparticules fluorescentes de polyéthylène ont été internalisées par les macrophages des 1 heures après stimulation et que ce phénomène est dépendant de la dose a 48 heures et du temps jusqu'à 24 heures. A partir des 24 heures, nous avons observé un ralentissement important de

l’internalisation. Les nanoparticules internalisées induisent l'activation d'un signal de mort cellulaire sur les macrophages qui génère des débris cellulaires qui contribueraient ainsi à l’entretien d’un cercle vicieux entre l’inflammation et le tissu environnant. Ces conclusions soutiennent une base cellulaire de la réponse inflammatoire macrophage - dépendante observée dans les tissus périprothétiques.

GENERAL CONTEXT

Total hip arthroplasty (THA) is a surgical procedure that replaces the damaged hip joint with a prosthetic device. It is considered as one of the most successful procedures performed today and its indication in the younger and active population is increasing (1). Of the bearing surfaces available, metal-on-polyethylene, metal-on-metal and metal-on-ceramic have been the most used (2). However, up to 20% of patients show evidence of aseptic osteolysis within 10 years (3), leading to implant loosening and surgical revision (4). Surgical revision is a surgical procedure able to reconstruct the joint by replacing a primary total or partial articular prosthesis and repair the defect by bone grafting according to pre and intraoperative assessment (5). Projections for the year 2030 estimate that indications for THA and surgical revision will increase by 154% and 137%, respectively, with severe economic consequences in public health (6). For this reason, long-term implant survival continues to be a major challenge in orthopaedic surgery. In this regard, better understanding of the pathophysiology of particle-induced osteolysis is essential for therapeutic development.

Currently, particle-induced osteolysis is understood as the final stage in the interaction of tribologic and biomechanical aspects of an implant on a susceptible host. Clinical studies have shown the retrospective data from 1960, however, no long-term preventive protocol, has been established to date (7). Improved biomaterials for the current frictional couples, such as cross-linked polyethylenes or new ceramics, have shown the decrease in wear production and consecutively wear rates of total joint replacements (TJR), promising a longer life span than the classical implants and improving the prognostic of the patients. While many case report series support this idea, only few relevant retrospective studies have reported their behaviour in a long-term follow-up (>10 years) (8).

After the proposition of the immunoactivatory role of wears debris in 2007 (9), the classical concept of an “inflammatory and osteolytic response under particles released from a low frictional system” becomes more complex. The current concept recognizes a specific response under the chemical structure, size and shape of released particles. Concerning the chemical structure of wear debris, the polyethylene has been the biomaterial more studied by it clinical and experimental relevance. The size of particles (polymeric chains, nanoscale and microscale particles) seems to be a critical activator of macrophages, determining differential ways of internalization and activation in primary phagocytes and then leading to the primary innate inflammatory

response or to the adaptive immune response. Thus, the study of biological interactions between micro and nanoparticles and macrophages might be a central issue in this field.

Of the approaches that have been proposed to study the biology of aseptic osteolysis, *in vivo* assays make it possible to examine the overall pathophysiology of osteolysis. While different animal species have been used for this aim (10,11), mouse models have become one of the most relevant tools for improving current knowledge in this field, highlighting the pathophysiology and proposing encouraging research strategies (12,13).

Considering the significant preclinical progress made in the past decade, certain relevant questions can be raised, such as: why has this progress so far not been translated into clinical success? Are the current models profitable and pertinent? What are the future challenges for a better understanding of the pathophysiology of aseptic osteolysis?

The present report gives an overview of current concepts of osteoimmunology in aseptic loosening of orthopaedic implants, the scientific approaches for its study and more specifically highlights the contribution and future challenges of mouse models in this field. Even though we mainly focus in the hip joint, by it relevance in the clinical practice, the biological concepts issued in this study might be also applied in all major replaced joints.

In the experimental part, this study intends to further understand the mechanisms of particle-induced osteolysis: 1) characterising the cellular populations of retrieved human periprosthetic pseudomembranes, 2) reproducing the inflammatory and osteolytic changes in the calvaria mouse model and then assessing the interference of ribonucleic acid (RNA) targeting the receptor activator of nuclear factor Kappa-B (RANK) as a new therapeutic approach and finally, 3) describing the early interactions between polyethylene nanoparticles and macrophages at cellular level.

BONE TISSUE

The bone is a specialized connective tissue, forming the skeleton of the body. Bone tissue has a central role in the biomechanics of the movements of the body, mineral metabolism and in haematopoiesis. The composition of bone tissue is summarized in **Table 1.**

Biomechanics: The bones are stiff lever and they must resist the deformation. The bones must also be flexible or elastic, to absorb and dissipate the energy. Finally, the bone must also be light to allow the mobility (14). The bone tissue is a viscous-elastic material whose mechanic properties are affected by its deformation grade. The flexibility properties of the bone are provided by the collagen, which give the bone the ability of support tense loads. On other hand, the fragility grade of the bone depends of the mineral constituents that give it the ability to support compressive loads.

Metabolic role in mineral homeostasis: One of the metabolic roles of the bone is related with the mineral homeostasis of Calcium (Ca^{+2}) Magnesium (Mg) and inorganic phosphate (PO_4), which are key components to the synthesis of bone matrix. Thus, in physiologic conditions, the bone and mineral homeostasis depends of the capacity of the body to trafficking these minerals from the intestinal absorption to the renal excretion. Furthermore, mineral homeostasis is under hormonal control (corticoids, calciotrophic hormones [Vitamin D and it metabolites and the paratohormone-PTH]). The imbalance in the bone turnover or in the mineral homoeostasis would imply the development of bone and mineral related disorders (14).

Hematopoietic: During the postnatal stage of development, the bone marrow is the primary site of hematopoietic stem cells (HSCs) maintenance and haematopoiesis (15)**.**

				Functions
Cellular phase (≈5%)	Osteoclasts			Bone remodelling
	Osteoblasts			
	Osteocytes			Protein synthesis of the organic fraction of the MEC
	Osteoprogenitors			
Extracellular matrix (≈95%)	Water (≈10%)			
	Organic phase (≈25%)	Fibrilar (≈90%)	Collagen 1	Structural
			Fibronectin	Adherence cells / matrix
			Elastin	Structural
		Inter-fibrilar (≈10%)	Proteoglycans	Diffusion of nutrients
			Glycosaminoglycans	
			Glycoproteins	
			Osteocalcin	Mineralisation
			Osteopontin	Adherence
			Bone sialoprotein	Mineralisation
	Mineral phase (≈65%)	Hydroxyapatite		
		Ions		

Table 1 Components of the bone tissue. Adapted from (16)

Bone Microanatomy

All bones of the human skeleton, though widely variable in function and shape, share a common anatomic organization. Globally, they are composed of dense cortical bone, which encloses an irregular medullary space containing cancellous bone that is composed of branching networks of interconnecting bony trabecular elements.

Cortical bone forms a relatively thick and dense outer wall and makes up about 80% of total skeletal mass (Figure 1A). The cortical surface is enveloped by the periosteum, a connective tissue that contains the cells that maintain, change, and repair this external surface (Figure 1B). The periosteum also contains blood vessels, sensory nerves, and dense fibrous tissue that are contiguous with the connective tissue elements of tendons, ligaments, and joint capsules. The remaining 20% of skeletal mass correspond to the cancellous bone and consists of interconnecting trabecular plates that share the medullary space with hematopoietic and fatty marrow. The inactive or resting trabecular surface is covered by a thin connective layer, the endosteum which, like the contiguous cortical endosteum, has widely spaced flat lining cells that are believed to have osteogenic potential, and form a barrier between the marrow and bone (17) (Figure 1C).

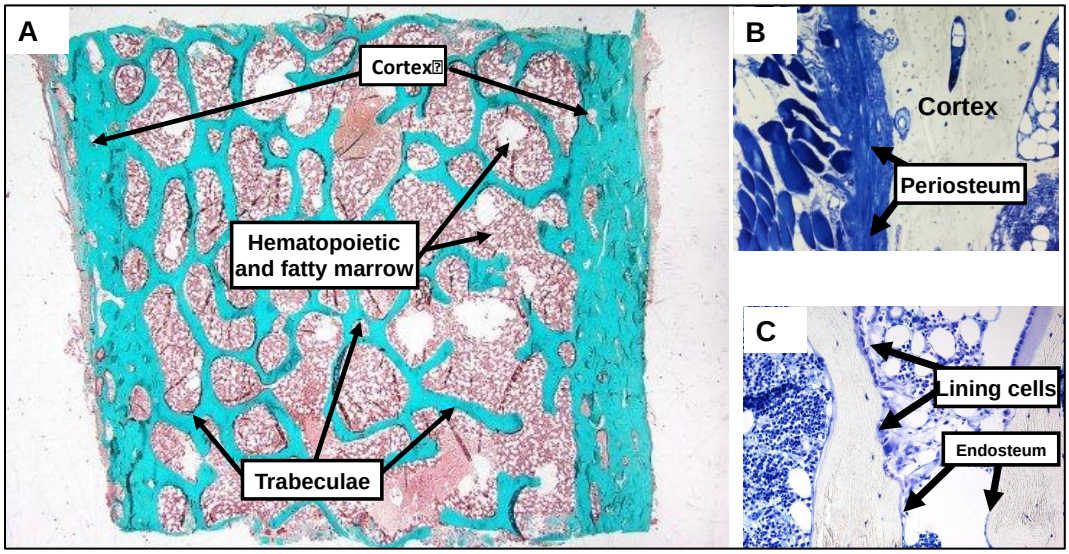

Figure 1. Bone microanatomy. Adapted from (17)

Both cortical and trabecular bones are composed of individual bone structural units (BSU), also called osteons, each of which represents the structural result of a focus of bone renewal (remodeling). Architecturally, cortical and trabecular BSUs are distinct. In cortical bone, BSUs may appear in cross section as concentric rings

(lamellae), forming cylindrical - shaped structures. In cancellous bone, the lamellae are flat and appear stacked in saucer shaped depressions (17) (Figure 2A and B).

Cortical BSUs are laminated bony cylinders that have central (Haversian) canals enclosing vascular structures, nerves, and a thin membranous lining (cortical endosteum) containing the flat and quiescent lining cells (Figure 2C). Cortical BSUs arise from Haversian and other communicating channels called Volkman's canals. They are about 0.4 mm in width and are several mm in length. They are oriented in a branching pattern and lie perpendicular to the long access of bone. Otherwise, the trabecular BSUs are laminated saucer-shaped structures that contain a relatively uniform volume of bone, each BSU representing a "quantum" of bone (17) (Figure 2D).

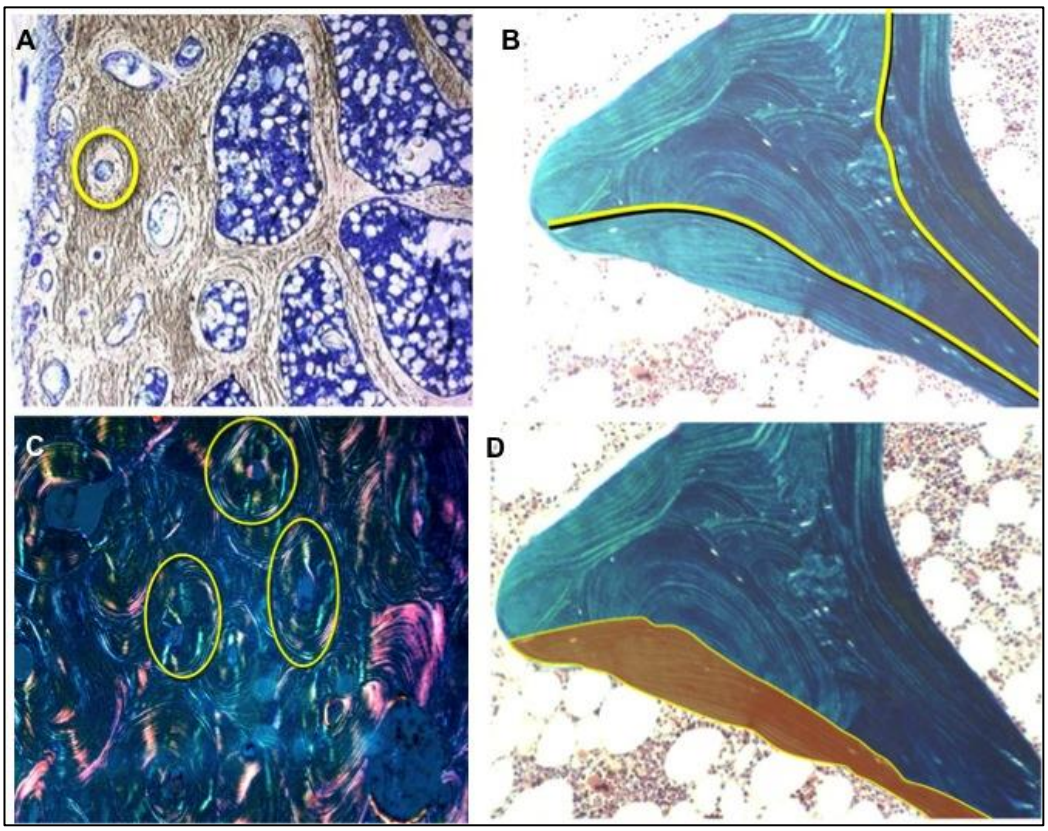

Figure 2. Cortical (A and C) and trabecular (B and D) bone structural units (BSUs). Adapted from (17)

Bone modeling, bone remodeling and basic multicellular unit (BMU)

Bone modelling (construction) is the process by which bone is formed by osteoblasts (OB) without prior bone resorption by osteoclasts (OC). This process is vigorous during growth and produces changes in bone size and shape (14).

Bone remodelling (reconstruction throughout life) is the process by the bone is constantly renewed (formed and resorbed) in response to a wide range of local and systemic factors. This dynamic process occurs in both cortical and trabecular (or cancellous) bone allowing a rapid response to changes in circulating calcium levels and, as has become more recently clear, some input into regulating hemopoiesis in adjacent bone marrow (14).

Osteoclasts and bone osteoblasts form basic multicellular units **(**BMUs**)** that function at discrete sites throughout the skeleton in a highly coordinated sequence of cellular activity (Figure 3). At any given remodelling site, bone resorption always precedes bone formation, resulting in the removal and subsequent replacement of a quantum of bone at each site. Under normal steady state conditions, the amount of bone removed is precisely replaced and there is no net change in bone mass. Only bone architecture is changed (17).

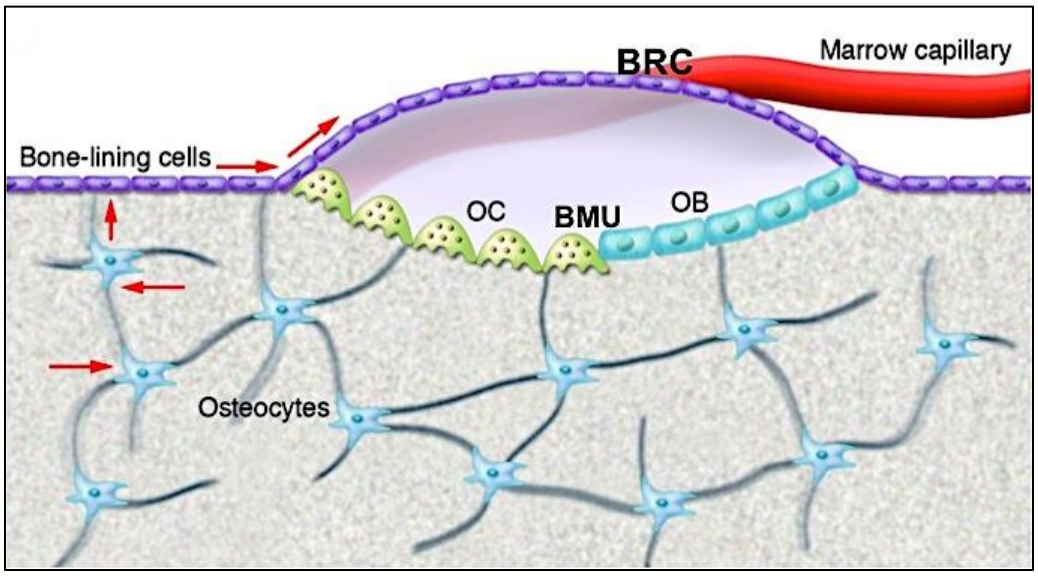

Figure 3. Bone multicellular unit (BMU) and bone remodelling chamber (BRC). (16)

The osteoblast lineage

Osteoblasts are the cells responsible for the synthesis of organic bone matrix and its mineralization. They are derived from MSCs. In adults, they are found primarily in the bone marrow stroma, periosteum and endosteum. The osteoblast maturation takes place via a series of complex steps of proliferation and differentiation from MSCs to mature osteoblasts and this involves many transcription factors (16) (Figure 4):

- Runx2 (Runt-related transcription for factor 2) (or CBFA-1 for core-binding factor-1 alpha subunit). This transcription factor binds to the promoter of genes involved in osteoblastogenesis including collagen 1 (COLL1), bone sialoprotein (BSP), osteocalcin (OCN) and osteopontin (OPN), to initiate the differentiation of MSCs to the pre-osteoblasts. In mice, the deletion of this gene leads to a complete absence of the endochondral bone model.
- Osterix (Osx) is also involved in osteoblast differentiation and therefore in bone formation. Indeed, mice deficient for Osx lack of osteoblasts, resulting in an absence of bone formation.
- The transcription factor activator protein 1 (AP1), compound of heterodimer proteins Fos and Jun families, is also an important regulator of bone formation. The expression of AP1 is induced by the transforming growth factor beta (TGF-β), parathyroid hormone (PTH) and vitamin D3 in osteoblasts. Different forms of AP1 will be expressed during the osteoblast differentiation. In the early stages of osteoblastogenesis, all the proteins Fos and Jun are expressed, and then they decline with the advance in the differentiation. Finally, AP1 in mature osteoblast consists only of Fra-2 and JunD.
- Dlx-5 plays an essential role in the control of the expression of BSP and OC by interfering with another factor, Msx2. Indeed, disabling the gene Dlx-5 in mice induced delayed ossification without altering morphogenesis. The over-expression of Msx2 ossification accelerates inactivation while delaying osteoblast differentiation, suggesting that Msx2 is a positive regulator of osteogenesis.
- The CCAAT/enhancer- binding proteins (C/EBPS) are an important transcription factor in adipocyte and osteoblast differentiation. For example, C/EBPδ and C/EBPβ regulate the expression of OCN and C/EBP-deficient mice suffering from severe osteopenia.

The expression of these transcription factors is under the complex interplay of cytokines or hormones, including: the bone morphogenetic proteins (BMPs), TGF-β, Wnt family proteins, the hedgehog proteins, fibroblast growth factor (FGF), estrogen and androgen. Thus, BMP2 by activating Smad1/5 and Smad4 stimulates the expression and function of Runx2. The anabolic Wnt proteins (Wnt3a and Wnt10) by activating the Wnt/β-Catenin also increase the expression of Runx2. Finally some of cytokines of the interleukin -6 (IL-6) family, via the activation of the transcription factor the Signal Transducers and Activators of Transcription-3 (STAT3), drive the expression of Runx2 and C/EBP (16).

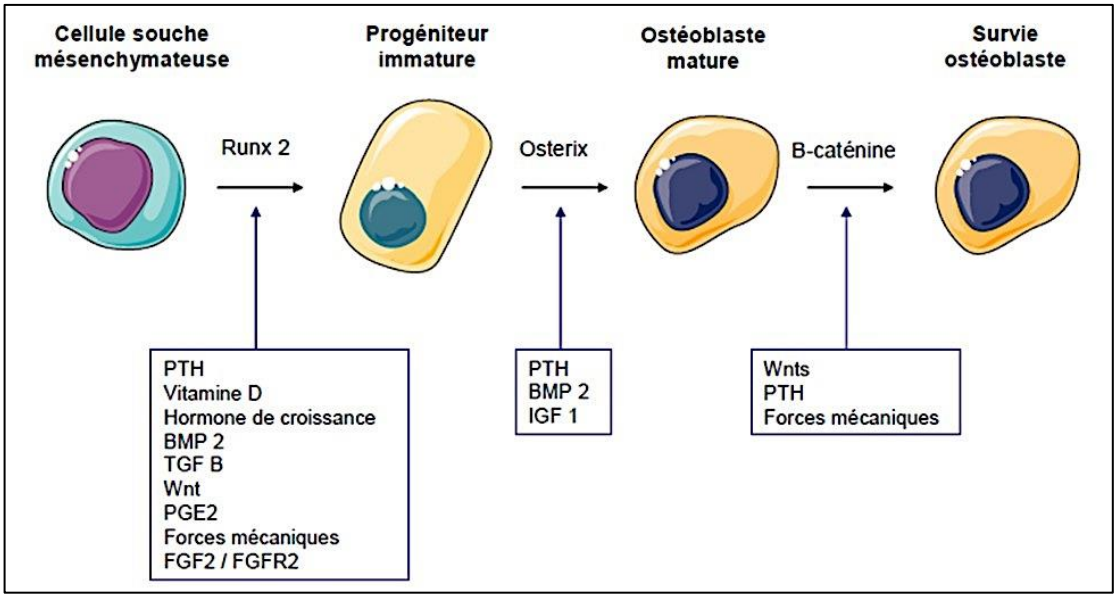

Figure 4. Transcription factors regulating the differentiation of osteoblast lineage. (23)

The pre-osteoblasts derived directly from MSCs and they located nearby places of bone formation (Figure 5 and Figure 6). These elongated cells have the capacity to divide but not synthesize the extracellular matrix. They begin to expression of some early markers such as osteopontin (OPN) or COLL1. The mature osteoblasts (Figure) are able to synthesize extracellular matrix and then, mineralize. This phenomenon occurs during the growth to adulthood and in bone remodeling. These cells have a basophilic cytoplasm, containing an abundant rough endoplasmic reticulum, numerous mitochondria and a well-developed Golgi apparatus, showing a very important activity of protein synthesis. They are placed on the osteoid, a non-mineralized bone

matrix, formed mainly of collagen, proteoglycans and glycosaminoglycans. Once osteoblasts are mature, they express (16):

- Alkaline phosphatase (ALP), an enzyme responsible of the hydrolysis of inorganic pyrophosphate that inhibits the calcification, thus promoting the mineralization of extracellular matrix.
- The collagen 1 (COLL1), forming about 90% of the proteins of the bone extracellular matrix. Formed by a triple helix of polypeptide chains, it is produced by the endoplasmic reticulum and then secreted into the extracellular matrix.
- Bone sialoprotein (BSP) and osteopontin (OPN) are the two most expressed non-collagenous proteins in bone tissue belonging to the family of Small Integrin-Binding Ligand N-linked Glycoproteins (SIBLINGS). These adhesive proteins bind the integrin membrane receptors, allowing the cell adhesion to bone matrix.
- Osteocalcin, a bone-specific protein, is expressed in large quantities and it corresponds to 10 to 20% of non-collagenous bone proteins. It contains carboxyglutamic acid residues (gla), which is dependent carboxylation of vitamin K. This protein expressed by mature osteoblasts late, seems to play a key role in bone resorption by stimulating osteoclast differentiation.

Outside these bone proteins, osteoblasts secrete a number of growth factors that play an important role in the regulation of bone metabolism, such as Transforming Growth Factors (TGF), Fibroblastic Growth Factor (FGF) and the Bone Morphogenetic Proteins (BMPs) (16):

- TGF is produced in a latent form by osteoblasts, then stored in the bone matrix in combination with a carrier protein, then released after the osteoclastic bone resorption. In vitro, TGF stimulates the proliferation of preosteoblasts and the production of collagen type-1 and osteopontin.
- BMPs (BMP-2, -4, -6 and -7), members of the superfamily of TGF-beta, are produced by osteoblasts and play a fundamental role in the control of bone formation. BMPs act at several levels by increasing the expression of Runx2 in osteoblast precursors and stimulating the expression of osteoblastic genes (alkaline phosphatase, type I collagen, osteocalcin) in osteoblasts.

- The FGF are important regulators of proliferation, function and apoptosis of osteoblasts. In vivo, FGF-1 and FGF-2 (or bFGF) stimulates bone formation in the endosteum and the periosteum in rats. Conversely, the invalidation of FGF-2 gene in mice decreases bone formation and induced osteopenia. Although FGF-2 modulates the expression of osteoblastic genes, some of these anabolic effects are indirect, induced by stimulation of the production of TGF by osteoblasts.

Osteoblasts also produce soluble regulatory molecules such as cytokines IL-6, Interleukin-11, the Tumor necrosis factor alpha (TNF-α), the Receptor Activator of Nuclear Factor kappa B Ligand (RANKL) or Osteoprotegerin (OPG), released into the extracellular medium or expressed on the cell surface acting on the osteoblast and osteoclast precursor cells (Figure 5). Some proteases, capable of regulating bone turnover by their action on the bone matrix proteins are also produced by the osteoblasts. This is the case of matrix metalloproteinases (MMPs), which MMP13 or collagenase 3 (16).

After the period of bone formation, most osteoblasts dies by apoptosis, a process of programmed cell death common to many tissues. The remaining cells can then turn into lining cells or osteocytes (16) (Figure 5).

The lining cells are inactivated or quiescent osteoblast cells, and form a monolayer of flattened cells containing little or fusiform cytoplasm and little organelles reflecting its reduced synthetic activity. Their main function is to ensure communication between the cellular environment and osteocytes entombed in the bone matrix. They also play a role during the initial phase of bone remodelling (activation). Indeed, they are able to perceive an initialization signal, leading to the degradation of the unmineralized organic matrix. Thus, the mineralized matrix is then exposed to the action of osteoclast precursors will migrate, merge and join the matrix (16).

The osteocytes are the most abundant cells of the mature bone and they are embedded in the mineralized bone matrix within a périostéocytaire space (Figure 5 and Figure 6). The cytoplasm of osteocytes contains abundant components of cytoskeleton, microtubules, intermediate and actin filaments. In contrast, the intracellular organelles are poorly developed, thus indicating a very low level of protein synthesis. Osteoblastic

markers previously expressed will gradually disappear (ALP COLL1, BSP, OCN) during the terminal differentiation into osteocytes.

The osteocytes forming an extensive network and them transmitting mechanosensory signals during the process of bone remodeling. Indeed, osteocytes interact with the collagen fibers that lining the osteocyte cavities through of the molecules integrin-like that act as mechanoreceptors, sensing the environmental mechanical stress applied to the bone. They then transmit the information to the osteoblasts and lining cells via gap junctions providing the functional adaptation of bone tissue (18).

The osteocytes also regulate the bone formation by secreting the protein sclerostin, which is one of their specific markers. Sclerostin is an antagonist of Wnt proteins and negatively control the activity of osteoblasts (19). While the regulatory mechanisms are not fully understood, it appears that the apoptosis of osteocytes would trigger the chemotaxis to the osteoclasts to the bone surface and therefore the beginning of bone resorption.

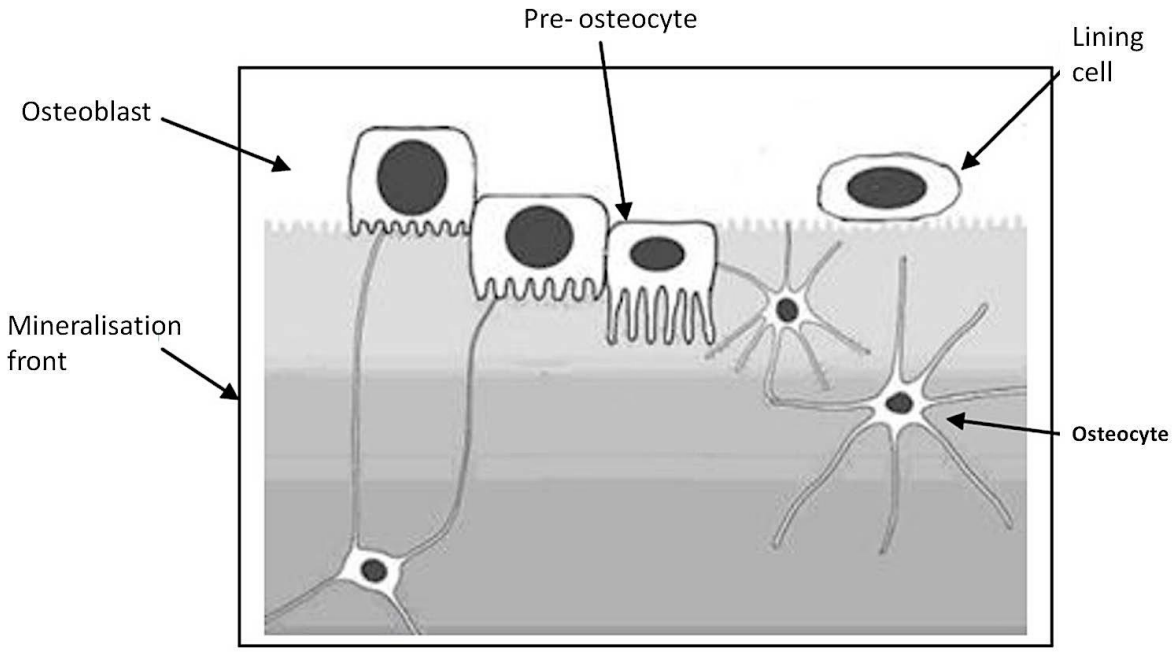

Figure 5. Evolution of the osteoblast lineage. (16)

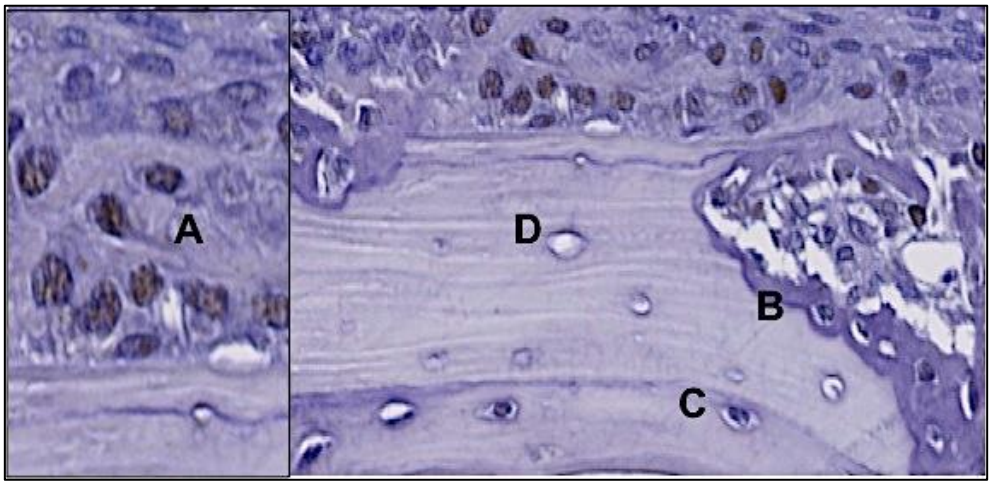

Figure 6. Osteoblast lineage cells detected by Osterix (left) and ALP (right) immunostaining. (A) Pre osteoblasts, (B) Osteoblast, (C) Osteocyte and (D) Osteocyte cavity. (Cordova *et al.*, 2014, submitted for publication)

Osteoclasts

The osteoclasts are the only cells in the body able to resorb the bone matrix. They are capable of degrading the organic phase by the secretion of enzymes in the resorption chamber and the inorganic phase by lowering the pH. Osteoclasts play a critical role in the development of the skeleton and in the maintenance of the bone mass and they are also involved in many bone diseases such as osteoporosis, tumor osteolysis or inflammatory rheumatism.

The osteoclasts have variable morphology. Though often appearing as large multinuclear cells, they are visible at the bottom of the Howship resorption pit, in contact with the calcified bone matrix by gaps. Positive identification may be made using acid phosphatase stains (Tartrate Resistant Acid Phosphatase-TRAP) (Figure 7). Osteoclasts have a developed Golgi apparatus, many peri-nuclear mitochondrial and they are rich in lysosomal enzymes such as TRAP or cathepsin K. In quiescent bone, osteoclasts are encountered infrequently, only about three being identified per 100 mm of trabecular surface, and therefore may be absent from an entire section. Under some pathologic conditions the number, size, and activity of osteoclasts may increase. Osteoclastic resorption of mineralized bone releases minerals in support of mineral homeostasis and products of collagenous protein degradation, including the collagen cross links, into the circulation. The relative

concentrations of cross links in blood or urine reflect the degree of bone resorbing activity and are considered to be “markers” of bone resorption.

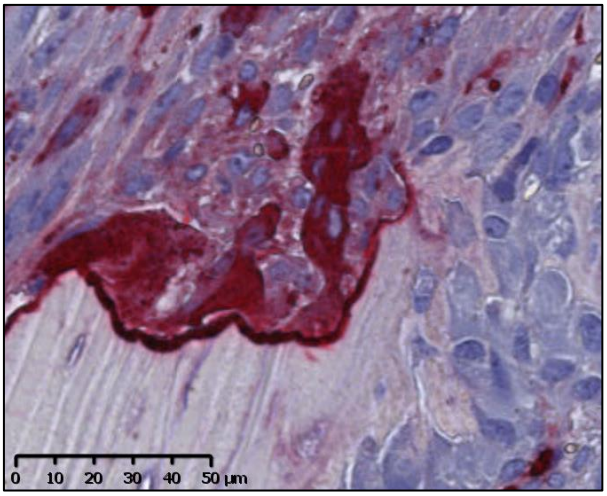

Figure 7. Osteoclast identified by TRAP staining. (Cordova *et al.*, 2014, submitted for publication)

The osteoclasts derive from the hematopoietic stem cells (HSCs) and more precisely from the mononuclear precursor called Macrophage-Colony Forming Unit (CFU-M) (Figure 8). The Macrophage-Colony Stimulating Factor (M-CSF) stimulates the proliferation of CFU-M to maintain a pool of mononuclear cells belonging to the monocyte/macrophage lineage. A small proportion of these cells is considered osteoclast precursors and is characterized by the absence of two osteoclast markers, TRAP and calcitonin receptor absorption inhibitor (CTR). The monocyte precursors are attracted to a resorption site, by chemotaxis, and then attach to the bone matrix to differentiate under the influence of M-CSF and RANKL, in the mononuclear/osteoclasts expressing CTR and TRAP. These cells, always under the effect of M-CSF and RANKL, fuse to form multinucleated cells that are not yet active and do not develop a brush border. The activation of osteoclasts is due to RANKL that will stimulate the formation of the brush border (20).

Between peripheral blood mononuclear cells (PBMCs), only certain monocytic fractions are capable of differentiating in mature osteoclasts in the presence of M-CSF and RANKL. The population most currently

used as an osteoclastogenesis model monocyte population expressing the CD14 marker (a co-receptor for lipopolysaccharide, LPS) (21).

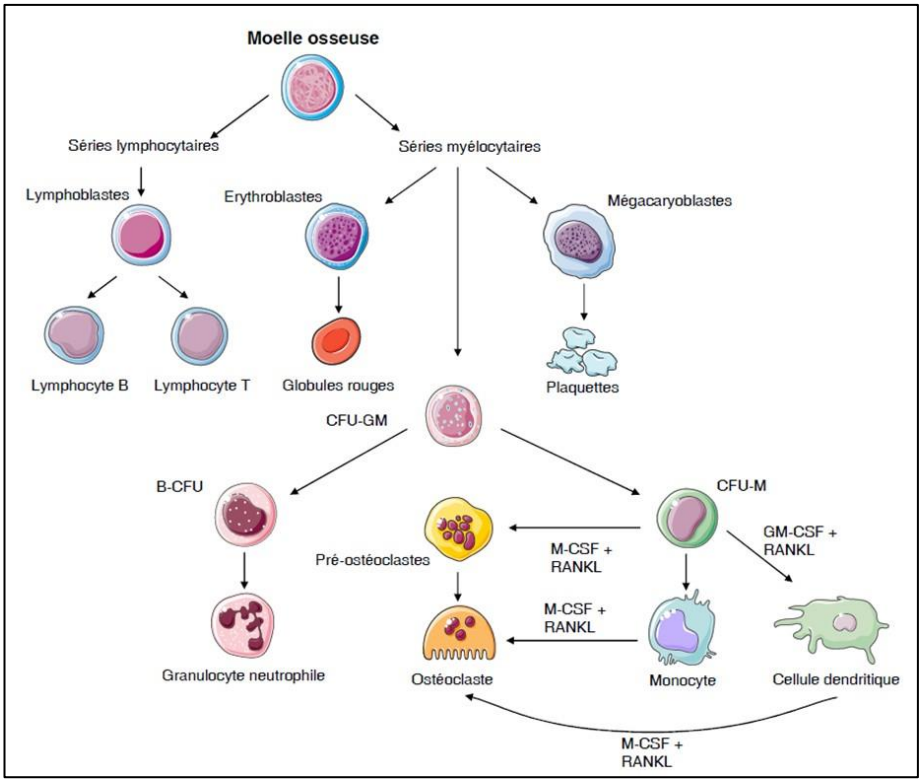

Figure 8. Differentiation of myeloid cells including the osteoclasts. (16)

The essential function of osteoclasts is the bone resorption. During the first phase of this process, a reorganization of the cytoskeleton of osteoclasts is observed: the actin microfilaments, vinculin and talin are organized into rings. This is essential for the formation of the clear zone area devoid of intracellular organelles and rich in actin filaments (22). It corresponds to a region where the plasma membrane is in contact with the bone, thus defining a closed space between the brush border compartment and the bone surface. The resorption process is performed in this compartment called resorption chamber and is performed in two stages: the dissolution of the inorganic (mineral) matrix prior to the degradation of the organic phase. Thus, the acidification of the absorption chamber (pH = 4.5) allows the demineralization of the matrix. This process involves ATP-dependent proton pumps. The pH within the osteoclast is maintained by a passive transport Cl^-

/$HCO3^-$. Finally, a chloride channel guarantees electroneutrality. The digestion of the organic matrix is carried out under the action of proteolytic enzymes (cathepsin K, metalloproteases or collagenases) contained in lysosomes (Figure 9) (23).

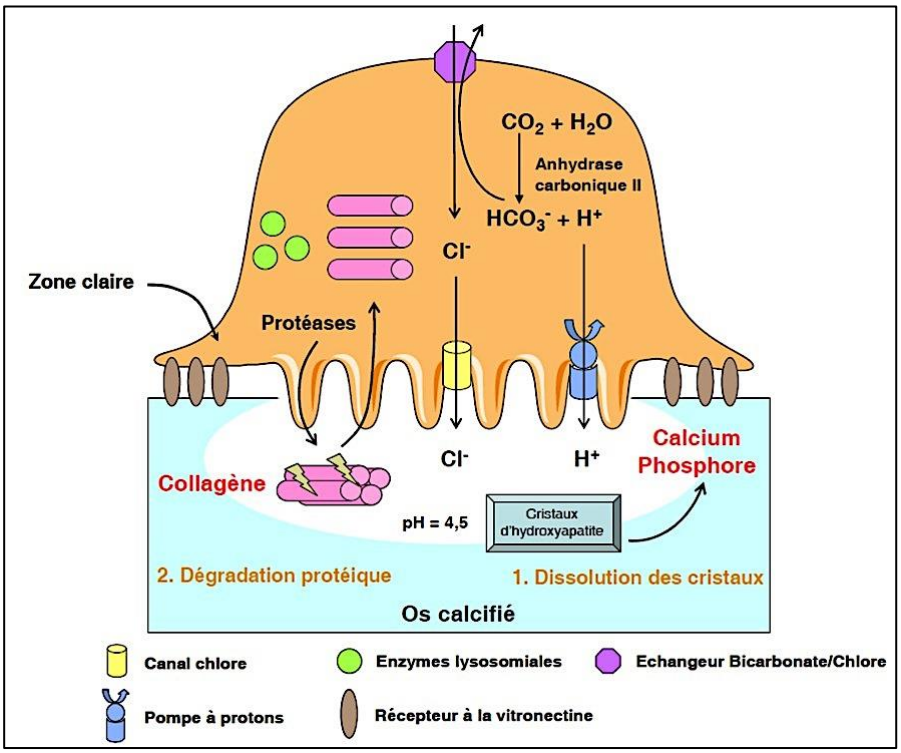

Figure 9. Activated osteoclast in the bone resorption pit. (24)

The triad RANK/RANKL/OPG mediates the intercellular communication between osteoblasts and osteoclasts and plays a fundamental role in the control of osteoclastogenesis (Figure 10). RANKL is a transmembrane cytokine that can be cleaved by proteases to generate a soluble form. RANKL binds with high affinity to its receptor RANK expressed on the surface of osteoclasts. The RANKL/RANK interaction is essential for the differentiation and survival of osteoclasts by the activation of different signaling pathways. In mice invalidated for RANKL or RANK genes, exhibit defective osteoclast activation, resulting in osteopetrosis (25).

OPG is a soluble glycoprotein, in particular produced by osteoblasts, which acts as a decoy receptor of RANKL. The ratio between the level of expression of OPG and RANKL by osteoblasts therefore allows the control of bone resorption. Indeed, it has been shown that deletion of the gene OPG resulted in severe osteoporosis characterized by excessive resorption (26), whereas the overexpression of OPG causes osteopetrosis (27). Various factors are capable of regulating the homeostasis of bone by acting on the triad RANK/RANKL/OPG (25,28).

- Runx2 regulates directly the expression of RANKL and OPG genes in osteoblasts, providing a molecular link between bone formation and resorption.
- PTH inhibits the secretion of OPG and increases the expression of RANKL by osteoblasts (29).
- Interleukin-1 beta (IL-1β) and TNF-α stimulate the production of M-CSF and RANKL by the osteoblastic precursors.
- IL-6 and glucocorticoids also stimulate the expression of RANKL
- Physiological doses of Vitamin D inhibit the stimulation of the expression of RANKL by PTH.
- The TGF- β, estrogens and BMPs increase the expression of OPG. The drop in estrogen levels during menopause thereby promotes the development of osteoporosis.

This molecular triad contributes to bone remodeling. Any disruption of this balance between the phases of bone formation and bone resorption is likely to induce the osteocondensant or osteolytic diseases.

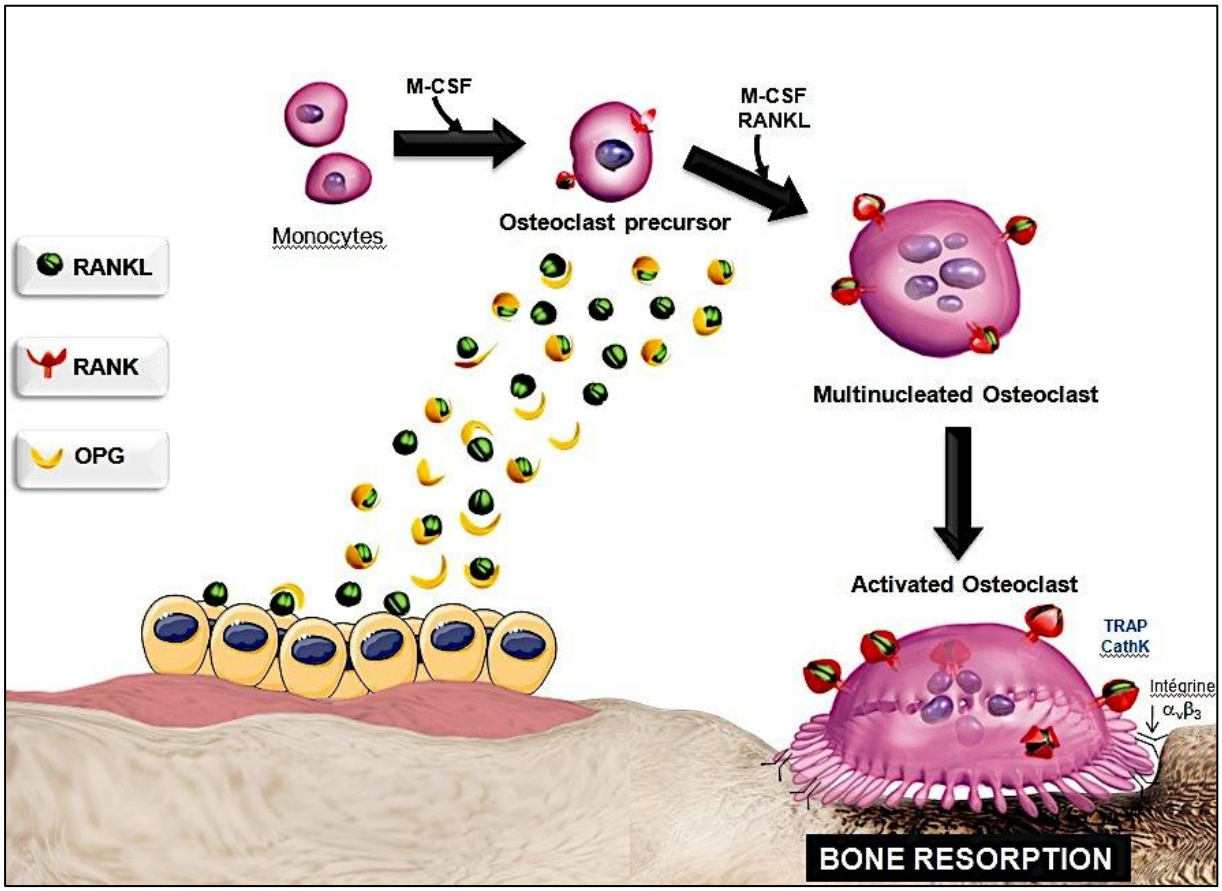

Figure 10. Role of the triad OPG/RANK/RANKL in osteoclast differentiation. Adapted from Amgen® and (28)

Bone remodelling cycle

The sequential events of the bone remodelling cycle are driven by an evolution of cellular events that occurs over a time period of three to six months, comprising fourth continuous stages: a) activation, b) resorption, c) reversal and d) formation (16, 17) (Figure 11).

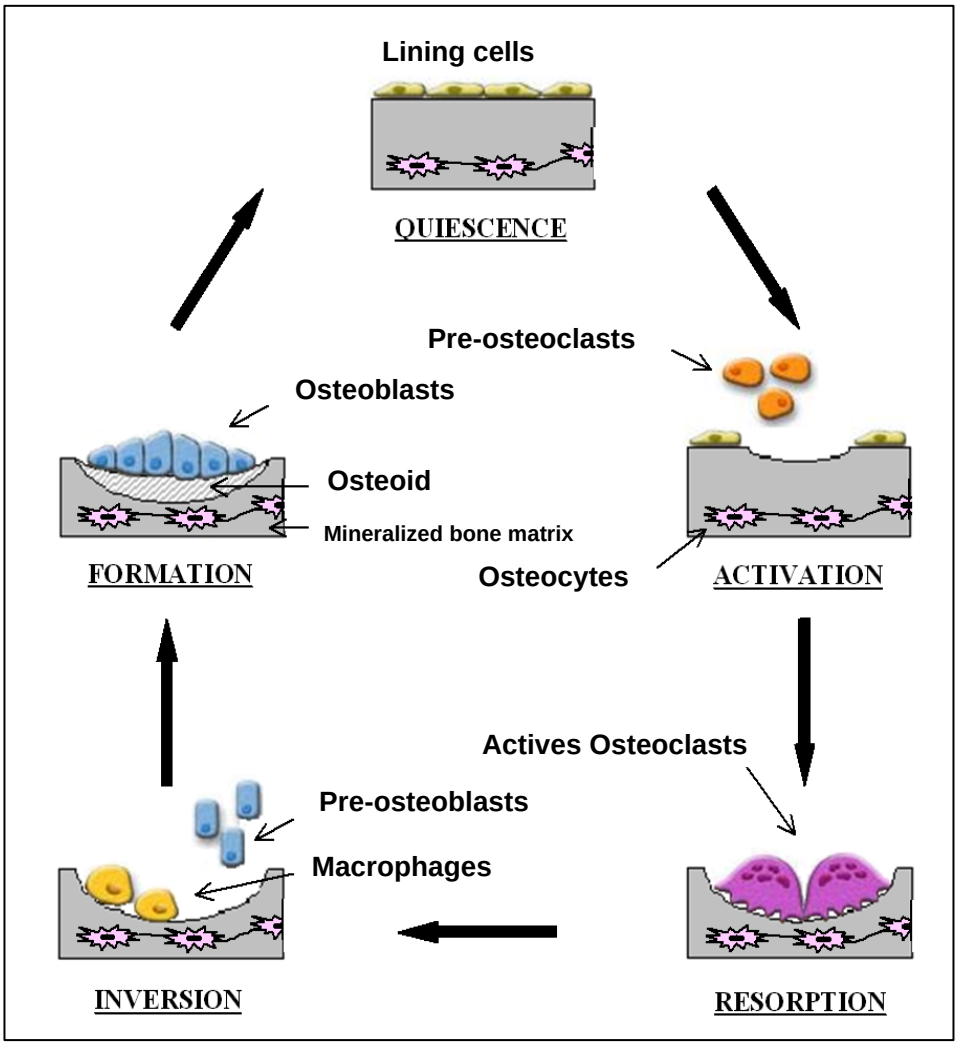

Figure 11. Bone remodelling cycle. (16)

a) Activation – a quiescent bone surface becomes populated with cells that have been recruited from osteoclast precursors and are destined to become bone-resorbing osteoclasts. Lining cells produce collagenase, which exposes the mineralized bone surface for bone resorption (16, 17) (Figure 11 and Figure 12A).

b) Resorption – mature osteoclasts remove a finite quantum of mineralized bone. Cells derived from circulating mononuclear phagocyte precursors are recruited to become bone-resorbing pre-osteoclasts. Pre-osteoclasts become mature osteoclasts and attach to the exposed mineralized bone surface, to form an isolated and sealed microenvironment forming the ruffled membrane, that is rich in both chlorhydric acid (HCl) and lysosomal enzymes (cathepsin K). Mature osteoclasts remove mineral and organic components of mature bone, leaving serrated footprints, or Howship's lacunae, on the surface (16, 17) (Figure 11 and Figure 12B).

c) Reversal – osteoclast activity and numbers decline and are replaced by pre-osteoblasts. Osteoclasts ultimately undergo cell death, or apoptosis and the resorption lacunae become populated by mononuclear preosteoblasts. Preosteoblasts are destined to become bone-forming osteoblasts. Preosteoblasts can be visually identified by their proximity to the resorption surface, clear cytoplasm, single nuclei, and positives for alkaline phosphatase (ALP) stain. Once they mature into osteoblasts, they appear as mononuclear cells with prominent nucleoli and deeply stained cytoplasm. Osteoblasts form a cellular monolayer on the resorption surface previously abandoned by osteoclasts (16, 17) (Figure 11 and Figure 12C).

d) Formation – preosteoblasts become mature osteoblasts and secrete bone matrix, which subsequently undergoes mineralization. Osteoblasts secrete type I collagen, called osteoid, from their basal surfaces onto the previously resorbed surface. Osteoid forms the organic matrix of bone. Some osteoblasts become entrapped in osteoid to become osteocytes. As bone mineralizes, osteocytes tend to become pyknotic but retain metabolic responsiveness to PTH and other stimuli. Osteocytes retain communication with the surface and with other cells through a system of microtubules called canaliculi. Osteoblasts secrete collagen matrix directly on the resorption lacunar surface. The resulting scalloped interface between old bone and new matrix is called the reversal or cement line (16, 17) (Figure 11 and Figure 12D).

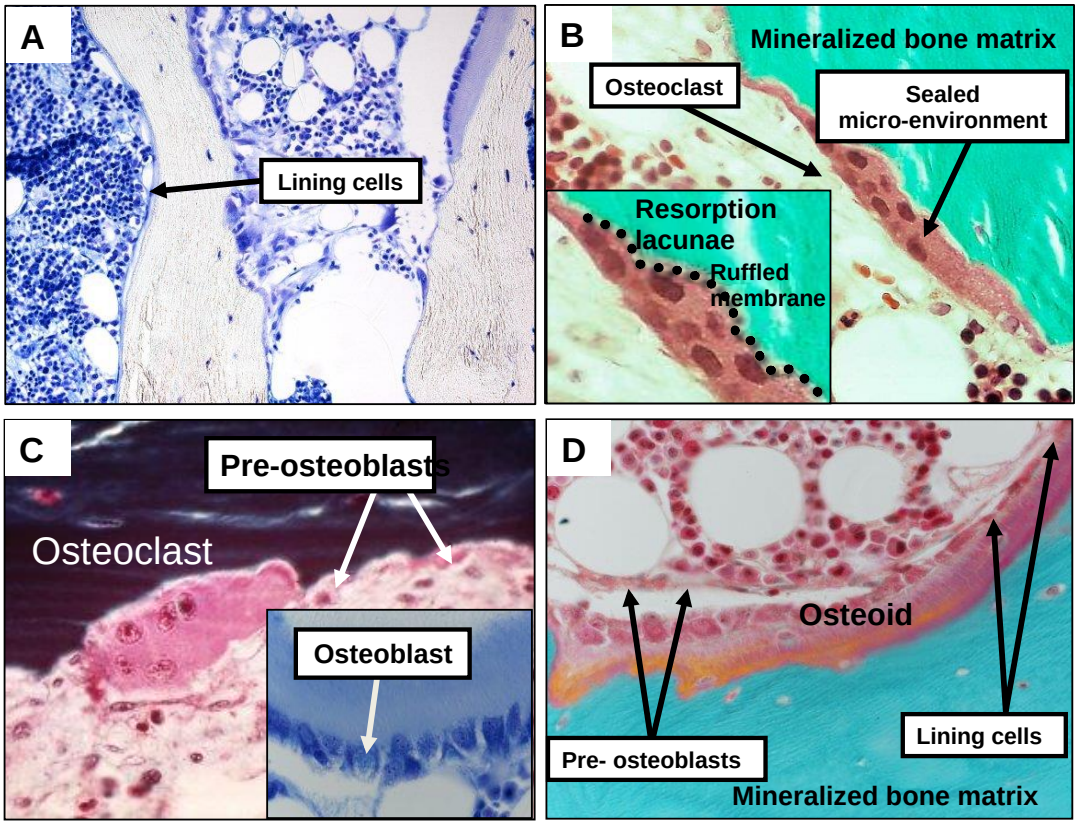

Figure 12

Cells involved in the bone remodelling cycle. (A) Activation phase, (B) resorption phase, (C) reversal phase and (D) formation phase. Adapted from (17)

Type I collagen is a triple helical structure composed of two α1 chains and one α2 chain. Gly-X-Y repeating triplets characterize collagen-α chains, where X and Y are usually proline and hydroxyproline, respectively. Type I collagen is synthesized in a procollagen form which undergoes post-translational hydroxylation and glycosylation of selective residues. It further undergoes removal of terminal sequences before being secreted in its mature form from the basilar surface of osteoblasts into the underlying extra cellular space. Under normal conditions, collagen molecules establish covalent C-to-N cross links that result in both end-to-end and side-to-side alignment, forming mats of aligned and interconnected collagen molecules.

Collagen layers periodically alternate their spatial orientation 90°, resulting in the layered or lamellar bone configuration seen in normal BSU. Under conditions of rapid turnover, e.g., normal growth, fracture healing, or under some pathologic conditions as illustrated, osteoid is deposited in disorganized fashion and is called woven bone in contrast to lamellar bone (Figure 13). Osteoblasts secrete collagenous and noncollagenous proteins into circulation, including the C and N-terminal fragments of procollagen, alkaline phosphatase, and osteocalcin. Concentrations of these products in serum and urine serve as "markers" of bone formation and turnover. The reversal line defines the limit of bone erosion and the original site of bone formation. The persistence of a serrated interface indicates that mineral deposition has not begun at this location (17).

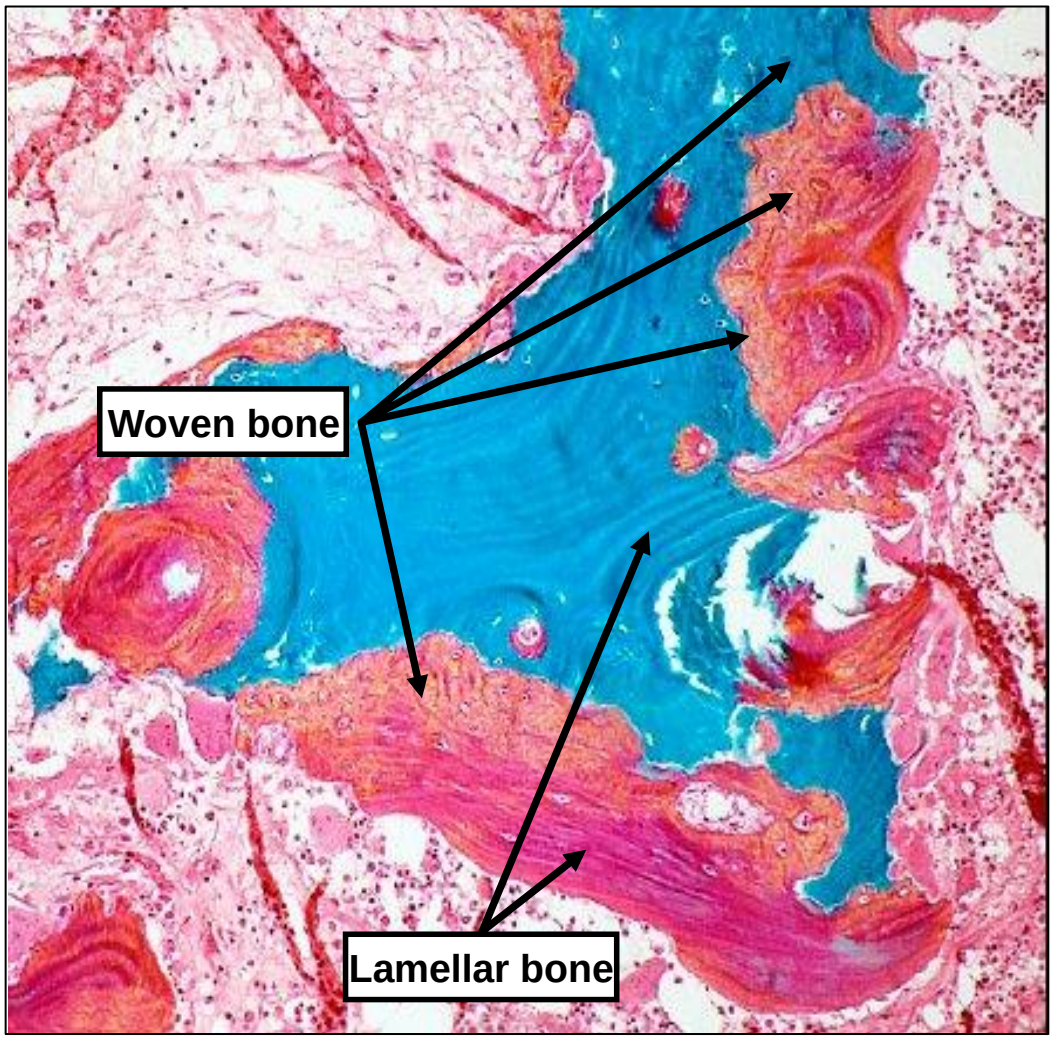

Figure 13

Woven and lamellar bone. Adapted from (17)

Ten to fifteen days after the secretion of osteoid, it undergoes maturational changes that prepare it for the initial deposition of calcium phosphate crystals. This occurs along an interface between mineralized and unmineralized bone, called the mineralization front **(**Figure 14 A, B and C). As early mineralization proceeds, the serrated reversal line becomes obscured and the mineralization front becomes a smooth linear interface (17).

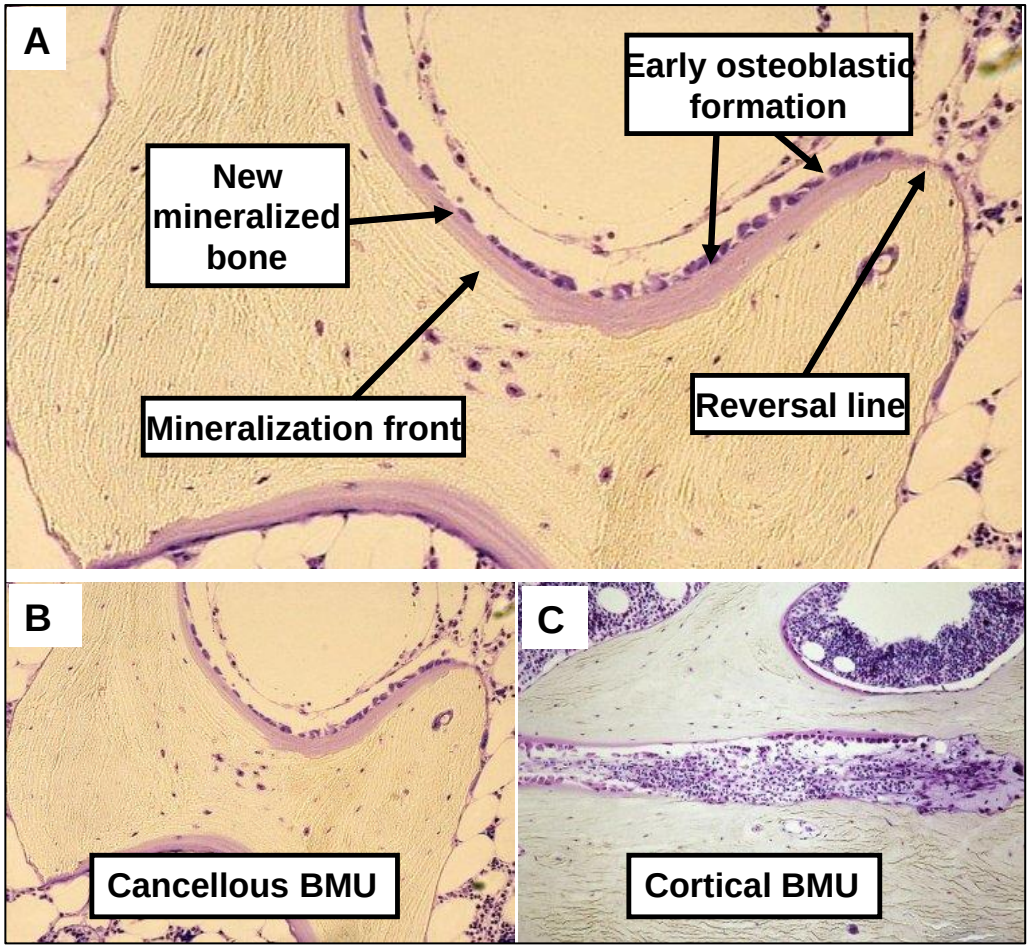

Figure 14

Mineralization front (A), cancellous (B) and cortical (C) BMUs. Adapted from (17)

Between the BMU and bone marrow there is a structure called the bone-remodeling compartment (BRC) (Figure 15). The BRC is lined by sinusoidal vascular structures whose marrow interface is made up of lining cells that form a canopy over the remodeling site. The BRC is thought to be a component of the BMU providing a local environment for regional cell signaling and the coordination of the coupling of formation to

resorption. Though the remodeling cycle begins with osteoclastic resorption ands ends with osteoblastic formation and mineralization, osteoclasts and osteoblasts are otherwise simultaneously present in different regions of the same BMU during most of the active remodeling cycle. Lead by osteoclastic resorption, the BMU moves across the surface of cancellous bone. Resorption is succeeded by formation, which eventually becomes new mineralized bone. Increases in remodeling space (turnover) are associated with an increasing tendency for fracturing. Its size is a limiting factor for increasing bone mass with drugs that reduce turnover (eg. Bisphosphonates). The remodelling space (RS) refers to that volume of bone that has undergone resorption or will undergo formation and mineralization, and which therefore does not contribute to mineralized bone mass. The RS is directly related to bone turnover, and represents the skeleton's potential for increasing bone volume, mass, and strength. The cancellous bone remodeling occurs over a trabecular surface, whereas cortical remodeling occurs within a cylinder. Bone cell function and the sequence of cell activities are otherwise similar. Cancellous BMUs occur in greater numbers, causing the cancellous bone turnover rate to be about ten-fold that of cortical bone (30).

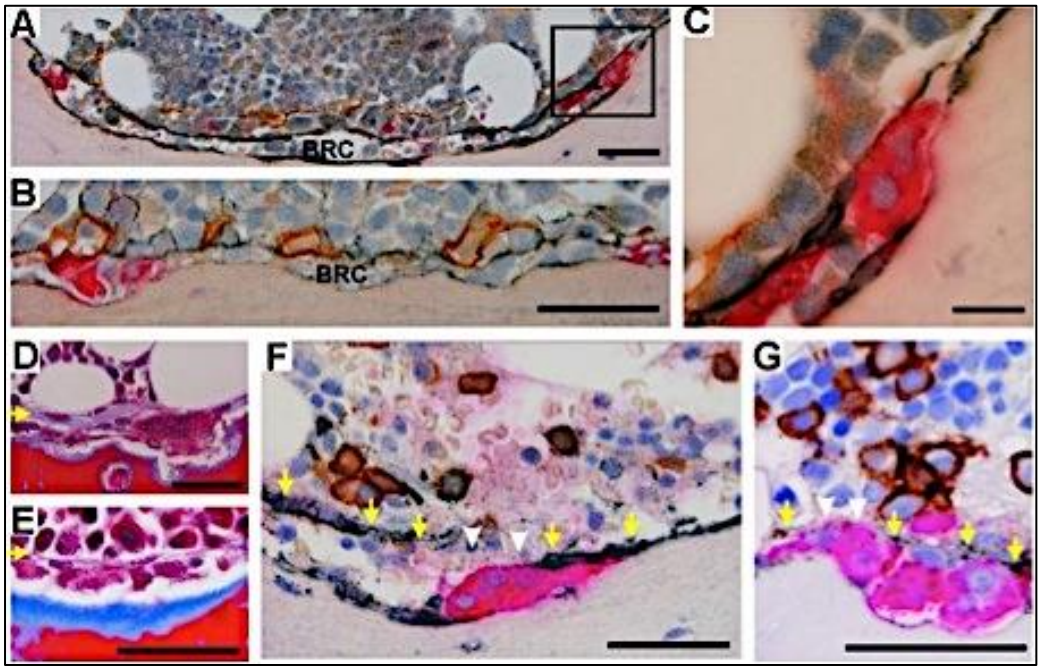

Figure 15

Histological appearance of the BRC: (A) Cross section of a complete BRC, the lining cells are stained in NCAM positive (black); (B) CD34-positives capillaries (brown); (C) Magnification of osteoclasts (red) (inset in (A)); (D) and (E) BRC containing bone (D) and osteoid (E) eroded surfaces; (F) and (G) are two examples of contnouos (yellow arrows) and disrupted canopies (white arrows). According to (30)

HIP JOINT ANATOMY: ARTICULAR SURFACES

The hip is a classical ball-and-socket synovial diarthrodial joint: a) it has a joint cavity; b) the joint surfaces are covered with articular cartilage; c) it has a synovial membrane producing synovial fluid, and d) it is surrounded by a ligamentous capsule (31).

The acetabulum is formed by the innominate bone with contributions from the ilium (approximately 40% of the acetabulum), ischium (40%) and the pubis (20%). The actual articular surface appears a lunate shaped when viewed looking into the acetabulum. Within the lunate, or horseshoe shaped articular cartilage, there is a central area – the central inferior acetabular fossa. This fat filled space houses a synovial covered fat pad and also contains the acetabular attachment of the ligamentum teres. Inferior to this, the socket of the hip is completed by the inferior transverse ligament (31).

Attached to the rim of the acetabulum is the fibrocartilaginous labrum. It plays a role in joint stability and in distribution of forces around the joint. It has also been suggested it plays a role in restricting movement of synovial fluid to the peripheral compartment of the hip, thus helping exert a negative pressure effect within the hip joint. The labrum runs around the circumference of the acetabulum terminating inferiorly where the transverse acetabular ligament crosses the inferior aspect of the acetabular fossa. It attaches to the bony rim of the acetabulum and is quite separate from the insertion of the capsule (31,32) (Figure 16).

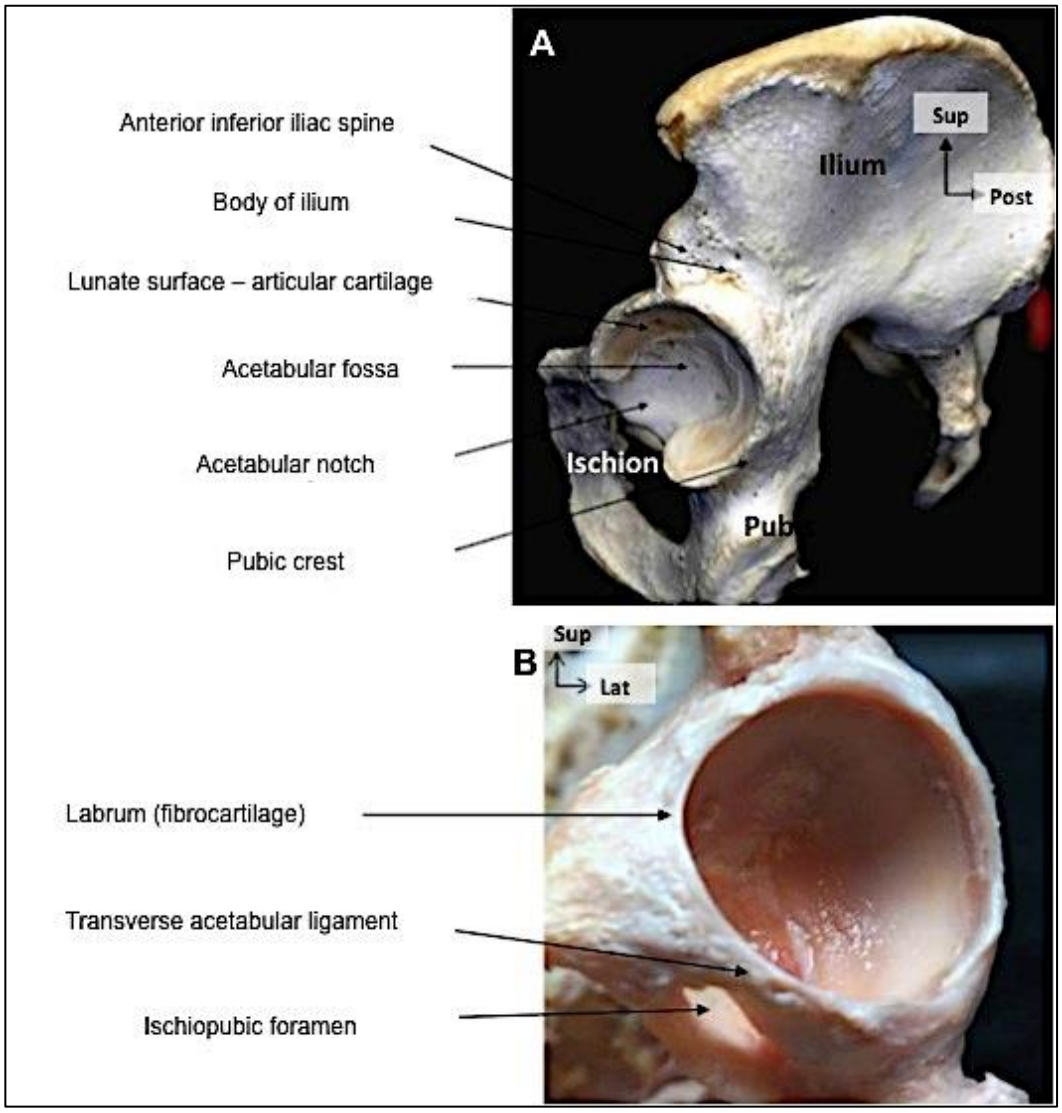

Figure 16. General view of hip bone: (A) acetabular fossa and (B) fibrocartilaginous labrum. (32)

The femoral head is covered with a corresponding articular cartilage beyond the reaches of the acetabular rim to accommodate the full range of motion. The covered region forms approximately 60 to 70% of a sphere. There is an uncovered area on the central area of the femoral head – the fovea capitis – for the femoral insertion of the ligamentum teres (Figure 17). The ligamentum teres, while containing a blood supply does not contribute to the stability of the joint. It is covered in synovium, so while it is intra-articular it is actually extra-synovial

The head of the femur is attached to the femoral shaft by the femoral neck. The neck-shaft angle is usually 125±5° in the normal adult. Thus, the femoral shaft is laterally displaced from the pelvis, thus facilitating freedom for joint motion. The neck-shaft angle steadily decreases from 150° after birth to 125° in

the adult due to remodelling of bone in response to changing stress patterns. The femoral neck in the average person is also rotated slightly anterior to the coronal plane. The neck is most narrow midway down the neck (31).

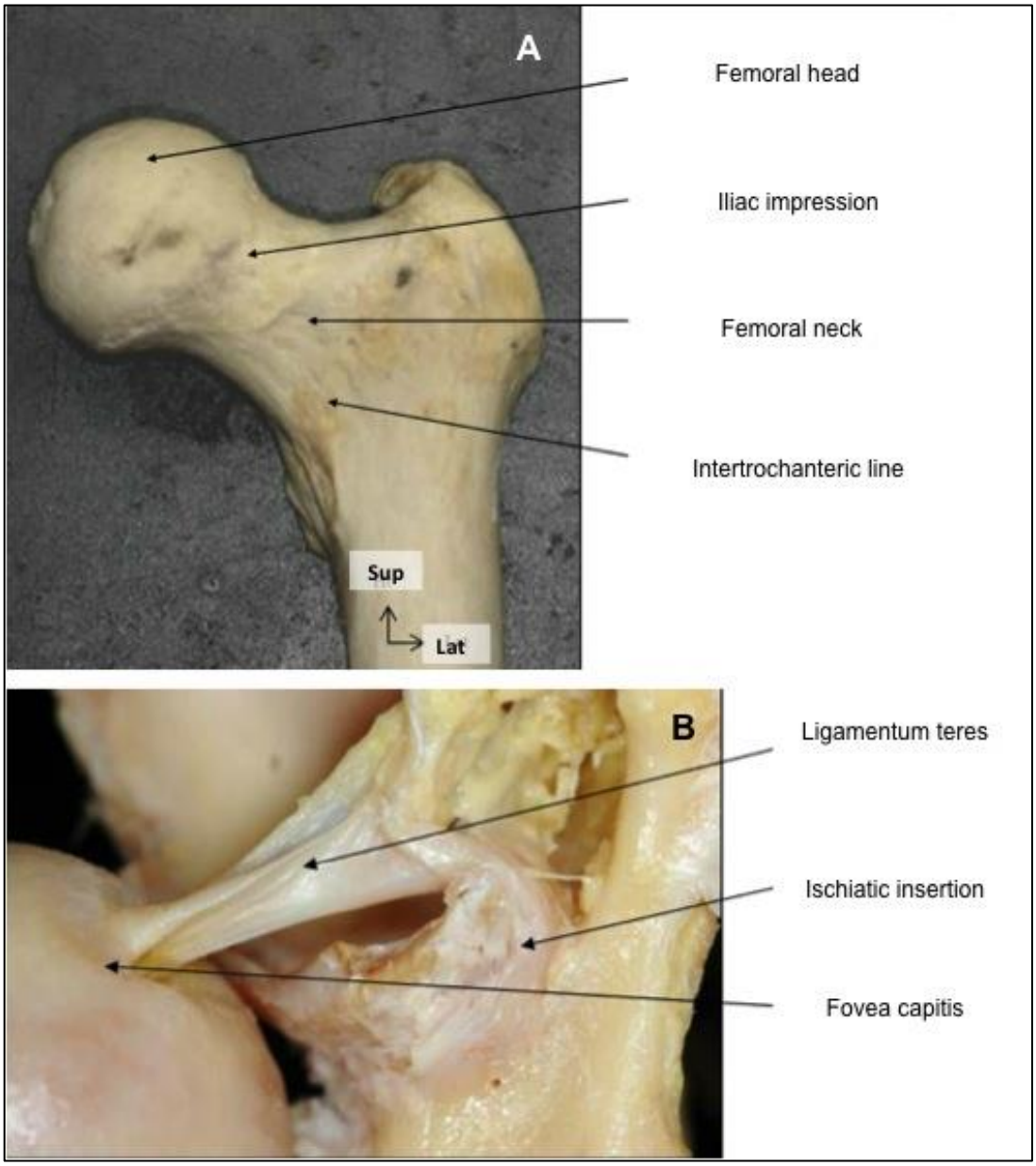

Figure 17. Proximal femoral epiphysis. (A) Femoral head and (B) femoral articular surface recovered by a cartilage layer and Teres ligament joining the fovea capitis with acetabular the notch. (32)

TOTAL JOINT REPLACEMENT: TRIBOLOGY AND BIOACTIVITY OF BEARING SURFACES

The tribology of artificial joints includes the wear behaviour of the implants' bearing surfaces (33). During the wear process, worn sub-micrometric particle debris is released normally or abnormally from the bearing surfaces to the bone microenvironment as a result of adhesive, abrasive, third body, fatigue or corrosive wear (33,34). The wear particles cause the secretion of pro-inflammatory cytokines by macrophages, production of pro-resorptive cytokines by osteoblasts and fibroblasts, stimulation of osteoclastogenesis, induction of osteolysis and subsequently the loosening of the implant (4). The sources of the particles can be either metallic or polymeric, the former including titanium (Ti) and chrome-cobalt (Cr-Co) and the latter consisting of ultra-high-molecular-weight-polyethylene (UHMWPE) from acetabular cups and polymethylmethacrylate (PMMA) from bone cement extensively used in cemented THA replacement. While wear debris of Ti, Cr-Co or PMMA is released under abnormal function of the prosthesis, UHMWPE particles are released normally during the life-span of the prosthetic device (35). Thus, production and accumulation of UHMWPE wear debris is an inherent phenomenon of implant use (35) (Figure 18).

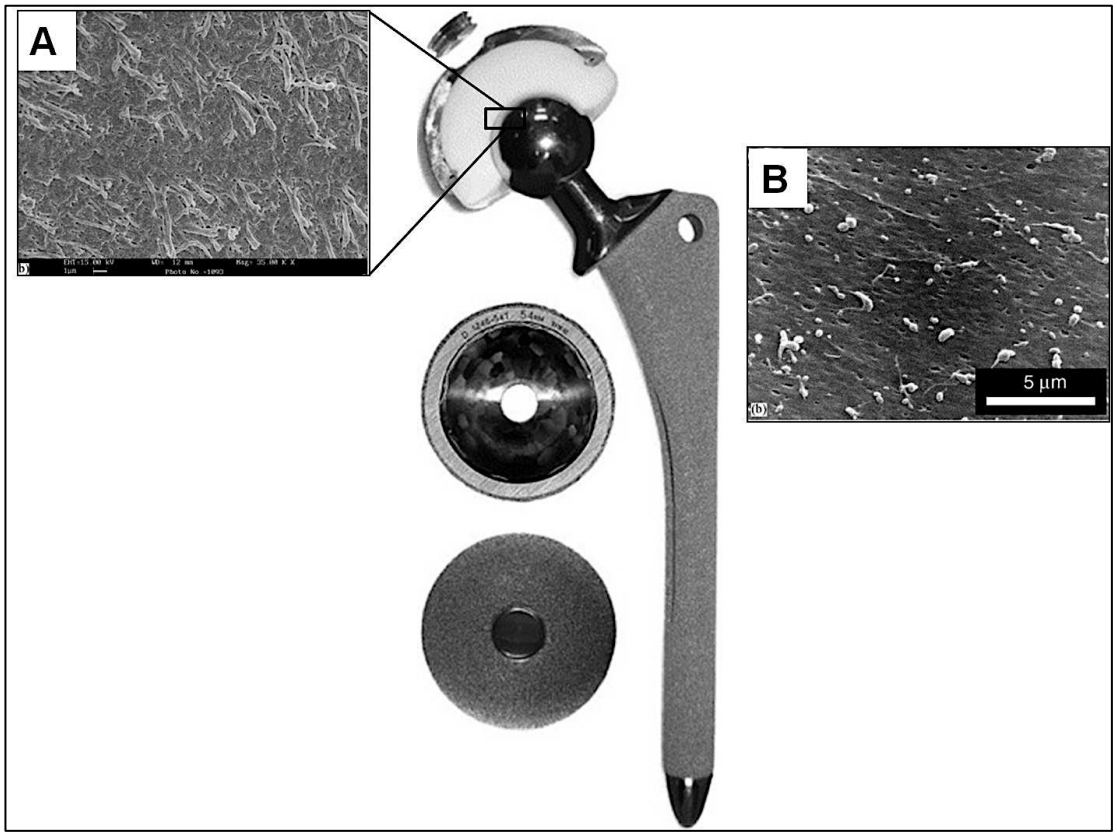

Figure 18. Scanning electron micrograph of bearing surface of polyethylene acetabular cup (A) and polyethylene wear particles (B) worn in hip wear simulator for 3 million cycles against Cr-Co head. Adapted from (36)

Metal-on-Polyethylene couples

The use of metal-on-UHMWPE bearing surfaces in hip implants was proposed by Charnley in 1961 (Figure 19 and Figure 20). This low frictional system is comprised of an acetabular UHMWPE cup articulating against a small diameter metallic femoral head (37). Its success is due to the combination of excellent mechanical properties and biocompatibility; however UHMWPE, which has become the material most commonly used as a prosthetic surface after the failure of polytetrafluoroethylene (PTFE, Teflon) (2), has shown limitations in the long term due to the generation of debris (38). In the past decade, a first-generation cross-linked polyethylene has shown lower wear rates and a decreased incidence of periprosthetic osteolysis compared to UHMWPE in the medium term; however the problem seems to persist: the cross-linked polyethylene still releases phagocytable wear nanoparticles, strongly related to its higher bioactivity (39). Furthermore, the residual oxidation and potential material fracture raise questions about its effectiveness.

Recently, a second-generation cross-linked polyethylene has been developed. New methods of stabilization (annealing and remelting) and incorporation of vitamin E (blended polyethylenes) have led to reduced oxidation and fracture risk, and a lower rate of wear (38). The clinical performances of cross-linked polyethylene and UHMWPE were analysed in a randomized trial (40) and in a meta-analysis (41) at intermediate follow-up. Both studies matched for the significant decrease in wear rates and in the low risk of developing loosening observed in new polyethylenes. A recent long-term multicentre study examining the benefits of cross-linked polyethylene in patients after THA showed an improvement in the prognosis of implant survival of up to 13 years (8). Despite these encouraging data, the need for longer-term follow-up is central to determining the differences in the need for surgical revision. Furthermore, the biological role of wear nanoparticles released by new polyethylenes remains unknown and seems to be an interesting subject of research for the coming years. In this context, we believe that UHMWPE will remain the biomaterial of reference.

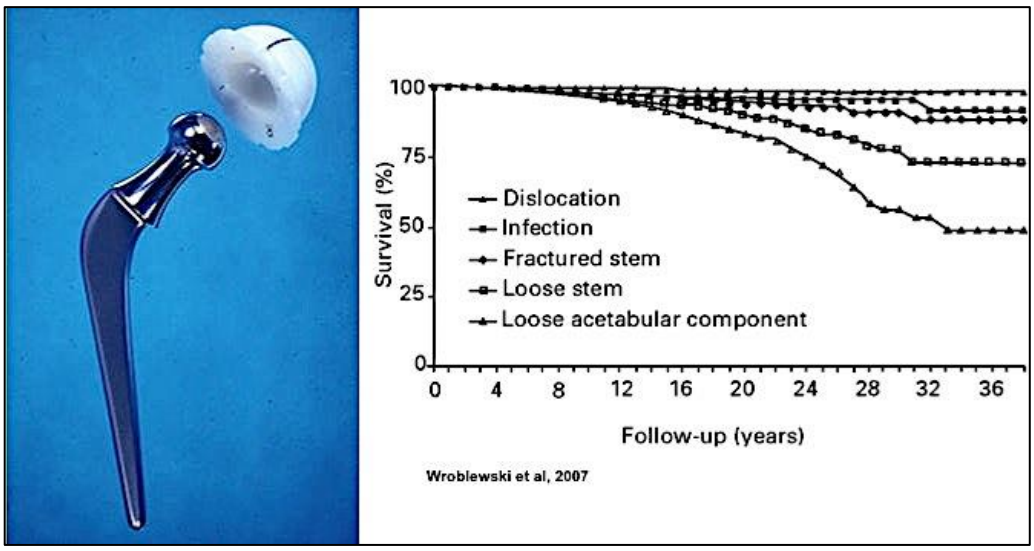

Figure 19. Charnley low - friction arthroplasty and it percentage of survival after 38 years. (42)

Figure 20. Charnley low - friction arthroplasty. (Image provided by courtesy of Professor F. GOUIN)

Other currently used alternatives for total hip arthroplasty include metal-on-metal and ceramic-on-ceramic bearing surfaces (Figure 21). In general, these have shown better mechanical properties and lower wear rates than the classic metal-on-UHMWPE couple and are an alternative to reducing the prevalent osteolysis and aseptic loosening in THA (43). However, the persistent risk of fracture for ceramic (33), the potential risk of development of hypersensivity reactions (9) and chronic exposure to metallic ions with metal-on-metal couples (44) cast doubt on the real advantages over metal-on-UHMWPE couples. Finally, although modular systems have shown advantages in adapting to anatomical difficulties, there is a risk of micro-displacement of metal interconnectors and wear production (45). We will now briefly describe the current tribological and bioactive concepts of each type:

Metal-on-Metal couples

Better postoperative stability, improved tribological properties and the ability to use larger diameter femoral heads on Cr-Co has led to an increase in its indications in younger and active patients in the last decade (46,47) (Figure 21B). However, early use prolongs the exposure to metal products (ions and/or nanoparticles),

increasing the need for surgical revision by adverse responses associated with metal debris (ARMD) rather than aseptic loosening. Similarly, a severe increase in serum cobalt (Co) concentrations (up to 160-fold) in patients treated with stemmed-large-head-metal-on-metal THA, hip resurfacing arthroplasties (HRAs) and modular systems, has been reported (48). The chrome-cobalt-molybdenum (Cr-Co-Mo) alloy present in the second-generation metal-on-metal devices has been related to the production of nanoparticles and ions by electrochemical corrosion (46,49–51) requiring special toxicological consideration. The predominating Cr-Co-Mo nanoparticles (50 nm or less) induce the reactivity of local tissues, mediated by the monocyte/macrophage response. They are internalized by diffusion (10-30 nm wide) or receptor mediated-endocytosis (RME), a specific endocytosis that is clathrin- or caveolae–mediated (120 or 80 nm wide, respectively)(52). Also, pinocytosis, a non-specific mechanism of endocytosis, has been proposed as an alternative means of internalization (52). Once the nanoparticles are in cytosol they increase the secretion of proinflammatory cytokines by having a direct effect on the nuclear factor-kappaB (Nf-kB). Another way of explaining the increase in reactivity in phagocytic cells by metallic nanoparticles, is the activation of inflammasome, an intracellular danger-signal protein complex, in a particle concentration-dependent manner (52,53).

On the other hand, the ionic sensitivity of local tissues leads to perivascular lymphocytic infiltration independent of the presence of wear debris. This response seems to be a type 4 delayed hypersensitivity response (9,52), but this issue remains controversial. The mechanism proposed is the loss of anti-corrosive capacity of Chrome by the effect of local biologic fluid, fritting and wear production (52). In this form, Cobalt is released into the synovial fluid and internalized by local macrophages leading to necrosis and intracellular corrosion by oxidative stress with an increase in production of reactive oxygen species (ROS). Thus, the NF-kB pathway is up-regulated, increasing the release of pro-inflammatory cytokines which re-stimulate the necrosis-oxidative stress vicious cycle (52). Ion accumulation was primarily related to local hypersensitivity or systemic toxicity (44). Furthermore, elevated serum levels of ions were associated with early failure of metal-on-metal devices (large femoral head in metal-on-metal THAs, metallic modular systems and metal-on-metal hip resurfacing systems) by ARMD, metallosis and osteolysis (51), leading to aseptic lymphocyte-dominated

vasculitis-associated lesions (ALVAL), a new pathological entity characterized by the presence of pseudotumoral soft tissues (46,49–51).

Ceramic-on-ceramic couples

The use of ceramic-on-ceramic *(aluminum or zirconium oxide)* has reduced the production of wear and loosening of the implant and is a good candidate for indications in a younger population (Figure 21B). However, it has shown low mechanical properties with an increased risk of fracture (33). Currently, the use of third generation ceramics has considerably improved their mechanical and tribological behaviour (54,55). A number of retrospective studies, performed in active patients (age 50 years on average) and analyzing their long-term behaviour, have shown the low incidence of aseptic loosening, with a high percentage of success in primary THA and only an exceptional need for surgical revision (54,55). Ceramic-on-polyethylene couples have also been proposed to minimize wear debris production (56). Ceramic heads were harder and more resistant to scratching and showed a reduction in liner wear rate than classic Cr-Co heads, suggesting a decrease in the risk of developing aseptic loosening (57,58). Despite these encouraging results, the microseparation described in zirconium femoral heads, the incidence of fracture, the great challenge for surgical revision due to the inability of using a ceramic head a second time and the risk of chipping the ceramic, do not make this the most popular choice (4).

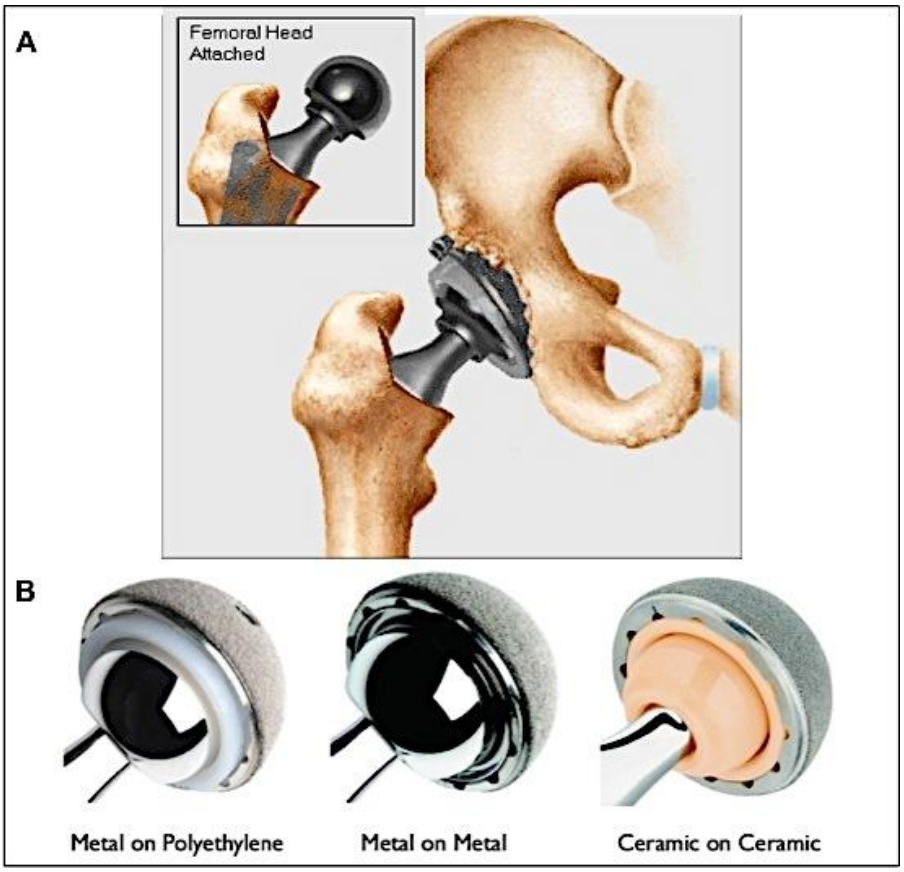

Figure 21. Bearing surfaces more often availables for total hip arthroplasty. (59)

Role of PMMA in aseptic loosening

While the head-cup interface has been highlighted as a main source of wear products, other bearing surfaces such as acetabular-cement and stem-cement interfaces should also be considered (Figure 22). The evidence available concerning the behaviour of the former is controversial, suggesting that cemented acetabular components have a better tribological performance and reliability than uncemented (60,61). Otherwise, the stem-cement interface is an important source of "fretting", the contact wear products generated by low-amplitude oscillatory micromotion under physiological loading (62,63). Femoral stem wear became one of the major sources of wear products after the introduction of improved biomaterials for the head-cup interface (62). The fatigue failure of PMMA leads to debonding of the femoral stem with the subsequent development of aseptic loosening (64,65). On the other hand, the morphology of the stem surface seems to play a critical role in generating fritting wear. Microporous rather than polished stem surfaces were significantly more associated with fretting wear production in the joint simulator (63). The confirmed role of bone cement in the genesis of

experimental stem-cement debonding and the subsequent generation of wear or fritting products was reaffirmed by clinical retrospective survivorship analysis confirming the lower lifespan of cemented compared with cementless THA at long-term follow-up. These data explain the general clinical popularity of cementless THA over cemented THA (66,67).

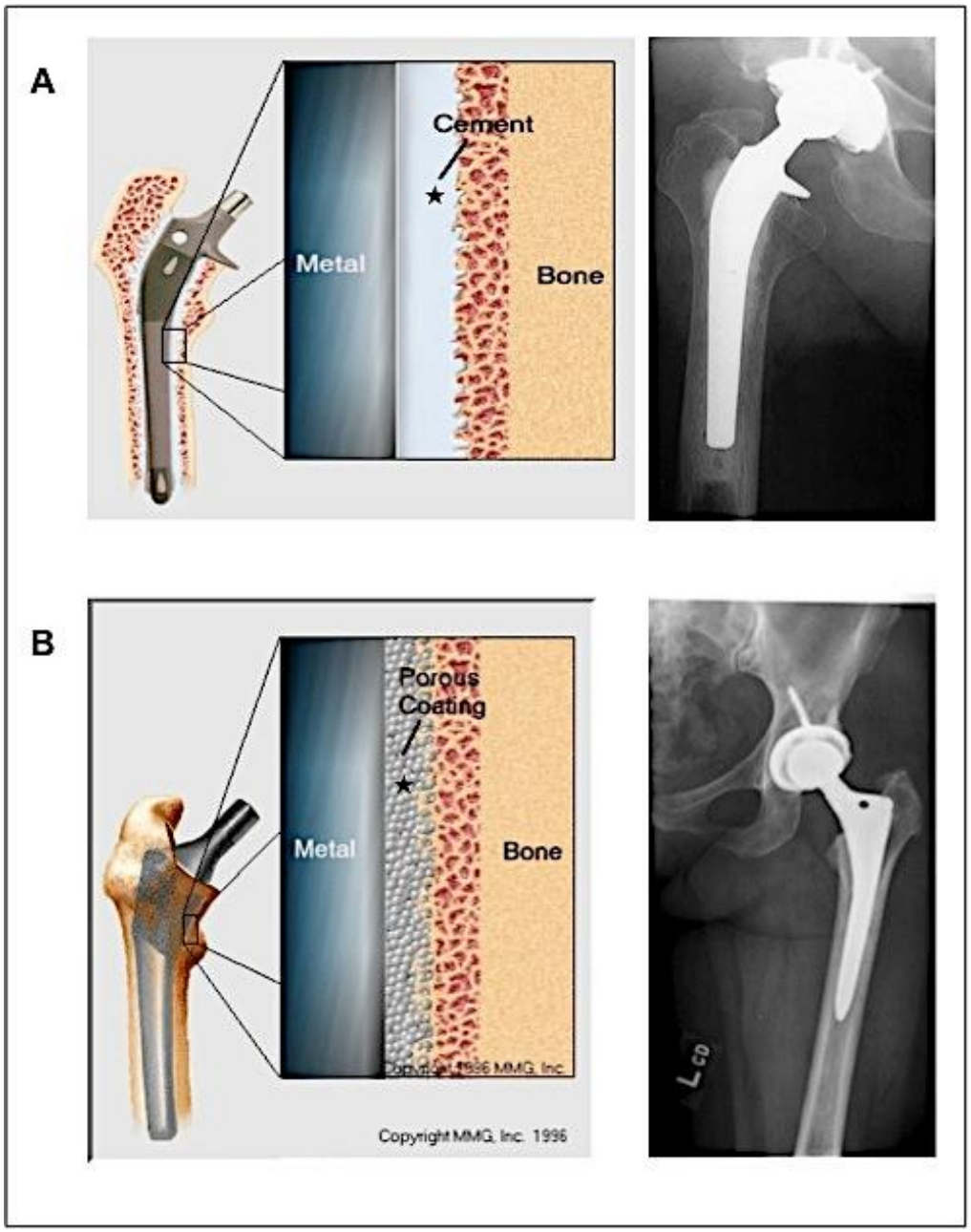

Figure 22. Metal-bone interface in cemented (A) or cementless (B) femoral stems of total hip arthroplasty. (59)

THE CELL INTERACTIONS WITH WEAR PARTICLES

In the field of aseptic loosening, *in vitro* approaches have served to highlight the interactions between particles and the most competent cells involved in inflammatory-osteolytic process: macrophages, osteoclasts and osteoblasts (Figure 23).

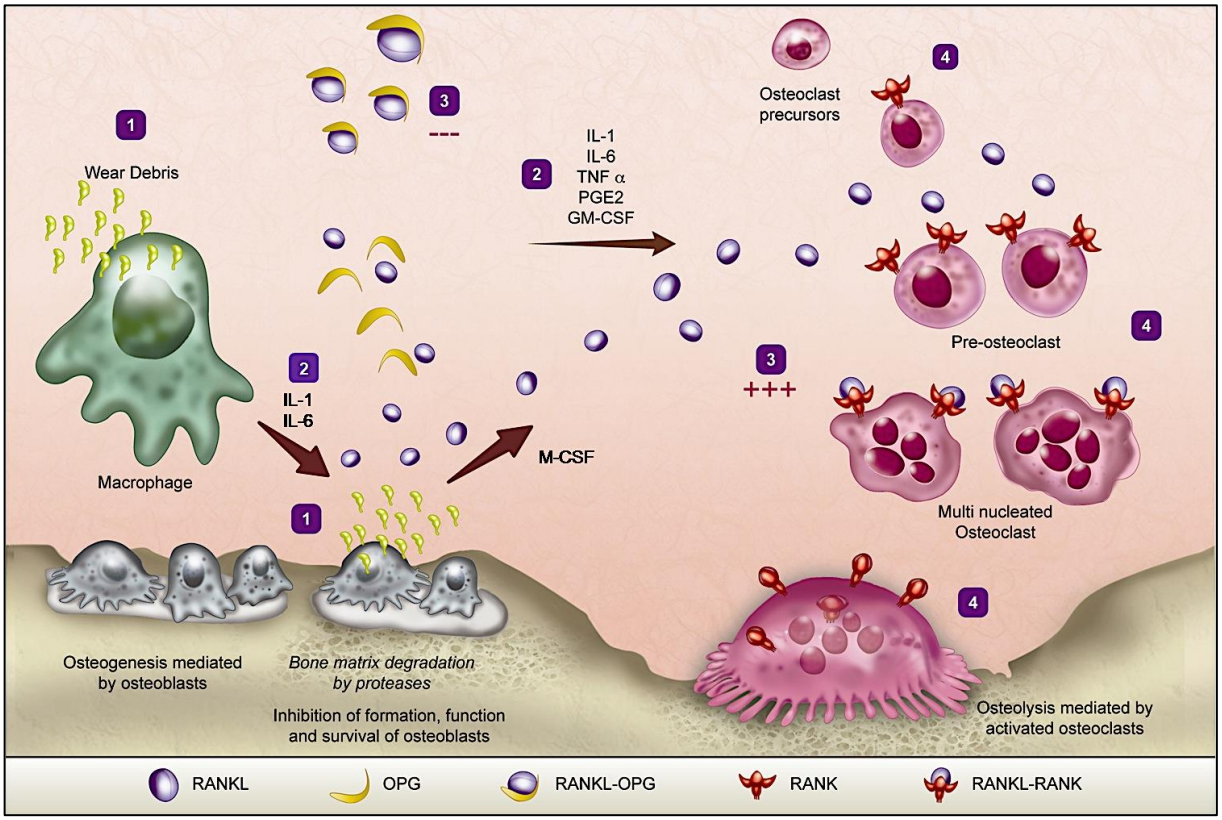

Figure 23. Simplified molecular mechanisms induced by wear debris particles in the periprosthetic niche.

(1) Wear debris particles stimulate macrophages and osteoblasts. (2) Activated macrophages secrete chemokines, pro-inflammatory cytokines (IL-1β, IL-6 and TNF-α), prostaglandine E2 (PGE2) and GM-CSF, inducing directly the recrutment, differentiation of pre osteoclasts in mature osteoclasts. (2) IL-1β and IL-6 activate indirectly the differentiation of osteoclasts through the secretion of RANKL by activated osteoblasts. (3) RANKL/RANK (+++) signalling between activated osteoblasts and pre osteoclasts in presence of M-CSF. (4) Recrutment, differentiation of osteoclast precursors into activated osteoclasts and subsequent osteolysis in resorption pit. (Cordova LA. *et al*., unpublished data)

Macrophages and wear particles

Monocytes / macrophages belong to the family of mononuclear phagocytes. These cells originate from multipotent precursors from bone marrow, hematopoietic stem cells, which differentiate into myeloid precursors (Figure 24). Myeloid precursors can then give the granulocyte and monocyte lineage. Newly formed monocytes leave the bone marrow, so to reach the bloodstream where they represent between 5 and 10% of the leukocytes. This monocyte population is characterized by the expression of receptor to M-CSF, Colony stimulating factor 1 receptor (CSF-1R) and coreceptor lipopolysaccharide (LPS), the CD14 marker. They will remain in the bloodstream for 1-3 days and then, through the endothelial barrier by diapedesis, they go into the various tissues of the body, they then differentiate into residents macrophages or inflammatory depend of the local context. Monocytes therefore represent "cell tank" while macrophages are essential effector cells in the initiation of the innate immune response to pathogens, and bridging the gap with adaptive immunity (16).

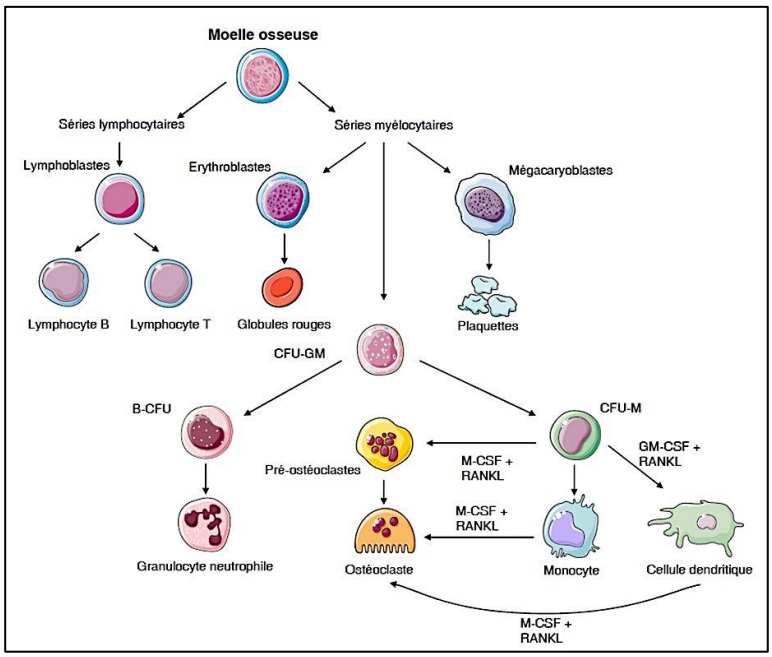

Figure 24. Differentiation of myeloid lineage. (16)

Originally, human monocytes were described and identified due to their morphology but the development of flow cytometry has better characterize through the expression of it LPS coreceptor, CD14. This technology has also helped to highlight the existence of new sub-populations based on the expression of the marker CD16 (RFcγIII). These new populations express strongly the moleculaes of major histocompatibility complex class II

(MHC II) and produces less TNF-α in response to stimulation by a ligand of Toll like receptor (TLR). Based on the expression of these two surface markers, three sub-populations are described in the literature: a) The classic macrophages ($CD14^{High}CD16^{-)}$, that correspond to 85% of circulants monocytes in healthy patients and they express strongly CD14, the chemokine receptor CCR2 and less the CX3CR1. They are a great capacity to phagocytose and to secrete proinflammatory cytokynes such as TNF-α, IL-6 and IL-1. b) The non-classic macrophages ($CD14^{Low}CD16^{High)}$ corresponding to 10% of circulant macrophages and they express slightly CCR2, strongly CX3CR1, CCR5 and MHC II. They seem to be more mature and closer to the resident tissue macrophages (Figure 25). Finally, c) the intermediate macrophages ($CD14^{HIGH}CD16^{LOW}$) have been also recognized.

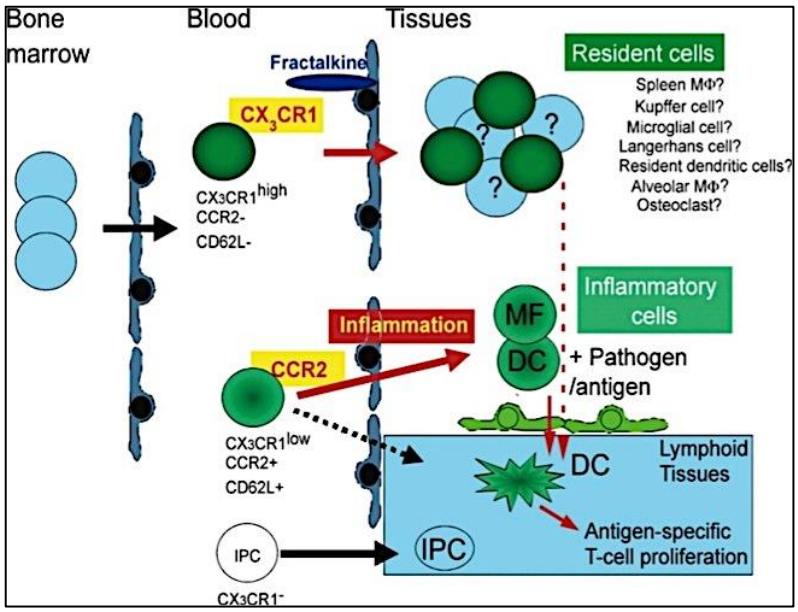

Figure 25. Distribution of circulant, residents and inflammatory macrophages. (68)

While macrophage diversity includes a large spectrum of phenotypes, rather than distinctly proinflammatory or antiinflammatory populations, differing cytokine production profiles have been described for M1 and M2 macrophages. The cytokine release profile of M1 proi-nflammatory macrophages includes increased TNF-α, IL-1β, IL-6, IL-12, IL-23 and type 1 interferon, as well as expression of inducible NO synthase (iNOS), CCR7 and HLA-DR. The cytokine release profile of M2 anti-inflammatory macrophages

includes increased IL-4, IL-10, IL-13, and IL-1ra production, as well as expression of CD206, Ym1, CD163, CCL1, CCL18, FIZZ1, Arginase 1 and chitotriosidase. These distinctions provide a useful tool to identify the phenotype of the different macrophage population in tissue specimens or in vitro studies (69) (Figure 26).

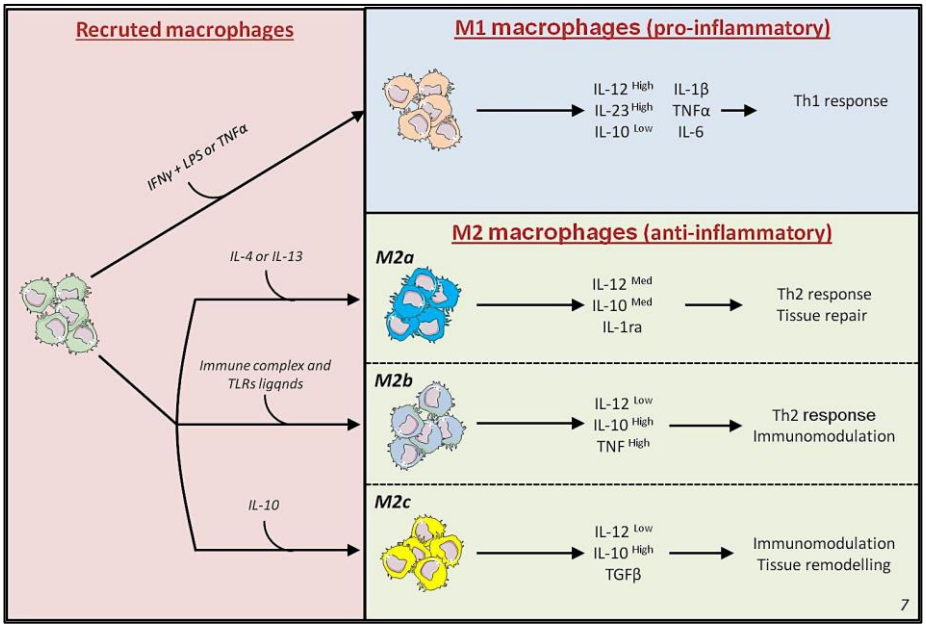

Figure 26. Macrophage phenotypes and subpopulations. (16)

There is strong evidence that points to macrophages as the key cells implicated in periprosthetic inflammation and osteolysis wear debris (35). The presence of macrophage-like cells surrounding large particles of polyethylene in pseudomembranes confirms this finding (70). The chemo-attraction of macrophages by chemokines, such as monocyte chemoattractant protein-1 (MCP-1), the most important chemokine regulating cell trafficking and infiltration of monocyte/macrophages in chronic inflammation, is a key step in the early inflammatory process (71). Furthermore, the presence of wear particles within phagocytable range (0.1 – 20 µm) inside the macrophages suggests that the cells actively engulf particles, which subsequently leads to the release of pro-inflammatory mediators such as cytokines TNF-α, IL-1β, prostaglandin E2 (PGE2), GM-CSF and IL-6 into the cell culture supernatant (35). The expression of inflammatory cytokines in macrophage-particle cultures can be modulated by particle composition (4), size (72), shape (73) and surface area (74). However, it remains unclear which parameters are the most important (73). Regarding the size, Endres *et al*.

and Pal *et al*. tested the effect of UHMWPE nanoparticles on monocyte/macrophage response, reporting an inverse relationship between particle size and bioactivity (75).

Naive's macrophages, resident in inflamed tissues (M0), have the ability to react to the environmental stimulus, leading to modification of their phenotype: microbial LPS, interferon gamma (IFN- γ) or TNF-α induce the pro-inflammatory phenotype (M1) and IL-4 or IL-13 induce modification to the anti-inflammatory phenotype (M2), promoting tissue repair (76).

The paradox of 80-90 % of implants surviving despite the continuous release of wear debris could be explained by the majority presence of M0 and M2 in peri-implant tissues (34,77). Otherwise, the aggressive osteolysis could be related to the activation of pattern-recognition receptors (PRRs) in M0 (34). PRRs are proteins expressed by the innate immune system to identify pathogen-associated-molecular-patterns (PAMPs), such as the LPS or endogenous damage-associated molecular-patterns (DAMPs) such as ROS (78). LPS would provide the initial danger signal to promote the differentiation from M0 to pro-inflammatory macrophages (M1). Interestingly, the macrophage phenotype has been experimentally modulated, from a pro-inflammatory subpopulation (M1) to an anti-inflammatory phenotype (M2) in human macrophages isolated from retrieved pseudomembranes, confirming the plasticity between both phenotypes and proposing a potential therapeutic approach (79). Based on these findings, the biofilm-derived bacteria and LPS may play an underestimated role in the implant loosening process (80). Clinical and experimental studies have confirmed that LPS have a high affinity to wear debris and play a significant role in the activation of PRRs and subsequent induction of bone loss (81–85). Based on this proposal, the classic paradigm of "aseptic loosening" could be modifiable by "septic loosening" caused by bacteria housed in the implant biofilm and recognizable only by new methods of detection (34).

Otherwise, Toll-like, NOD-like, AIM-like and RIG-I-like receptors (TLRs, NLRs, ALRs and RLRs respectively) have been described (86,87). All of them are opsonin-dependent PRRs activated by immune or non-immune molecules (88,89). TLRs' signalling pathway is a key step for activating transcription factors of pro-inflammatory cytokines in immune cells (70,87). TLR2 is engaged by exogenous short chains of polyethylene, activating NF-kB (Figure 27) (70,90). Co-ions released from metal-on-metal implants promote

the homodimerisation of TLR4, leading to the synthesis of pro-inflammatory cytokines and co-stimulatory molecules in macrophages (34,91). Additionally, other endogenous DAMPs signal through TLR2 and TLR4 pathways (70). On the other hand, endocytic PRRs, the scavenger receptors, promote the engulfment and destruction of charged ligands independent of the opsonisation process (92). The macrophage receptor with a collagenous structure (MARCO) is a scavenger receptor, which has been reported to be highly expressed in $CD68^{+}$ positive macrophages and foreign body giant cells in interface membrane linings and stroma around cemented implants (92). Activation of these sensors by particles may therefore induce the recruitment of the cellular infiltrate, initiating an acute inflammatory response and linking innate with adaptive immune responses (88).

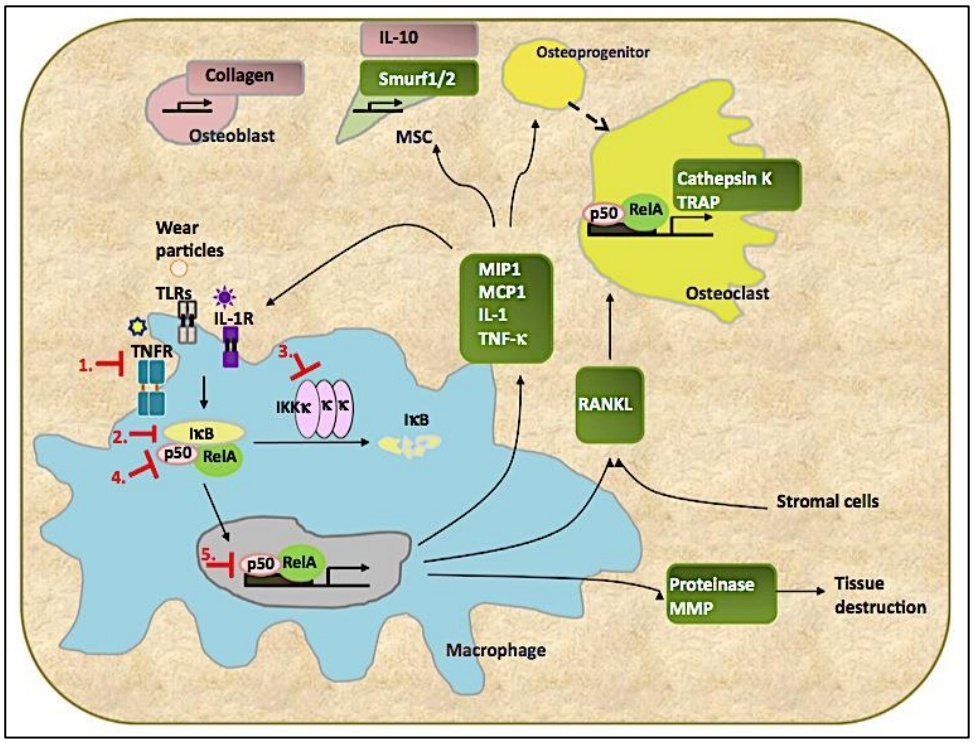

Figure 27. The central role of NF-KB in the orchestration of inflammatory and osteolytic response under wear debris challenge in periprosthetic tissues.

Wear particles activate NF-KB (inside the nucleum of macrophage) by TNF (TNFR) and IL-1 (IL1R) signalling and TLRs pathway. NF-KB up regulates the synthesis, expression and secretion of chemokines (macrophage inflammatory protein-1 [MIP1] and Monocyte chemoattractant protein-1 [MCP1]), proinflammatory cytokynes (IL-1, TNF-α), pro-osteoclastogenic cytokynes (RANKL), proteinases to bone matrix resorption (MMP and others) and also inhibitors signals for osteoblasts and MSCs. (90)

In another way, a cross-control of immune response through the expression of estrogenic receptors (ERs) by periprosthetic macrophages has recently been reported (93). Their blockade results in a decrease of TNF-α in mouse macrophages activated by polyethylene particles. The macrophagic response to wear particles may therefore be modulated through ERs and their ligands (93).

With respect to the mechanistic understanding of intracellular macrophage activation, Caicedo *et al.* proposed the NACHT, LRR, and PYD domains containing protein-3 (NALP3) inflammasome, a macrophagic intra-cellular stress response triggered by the presence of phagocytized metallic debris (53). Confirming this finding, the titanium-induced inflammation triggered by macrophage TLR signalling and intra-cellular activation of the NALP3 inflammasome has been shown to induce increased IL-1β secretion and IL-1-associated signalling and to promote the recruitment of neutrophils (70). A differential activation of NALP3 inflammasome has been described for larger or smaller particles of polyethylene, Ti, Silica, Cr-Co and PMMA (70). While the larger lead to ROS-mediated inflammasome activation triggering a classic foreign body reaction (giant cells surrounding the largest wear particles); the smaller trigger the cytosolic cathepsine-mediated inflammasome activation after endosomal destabilization (70). These events may therefore propose the inflammasome as a critical mediator for orthopaedic wear-induced osteolysis maintaining the chronic inflammation, inducing periprosthetic bone loss and ultimately leading to implant failure (70). Experimental models blockading NALP3 inflammasome components propose this pathway as a viable therapeutic target for the treatment of periprosthetic osteolysis (94).

Osteoclasts and wear particles

The presence of UHMWPE wear particles in the periprosthetic bone microenvironment enhances the differentiation of osteoclast progenitors into mature osteoclasts in response to the cytokines released by activated macrophages and osteoblasts (95). In the past decade, major advances in understanding the osteoblastic regulation of osteoclastogenesis, mediated by the RANKL/RANK/OPG system, have been made

(96). For example, it has been shown that OPG expression by human osteoblasts was significantly inhibited in the presence of UHMWPE particles, leading to a decreased OPG/RANKL ratio and subsequent stimulation of osteoclastogenesis *in vitro* (97). Furthermore, the intracellular activation of osteoblastic cells by phagocytosis mediator proteins ERK1/2-CEBPβ may be a key inflammatory pathway that links phagocytosis of wear particles to inflammatory gene expression in osteoprogenitor cells (98).

Osteoblasts and wear particles

Normal bone formation by osteoblasts is essential for implant survival. Disruption of osteoblast function by wear particles was hypothesized to be an important factor influencing the balance in bone remodelling and thereby decreasing the survival of implants due to aseptic loosening. Several authors have reported an inhibitory effect of Ti particles on osteoblast function by various mechanisms: suppression of gene expression of collagen type 1 (99), triggering apoptosis (99) and alterations of adhesion (100) with a consecutive decrease in cell viability (99,101). Moreover, different particle types and surfaces were tested, identifying cobalt-based and rough-surface particles as the most cytotoxic compositions and, inversely, zirconium oxide (ZrO_2) particles as the most innocuous (99,101). Exposing osteoblasts to UHMWPE particles *in vitro* decreases their osteogenic activity (mineralization, proliferation, alkaline phosphatase activity, and osteocalcin production) mediated by an increase in RANKL expression and induction of a catabolic phenotype (39,75).

MOUSE MODELS AVAILABLES FOR THE STUDY OF PERIPROSTHETIC OSTEOLYSIS

Different species have been used to test biological and biomechanical parameters, two aspects closely related to aseptic implant loosening (102). These include sheep (10) dogs (103), rabbits (11), rats (104) and mice (13,105). The use of large animals has obvious advantages, especially if the desired outcome is the global understanding of the behaviour of the implant in the host. However, the cost of maintenance and the need for multiple therapeutic interventions in a large animal do not make these options the most used as a primary *in vivo* approach. For this reason, mouse models appear to be the most effective alternative, due to the low cost of maintenance, the facility in reaching sufficient numbers of individuals to strengthen statistical results and the diverse options in genetic or immune features available (13,106). Mouse models have been exploited with two major aims: the reproduction of a human clinical phenotype (modelling) and the development of therapeutic assays.

To model particle-induced osteolysis *in vivo*, it is necessary to establish a causal effect between the particles and inflammatory osteolysis and to unveil the mechanisms involved, identifying their critical markers. The first aim has been well achieved in mice, demonstrating that the UHWMPE-induced formation of granulomas and subsequent development of osteolysis is highly dependent on the size and shape of the particles (35). Moreover, Wooley *et al.* suggested an important role for UHMWPE particle size, introducing the concept of a "critical particle size" (<20 μm) required to induce significant reactions *in vivo* (107). The desired second aim of unveiling the mechanism of particle-induced osteolysis is based on a classical paradigm: macrophage-mediated inflammatory responses and increased osteoclastogenesis lead to an imbalance between bone formation and resorption (102). In this sense, in the past decade the biological interactions between particulate debris and immune response have been better understood. Goodman suggests a differential immune response according to the biomaterial involved (9). While polymers (UHMWPE and PMMA) seem to trigger an unspecific response, metals (Cr-Co and Ti) are thought to trigger a type IV hypersensitivity reaction. The cellular effectors in the non-specific (polymeric) response appear to be mainly macrophages and fibroblasts, with a secondary modulator role for lymphocytes. By contrast, during the specific response, T lymphocytes may play a major role in the maintenance of chronic inflammation, however their exact role in implant-

loosening is still unknown (9). Consequently, understanding the exact role of macrophages and lymphocytes is the key to understanding the immune modulation induced by particles.

Several animal models have demonstrated an activation of macrophages in response to a variety of wear debris particles. Goodman *et al.* reported a foreign body giant cell reaction and prosthetic loosening that generated elevated levels of PGE2 in rabbits (108). Spector *et al.* showed that macrophages produced elevated levels of PGE2 and IL-1 in a canine osteolytic model (109). These findings were also confirmed in rat models (110). Furthermore, new advances in *in vivo* imaging have served to confirm macrophage trafficking and have revealed the role of MCP-1 in macrophage recruitment in the presence of UHMWPE wear particles *in vivo* (111), as well as the role of transcription factor NF-κB in UHMWPE particle-induced osteolysis (112). The immunomodulatory role of the sphingosine-1-phosphate (S1P) system regulating the release of pro-inflammatory cytokines and T cell activation have been reported in a mouse collagen-induced arthritis model (113) suggesting a potential role in particle-induced osteolysis.

Interestingly, a paradoxical role of estrogens in mice has recently been proposed. While a classic bone protective function has been attributed to estrogens in humans, a contrary effect has been shown in mice, where estrogen deprivation is associated with a protective effect in a particle-induced osteolysis model (93). These findings support a pro-inflammatory and pro-osteolytic effect of estrogens in periprosthetic tissues in mice, probably mediated by estrogen receptors expressed by periprosthetic macrophages (93,114). Furthermore, an immunomodulatory effect of IL-4 on periprosthetic macrophages activated by UHMWPE particles has also been observed. IL-4 produced by activated macrophages seems to exert immunomodulatory activity through the polarization of macrophages from the pro-inflammatory sub-population (M1) to the anti-inflammatory (M2) phenotype (79,93).

The development of immunologically-compromised mouse models has served to sustain the concept of the involvement of the immune response in particle-induced osteolysis (53,70,115). Lymphocytes and macrophages are considered the main cellular targets in this process. Taki *et al.* reported a similar osteolytic response to polyethylene or Ti particles in a Pfp/Rag2 double knock-out calvaria model of lymphocyte-deficient mice (116). These results suggest that lymphocytes are not implicated in the osteolytic mechanism.

Consistent with these findings, Purdue *et al.* reported a similar capacity to develop granuloma and osteolysis under polymeric stimulus in lymphocyte-deficient mice (4). However, a lymphocytic infiltrate has been observed around metal-on-metal arthroplasties and this is correlated with poor clinical implant performance (4). Taken together, these results suggest that lymphocytes may be implicated in a metal-specific response, but not in a polymeric non-specific response. Finally, Ren *et al.* highlighted the key role of macrophages in the UHWMPE particle-response in nude mice, showing the systemic trafficking of reporter macrophages and localized osteolysis after polymeric particle stimulation (117). Despite these important advances, further studies in osteoimmunology are necessary to clarify their real importance.

Local osteoclastic bone resorption is influenced by different cytokines in *in vivo* models. Among these, TNF-α seems to play a main role since it directly stimulates osteoclast formation, differentiation and activity (95). However, the essential cytokine network proteins controlling the recruitment of functional osteoclasts in wear particle-induced osteolysis *in vivo* seem to be the proteins of the RANK/RANKL system (118). UHMWPE particles induce inflammation, but not osteoclastic bone resorption in $RANK^{-/-}$ mice (118). However, other routes for osteolysis activation have been reported. Yao *et al.* and Nakashima *et al.* unveiled the capacity of macrophages and fibroblasts activated by wear particles to directly initiate the resorption mediated by MMP-1, MMP-2 and MMP-9 (119,120).

The identification of relevant inflammatory and osteolytic markers in mice includes biomarkers that can be found in clinical and *in vitro* studies as well. Among those are the cells of the immune response, osteoprogenitor cells, pro-inflammatory (IL-1, IL-6, TNF-α, PGE2 and others) and pro-osteoclastic cytokines (RANK, RANKL, IL-1 and TNF-α), pro-osteolytic factors such as MMP-2 and MMP-9 (121) and neuropeptides (calcitonine and Calcitonin gene related peptide α-CGRP]) (122) or vascular signals (vascular endothelial growth factor [VEGF]) (123).

The air pouch model

Wooley *et al.* developed a model to study the cellular reaction and expression of cytokines after the introduction of metals (Co-Cr, Ti-6Al-4V) and polymeric biomaterials (UHMWPE and PMMA) within subcutaneous spaces previously created, named "air pouches" (124). Ren *et al.* modified this model by co-implanting bone sections from syngeneic mice and particles into the air pouches (105) (Figure 28). These studies showed macrophage infiltration and production of pro-inflammatory cytokines in the bone inside the air pouch, which then underwent resorption (105).

The air pouch model has served as an initial "proof of concept" in the targeting of anti-inflammatory or anti-resorptive events related to particle-induced osteolysis. However, this model fails with respect to the reproducibility of the normal anatomic condition, because the bone is implanted in an ectopic site without its usual physiological environment, including blood supply, vascular, nervous and hormone control. These factors may be key aspects in the development of particle-induced osteolysis, considering the role of vascular and nervous peptides and soluble factors (hormones, cytokines and growth factors) involved in the control of bone homeostasis.

The calvaria model

In the calvaria model, a 1×1 cm area of calvaria is exposed by a midline sagittal incision with careful conservation of the periosteum, and particles are then placed on this surface (125) (Figure 28). This model has served as an important tool for understanding the mechanisms involved in inflammatory bone resorption in a physiological bone site (126). Merkel *et al.* showed that Ti particles lead to inflammation, osteoclast formation and bone resorption and proposed a key role for TNF-α in periprosthetic osteolysis after blocking the action of TNF-α by deletion of genes encoding its receptors (p55TNF and p75TNF) (125,126). Other mediators such as IL-1 and IL-10, as well as cyclo-oxygenase (COX) 1, COX2, and PGE2, have been

studied with this model. The injection of IL-1 stimulated bone resorption, demonstrating the responsiveness of the calvaria model to this inflammatory mediator (127). The anti-inflammatory cytokine IL-10 has been shown to suppress wear debris-induced osteolysis (128). In the same vein, this model has been useful for proving the modulatory effect of IL-4 on the macrophage phenotype (129) in an innovative model of percutaneous injection of polyethylene particles on calvaria (130). Finally, COX2-deficient mice showed significantly less bone resorption induced by titanium particles than wild-type and $COX1^{-/-}$ mice (131). Recently, this model has been used to detect the presence of TLR-2 and TLR-4 in osteolytic zones induced by polyethylene (132). Otherwise, this model has served as proof of the concept for different therapeutic strategies in particle-induced osteolysis. Furthermore, an innovative and useful approach for this model has been reported, testing the reliability of the early diagnosis of bone loss after particle implantation by a nanopolymer (133).

In general, the main benefits of this model are the ability to test the host response in an orthotopic bone site, the possibility for splitting the calvarium and performing serial analyses, the rapidity of the development of osteolysis (about 7 days), the relatively low cost, the ability to screen a large number of experimental variables and the possibility for using small animal imaging to quantify bone loss. This model has made possible the use of transgenic strains in which the role of specific genes can be assessed for a better understanding of the pathophysiology and preclinical treatment of periprosthetic osteolysis. However, disadvantages are related to the fact that the calvarium consists of flat bones with membranous bone formation, rather than the endochondral ossification seen in long bones. Moreover, this model exhibits an acute (rather than chronic) effect and a lack of biomechanical factors related to osteolysis associated with wear debris, such as the presence of a load bearing implant, oscillatory fluid pressures and mechanical forces.

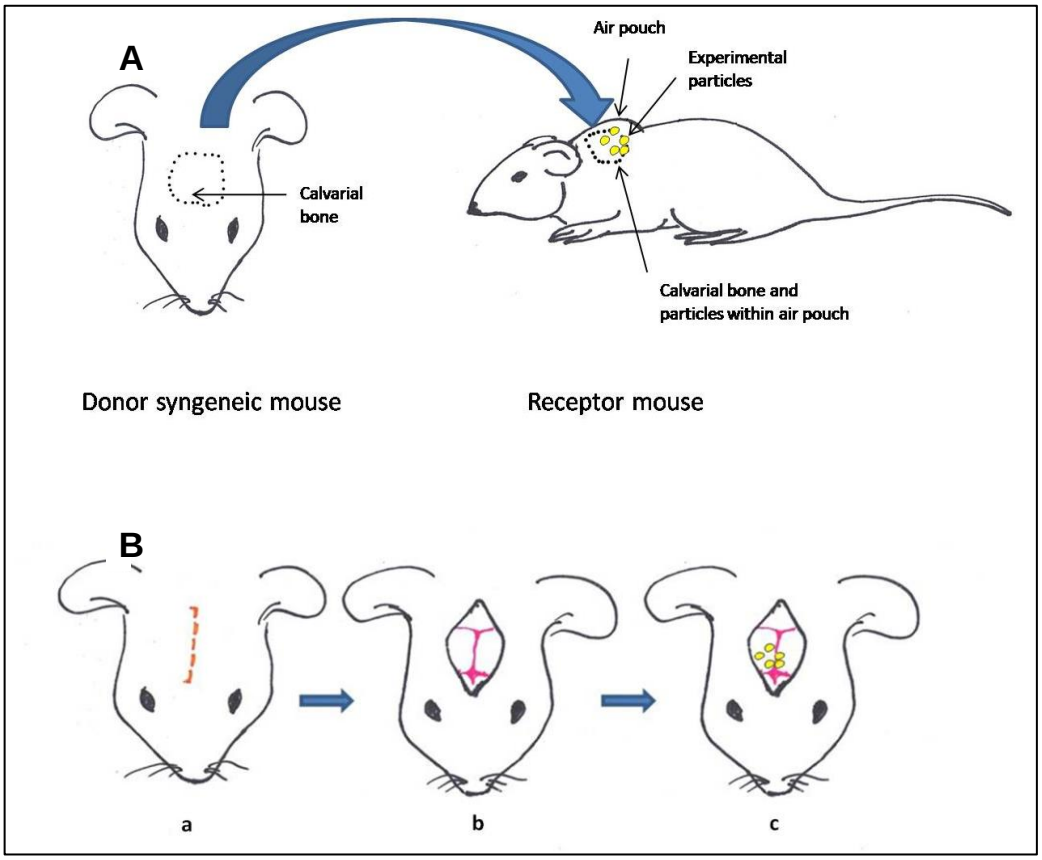

Figure 28. Air pouches (A) and calvaria (B) mouse model. (134)

Intramedullary implant models

A third generation of model was proposed by Warme (2004) and then modified and improved by Wooley *et al.* and Goodman *et al.* (13,106,135–137). All of these models coincide in a) the ability to analyze endochondral long bone behaviour in experimental conditions, b) the presence of intra-medullary load-bearing implants and c) the possibility for assessing the long-term effects of particles in the periprosthetic bone micro-environment. These models can be analyzed according to the anatomical site involved (femur or tibia) and the frequency of particle implantation:

The proximal tibia hemiarthroplasty model. The hemiarthroplasty model proposed by Yang in 2007 consists of a stainless steel or titanium rod inserted in an intra-medullar manner in the proximal tibia epiphysis (Figure 29). Mice receive intra-operative and later monthly infusions of titanium particles. This model corresponds to long-term knee implant failure (24 weeks) and makes it possible to characterize the biomechanical aspects such as the position of the implant, migration of the intra-medullary pin (by micro-computed tomography) as well as stability and traction resistance (pullout test). Furthermore, pathological

features can be studied, *e.g.* the effects of titanium particles on the expression of pro-inflammatory and osteoclastogenic cytokines (IL-1, TNF-α, IL-6 and RANKL) in periprosthetic tissue (106). Moreover, Shi *et al.* (137) described a significant infiltration of macrophages in the periprosthetic tissue accompanied by an increase in osteoclasts and Howship's lacunae and a decrease in new bone formation using this model. Early results from these experiments are promising and have confirmed that particles around the implants induce a pro-inflammatory response in periprosthetic tissues, and that the pro-inflammatory cytokines IL-1 and TNF-α are involved (106).

The distal femoral implant model with single implantation of particles. Proposed by Warme *et al.*, this model consists of the inclusion of an intra-medullary metallic load implant in the distal femoral epiphysis associated with an intra-operative single peri-implantation of particles (135) (Figure 29). Several authors describe the long-term effects (2, 10, 20 and 26 weeks) of a single dose of titanium (12,136) or UHMWPE particles (138). Using this model, IL-1 has been suggested as a modulator in the formation of the periprosthetic membrane (12). Furthermore, a single dose of UHMWPE particles showed a long term effect in up-regulating pro-inflammatory factors (IL-1, MCP-1, IL-6 and TNF-α) derived from mononuclear cells, suggesting that this mechanism may stabilize the chronic inflammatory state in periprosthetic tissues (138). However, this conclusion would seem unlikely since inflammation and formation of the membrane are likely to be required steps leading up to resorption.

The distal femoral implant with continuous intra-medullary infusion. Although distal femoral implants and tibia hemiarthroplasty with discontinuous or single implantation of particles have the advantage of being loaded implant models, they fail in providing a continuous release of particles of clinically relevant size, shape and volume. To remedy this, Goodman's group proposed another model in 2008 (13). Based on the *in vitro* and *ex vivo* validation of particle-release using an Alzet® pump (139,140), Ma *et al.* demonstrated that this model can ensure the constant presence of particles released from a subcutaneous osmotic pump in the femoral intra-medullary cavity, mimicking the human condition (13) (Figure 29). They successfully infused UHWMPE particles into the intra-medullary femoral cavity during 4 weeks. The model was characterized by micro-architectural and immunohistochemical analyses showing a reduction in bone volume. Ren *et al.*

suggested that macrophages are systemically recruited from the circulation and migrate to the implanted medullar cavity within 2 to 3 weeks (117). These cells may stimulate local osteolysis and up-regulate known bone-remodelling markers. An interruption of this migration is proposed as a potential therapeutic approach (117).

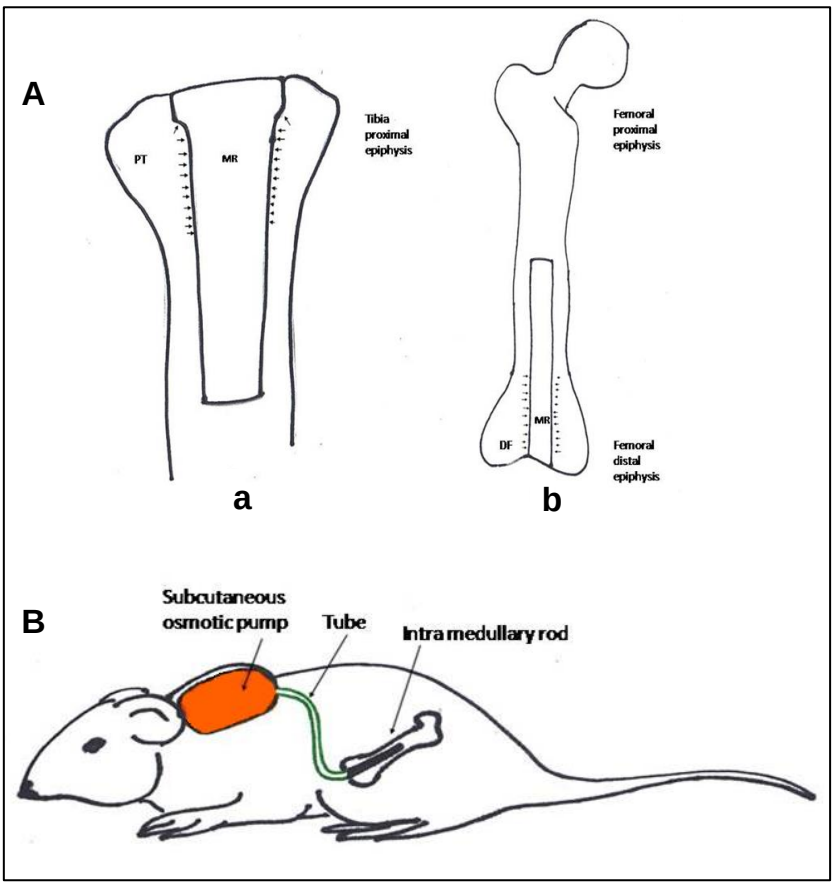

Figure 29.Intramedullary implant models. (134)

(A) Single implantation of particles in the proximal tibia hemiarthroplasty model (a) and in the distal femoral implant (b) and (B) continuous intra-medullary infusion in the distal femoral implant model

Certainly, intra-medullary implanted mouse models constitute a closer approach to the human situation than air pouch and calvaria models. However, the surgical manipulation of the epiphysis with the implant insertion in the carved channel may increase the risk of pathological fracture, giving a potential bias in the findings.

AIMS OF THE THESIS

Epidemiologic and registry studies were a good means of retrospectively resuming long-term behaviour in a large number of implanted patients and of identifying the risk or protective factors associated with the performance of the different implant alternatives. Regarding the behaviour of different bearing couples of a single brand THA obtained from the National Joint Registry for England and Wales, significantly higher rates of surgical revision were observed in: a) hard bearings (metal-on-metal and ceramic-on-ceramic) rather than metal-on-polyethylene, b) smaller femoral stems and c) obese patients (body mass index [BMI] ≥ 30) (141). Otherwise, Smith *et al*., report that the risk of surgical revision for metallic hemiarthroplasties (HRAs) increases with the smaller size femoral-head in patients of both sex, becoming comparable with the reference system (28 mm cemented metal-on-polyethylene stemmed THA). On the contrary, a gender difference was observed in implant survival: while large size femoral heads in men had a survival rate similar to that of the reference system, all kinds of femoral head HRAs in women showed poorer survival than the reference (142,143).

Clinical reports recognize osteolysis induced by wear debris as the main cause of aseptic failure leading to revision surgery (144). Currently, pro-inflammatory cytokines (tumour necrosis factor alpha [TNF-α], interleukin 1 [IL-1], interleukin 6 [IL-6], interleukin 12 [IL-12] and interleukin 23 [IL-23]), anti-inflammatory cytokines (interleukin 10 [IL-10]), pro-resorptive cytokines (receptor activator of nuclear factor κB [RANK] and receptor activator of nuclear factor κB ligand [RANKL]), anti-resorptive cytokines (osteoprotegerine [OPG] and IFN-γ), chemokines (MCP-1 and,MIP-1), PGE2, colony stimulating factors (M-CSF and granulocyte-macrophage colony-stimulating factor [GM-MSCF]), signalling sphingolipids (S1P), growth factors (platelet-derived growth factor alpha [PDGF-α], transformer growth factor alpha [TGF-α] and beta [TGF-β]), enzymes (ciclooxygenase-2 [COX-2] and matrix metalloproteinases [MMPs]), hormones, glucocorticoids and immune complex, have been described in the human response to wear debris (4,35,145). While preclinical studies have shown that targeting the osteoclasts (bisphosphonates) or cytokines involved in bone remodelling (blocking the pro-inflammatory or increasing the anti-inflammatory) results in significant inhibition of bone loss suggesting a good clinical response, the prospective clinical trials failed to confirm this hypothesis in the long-term (7). On the other hand, the inter-individual variability in implant survival after THA

has been associated with single nucleotide polymorphisms (SNPs) of proteins, receptors, intracellular mediators, pro-inflammatory cytokines and enzymes (146). Single-centre studies report that genes coding for stimulatory Gas subunit (GNAS1), a ubiquitously expressed cAMP-dependent G protein, TNF-238 A allele, TNF-α promoter transition, IL-6, MMP-1, MMP-2, TGF-β, OPG and mannose-binding lectin (MBL) were overexpressed in patients with aseptic loosening (146). These findings may facilitate the pre-operative identification of patients with a predisposition for periprosthetic osteolysis. In brief, despite the knowledge available concerning the symptomatic aspects and a potential genetic predisposition for implant loosening, there remains a lack of understanding of the natural history of the disease. Overall, the efficacy of new drugs or the performance of optimized biomaterials needs to be confirmed in further randomized clinical studies including longer follow-ups and relevant outcomes (7).

Preclinical study has been the most prolific strategy to deep in the understanding of the cell and molecular basis of particle-induced osteolysis and to test potential innovatives therapies. While multiple models have been developed, only air pouch and calvaria mouse models have been used regularly to perform therapeutic tests. Potential clinical applications are summarized Table 2, Table 3 and Table 4**.**

Author	Model	Therapeutic intervention	Strategy
Schwarz, 2000 [71]	Calvaria, Ti	Pentoxifylline (anti TNF-α) and alendronate.	TNF-α inhibition in activated macrophages and antiresorptive effect in mature osteoclasts
Childs, 2001 [90]	Calvaria, Ti	Etanercept	Osteoclast depletion via TNF-α blockade
Zhang, 2001 [74]	Calvaria, Ti	Celecoxib (Selective COX-2 inhibitor)	Blockade of cross talk with pro-inflammatory cytokines and Inhibition of prostaglandin production
Carmody, 2002 [73]	Calvaria, Ti	vIL-10 (AdvIL-10)	Antiinflammatory, inhibition of osteoclasdtogenesis and osteolysis via gene trasfer of IL-10
Childs, 2002 [91]	Calvaria, Ti	Recombinant RANK-Fc	Osteoclast depletion via RANK blockade (RANK-Fc)
Von Knoch, 2005 [92]	Calvaria, UHMWPE	Zoledronic acid (Zol) and Simvaststin	Antiresorptives via intra-cellular mevalonate pathway blockade in mature osteoclasts
Von Knoch, 2005 [93]	Calvaria, UHMWPE	Recombinant Fc-OPG	Osteoclastogenesis inhibition via exogenous OPG (OPG:Fc)
Zhang, 2007 [94]	Calvaria, PMMA/UHMWPE	Doxycycline (DOX)	Inhibition of osteoclastogenesis, pro apoptotic of mature osteoclasts and inhibition of MMP
Landgraeber, 2009 [95]	Calvaria, UHMWPE	Anti apoptotic	Macrophage and osteoblastic anti apoptosis
Kauther, 2011 [96]	Calvaria, UHMWPE	Calcitonin substitution	Inhibition of osteoclasts activity
Rao, 2012 [97]	Calvaria, UHMWPE	IL-4	Modulation of macrophage polarization (M1/M2)
Nich, 2013 [37]	Calvaria, UHMWPE	ERαKO or ER pan-antagonist	Macrophage response mediated by estrogen receptors (ER)
Kauther, 2013 [67]	Aged calvaria, UHMWPE	Neuropeptides such as Calcitonin/α-CGRP	RANKL-inhibition in aged cal-/cal- model
Yamanaka, 2013 [98]	Calvaria, PMMA	MAPK/JNK inhibitor and calcineurin/NFAT inhibitor cyclosporine-A	Blockade of JNK and NFAT pathways
Burton, 2013 [40]	Calvaria, PMMA	Caspase-1 deficient mice	Blockade of caspase-1 (effector of the NALP3 inflammasome)

Table 2. *In vivo* assays using calvaria model with clinical perspectives. (134)

Author	Model	Therapeutic intervention	Strategy
Yang S, 2002 [81] Yang SY, 2004 [82]	Air pouches, UHMWPE	IL-1Ra, viral IL-10	Blockade of IL-1 by gene therapy to prevent or retard the inflammatory response
Yang S, 2002 [83]	Air pouches, UHMWPE	Viruses encoding human OPG gene (rAAV-hOPG)	Inhibition of osteoclastogenesis by gene transfer targeting OPG
Ren, 2006 [84]	Air pouches, UHMWPE	Erythromycin	Reduction of cytokine production and osteoclast differentiation
Ren, 2007/Ren, 2011 [68,85]	Air pouches, UHMWPE	VEGF antibody and a VEGF receptor II inhibitor	Inhibition of inflammatory and osteoclastogenic response by blockade of specific monocyte/macrophage receptor
Zhang, 2011 [86]	Air pouches, Ti	Locally delivered lentivirus-mediated VEGF miRNA	VEGF gene silencing
Wang, 2012 [87]	Air pouches, UHMWPE	Local administration of adenovirus expressing siRNA-targeting BMPR-IB	Downregulating osteoclastogenesis through the RANKL-OPG pathway
Chen, 2012 [88]	Air pouches, Ti	Tetracycline	MMP-9 inhibition and downregulation of RANK/RANKL
Dai, 2012 [89]	Air pouches, metal	VEGF antibody (Bevacizumab)	Inhibition of inflammatory responses and osteolysis
Chen, 2012 [27]	Air pouches, Ti	p38 MAPK inhibitor	Downregulation of osteoclastogenesis

Table 3. ***In vivo*** **assays using air-pouches model. (134)**

Author	Model	Therapeutic intervention	Strategy
Yang, 2007	Proximal tibia hemiarthroplasty model /discontinous injection of Ti		Wear debris-induced prosthesis instability and osteolysis/feasibility of in vivo gene transfer
Shi, 2007	Proximal tibia hemiarthroplasty model /injection of PMMA		Macrophage infiltrate/osteoclasts/ inhibition of new bone formation
Warme, 2004	Distal femora model /single injection of Ti		Particle-induced intramedullary inflammation (IL-1/TNF-α)
Epstein, 2005	Distal femora model /single injection of Ti	IL-Irl-KO mice	IL-1 as an important modulator in the local inflammatory response
Epstein, 2005	Distal femora model /single injection of UHMWPE		Mononuclear cells perpetuate a chronic inflammatory response by expression of IL6/TNF-α/IL1b and MCP-1
Bragg, 2008	Distal femora model /single injection of Ti	IL-1R1KO mice	Multi-factorial role for IL-1 in the proinflammatory cascade
Ma, 2008	Distal femora model /continous infusion UHMWPE		Continuous infusion of particles to the murine bone-implant interface
Ren, 2011	Distal femora model /continous infusion UHMWPE		UHMWPE stimulate the systemic migration of remotely injected macrophages and local net bone resorption

Table 4. *In vivo* assays using intramedullary mouse models. (134)

Considering that epidemiological, registry, clinical and preclinical studies match in the inter-individual variability of implant survival after THAs, the lack of understanding of the full molecular basis of periprosthetic osteolysis and the need to develop new therapeutic approaches to transfer to clinical protocols, we propose a multilevel study to further the current knowledge of the biology of the periprosthetic niche including (Figure 30):

- Study 1: A human approach, to characterize the cellular profile of retrieved periprosthetic membranes.
- Study 2: The assessment of an innovative *in vivo* approach using the interference of the RNA (siRNA) technology targeting RANK in a mouse model of particle-induced osteolysis
- Study 3: An *in vitro* approach to describe the early interactions between the human macrophages and nanoparticles of polyethylene.

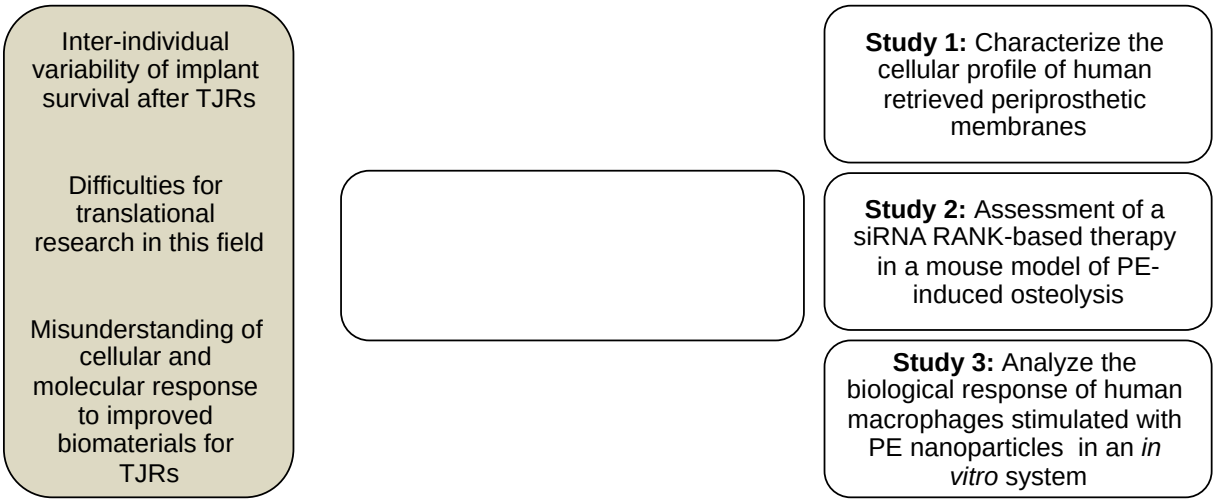

Figure 30. Rationale of the current study.

MATERIAL AND METHODS

STUDY 1

This descriptive clinico-histologic study was carried out with the approval of the ethic committee of University Hospital of Nantes and the Faculty of Medicine of University of Nantes.

Tissue collection samples

Synovium were collected during primary total joint replacements from seven patients and used as a control group. Fourth female and three male, average ages of 67.7±10.2 years old, all with a diagnosis of hip or knee osteoarthritis (OA) composed this group. Periprosthetic pseudomembranes were collected during revision joint replacements from seven patients, fourth female and three male, average age of 69.1±14.8 years old with clinico-radiographic and microbiological evidences of aseptic osteolysis around cotylo-femoral components, for total hip arthroplasty (THA), or femoro-tibial, for total knee arthroplasty (TKA) implants and with a mean of implant survival of 112.1±59.8 months. All revised patients received a metal-on-polyethylene total joint replacement.

Histology and immunohistochemistry

Harvested synovium and pseudomembranes were fixed in 4% buffered formaldehyde and then decalcified with 4.13% EDTA and 0.2% paraformaldehyde in phosphate buffered saline (PBS) for 96 hrs. using the KOS microwave histostation (Milestone, Kalamazoo, MI, http://www.milestonemed.com). After that, the samples were embedding in paraffin, 10 slides (3-μm-thick sections) were prepared from each sample. All slides were primarily stained with Haematoxylin & Eosin (H&E) to detect their cellularity. Tartrate-resistant acid phosphatase (TRAP) staining was performed to identify osteoclast-like cells in retrieved tissues by 1-hour incubation in a 1 mg/mL naphthol AS-TR phosphate, 60 mmol/L N,Ndimethylformamide, 100 mmol/L sodium tartrate, and 1 mg/ mL Fast red TR salt solution (all from Sigma Chemical Co.) and counterstained with haematoxylin. Primary anti-human CD68, CD3, CD4, CD8, CD117 monoclonal antibodies (Abcam, Cambridge, MA, http://www.abcam.com) were used for immunodetection of human macrophages, T cells and

it sub-populations (pan detection of T cells, human T helper/inducer cells – cross reacts with monocyte/macrophage and human T cytotoxic/suppressor cells), B cells and mast cells, respectively.

Histological images were acquired by the digital slide scanner NanoZoomer 2.0-RS (Hamamatsu, Japan) and then exported as a 10X field by viewing software NDP.view2 (Hamamatsu, Japan).

STUDY 2

siRNAs

All siRNAs were ordered from Eurogentec (Angers, France) with 3' overhanging dTdT and with annealed sense and reverse strands. Three primer sequence sense strands: 5'-GUGGAAAUAAGGAGUCCUC-3', 5'-CAGUAACUCCACGUUCAUC-3', and 5'-CUUCAAGGGUGACAUCAUCGU-3' were designed to target *Homo sapiens RANK* mRNA (NM_003839) at start positions 811, 1622 and 1661 and named *RANK*-811, -1622, and -1661 siRNA respectively. The antisense strands of those three designed *RANK* siRNAs also present perfect complementarity with *Mus musculus Rank* mRNA (NM_009399.2) at start positions 804, 1576 and 1616, respectively Furthermore, a siRNA duplex (sense strand 5'-UUCUCCGAACGUGUCACGU-3') which did not show significant homology with any mouse mRNA sequence according to BLAST database searches, was used as a negative control and designated as Ct-siRNA. A previously validated siRNA (*LucF*-siRNA sense strand 5'-CUUACGCUGAGUACUUCGA-3') was used *in vivo* as an innocuous siRNA (147).

While the three sequences of *RANK*-directed siRNAs were assessed in RANK-expressing human cells (HEK 293 RANK (+)), only two of them (siRNA *RANK*-811 and -1661 siRNA) were selected for assessment in murine cells (RAW) based on their efficacy in decreasing the RANK signal.

Cells

RANK-expressing HEK 293 cells

Human Embryonic Kidney 293 (HEK 293) cells which over expressed stably the human Receptor Activator of Nuclear factor κ B (RANK; official name Tumour Necrosis Factor Receptor Superfamily, Member 11a) (148), were cultured in Dulbecco/Vogt modified Eagle's minimal essential medium (DMEM) (Lonza, Switzerland) supplemented with 10% foetal calf serum (FCS) (Lonza, Switzerland).

RAW 264.7 and pre-osteoclast murine cells

Murine RAW 264.7 monocytic cells (American Type Culture Collection, Promochem, Molsheim, France) were differentiated into pre-osteoclasts as previously described (149). Briefly, they were cultured in phenol red-free α-MEM (Invitrogen, Eragny, France) supplemented with 10% FCS (Perbio, Erembodegem, Belgium) and 1% non-essential amino acids (Invitrogen). To induce pre-osteoclast formation, RAW 264.7 cells were cultured for 5 days in the presence of 100 ng/mL of human RANKL (R&D Sytem, UK). All experiments were performed in triplicate at least three times.

Particles of polyethylene

Pure polyethylene (PE) particles (Ceridust 3610™, Clariant, Gersthofen, Germany) were purchased. Particle morphology was assessed by surface-electronic-microscopy (SEM) (Jeol, model 6400F). Particle size and distribution were determined by 5 consecutive measures in a Coulter Counter ™ (Beckman Coulter Inc, US) with a mean size of 7.23 μm and with a distribution of d10=1.15, d25 = 3.94, d50 = 7.14, d75 = 10.28 and d90 = 13.05 (Figure 31). To eliminate endotoxins, the particles were washed in ethanol and then dried (114) and then aliquoted in singles and sterile eppendorf vials for manipulation in the surgical room.

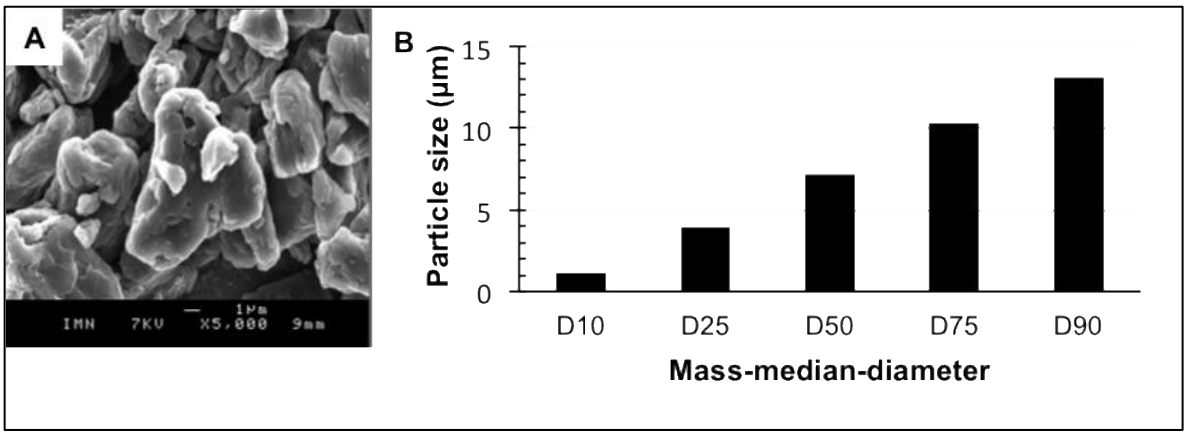

Figure 31. PE particle morphology by SEM (A) and size distribution by DLS (B).

siRNA transfection with INTERFERin™

All siRNAs were transfected using *Opti-MEM®* (Invitrogen, Eragny, France) and 2 µL of INTERFERin™ per well (Ozyme, Saint Quentin Yvelines, France) in triplicate. RANK-expressing HEK 293 cells (30,000 cells per well, in 24-well plates) and RAW 264.7 monocytic cells (45,000 cells per well in 96-well plates) were transfected with 1 nM siRNA or 10 nM siRNA, respectively.

Detection of RANK by flow cytometry.

Following siRNA transfection, RANK-expressing HEK 293 cells were incubated sequentially with 0.1 mg/mL anti-human RANK/TNFRSF11A antibody targeting human RANK (R&D Systems, UK) and a secondary fluorescent antibody (antibody Alexa Fluor488-rabbit anti-goat A11078). Fluoresence at cell surface was analyzed by flow cytometry (FC500 Beckman Coulter, Inc. Brea, CA, US). Flow cytometry results are expressed as a % of RANK inhibition with 0% corresponding to the median fluorescence intensity of cells transfected with Ct-siRNA. Nonspecific fluorescence was adjusted using isotype control (Rabbit IgG Control, R&D Systems).

Assessment of *Rank* expression by quantitative real time PCR (RT-PCR)

Total RNA was extracted from RAW 264.7 cells 48 h after siRNA transfection using NucleoSpin RNA II (Mechevey-Nagel). The first strand of complementary DNA was synthesized at 37 °C for 1 h from 5 µg of total RNA in a 50 µl mix containing RT buffer, 0.5 µg of random primers, 0.5 mM dNTP mix, 20 U RNaseOUT and 400 U murine moloney leukaemia virus-reverse transcriptase (all from Invitrogen). The real-time PCR contained 10 ng reverse-transcribed total RNA, 300 nM forward and reverse primers and 5 µl 2 × SYBR green buffer (Bio-Rad, Marnes la Coquette, France) in a final volume of 10 µl. Polymerase chain reactions were carried out in triplicate from several RNA extractions, in 96-well plates using the Chromo4 System (Bio-Rad). The listed oligonucleotides were used to amplify the *Mus musculus* receptor activator of nuclear factor kappa-B (*Rank*, 5'-TGCAGCTCTTCCATGACACTG-3' and 5'-CAGCCACTACTACCACAGAGATG-3'), Cytochrome c-1 (*Cyc 1*, 5'-TGTGCTACACGGAGGAAGAA-3' and 5'-CATCATCATTAGGGCCATCC-3') and 60S ribosomal protein L19 (*Rpl19*, 5'-TCGTTGCCGGAAAAACAC-3' and 5'-AGGTCACCTTCTCAGGCATC-3') were used as housekeeping genes. Analyses were performed using the Vandesompele method (150).

Implantation of polyethylene particles in mouse calvaria

The mice (Elevages Janvier, Le Genest Saint Isle, France) were housed in pathogen-free conditions at the Experimental Therapy Unit (Faculty of Medicine, Nantes) in accordance with the institutional guidelines of the French Ethical Committee (CEEA PdL 06 ethical committee, authorization number: 1280.01) and under the supervision of the authorized investigators. All surgical procedures were also performed according to international ethical guidelines for animal care (authorization number: 2012-198). C57BL/6 male mice (Janvier, Le Genest-Saint Isle, France) aged 10 weeks were surgically implanted using the adapted mouse calvaria model (151) with 20 mg of dried PE particles. Briefly, under general anaesthesia (2-3 % Isofluorane in 100 % oxygen at flow rate of 1L/min), a 0.5 x 0.5-cm² area of periosteum was exposed by a middle sagittal incision in previously shaved and aseptic head skin (Betadine, France). The dried polyethylene powder was uniformly spread over the periosteum with a sterile surgical spoon. The surgical approach was carefully closed with 5-0

non-absorbable sutures. A subcutaneous injection of Buprenorphine (Buprecar 0,1 mg/Kg) was performed after the surgical procedure (Palier 1 protocol). One group of mice underwent the same surgical procedure but without the polyethylene particle implantation (Sham group).

Zoledronic acid treatment

Zoledronic acid (ZOL) kindly provided by Novartis Pharma (Basel, Switzerland) was prepared in PBS and injected s.c. at 50 µg/kg twice a week (day 2 and day 5 after particle implantation).

Local injections of formulated siRNAs

For *in vivo* injections, siRNAs were premixed with an equal quantity of a Deoxyribonucleic acid (DNA) cargo in 150 m*M* NaCl as described (152) and mixed with an equivalent volume of cationic liposome DMAPAP/DOPE at a ratio of 6 nmol of cationic lipid per microgram of nucleic acid as previously described (153). The lipoplexes were formed at room temperature for at least 30 minutes. Injections of 100 µl of lipoplexes containing 2.5, 5 or 10 µg of siRNAs were used *in vivo*.

PE particle-implanted mice were randomly divided into four groups which received injections of either 2.5 µg *LucF*-siRNA (PE – 2.5 µg *LucF*-siRNA group n=3) or 2.5 or 5 or 10 µg of *RANK*-811 siRNA. Groups of mice were respectively named PE 2.5 µg *RANK*-811 siRNA, (n=3), PE -5 µg *RANK*-811 siRNA (n=5) and PE - 10 µg *RANK*-811 siRNA group (n=5). Each mouse in the PE particle-implanted groups received one injection of the designated lipoplex solutions in the calvaria site at days 1, 4 and 7 after surgery, while mice in the Sham group (no particles, n=3) received 100 µL of saline solution in the same site. The injection site was determined intermediate to the full cephalocaudal length of the sutured surgical approach and 2 mm laterally to the right of it. The inclination of the 26-gauge needle was oblique pointing medially until a soft contact with the bone surface. A continuous and slow pressure injection, to avoid the reflow of injected solution, was performed. All animals were sacrificed by cervical dislocation following isofluorane anaesthesia at day 9 after the surgical

procedure. We extended our standard protocol (7 days) by 2 days in order to achieve the administration of three doses of the proposed therapy.

Micro-computed tomography assessment

The analysis of bone microarchitecture was performed using the high-resolution X-ray micro-computed tomography (micro-CT) system for small-animal imaging SkyScan-1076 (SkyScan, Kontich, Belgium). Analyses were performed at necropsy (day 9). All calvarias were scanned using the same parameters (pixel size 9 μm, 50 kV, 0.5-mm Al filter and 0.8 degree of rotation step). Three-dimensional reconstructions and quantification of bone parameters were performed in a cylindrical volume of interest (VOI) (ratio 0.5 mm, height 1.143 mm, VOI=0.89 mm^3; Figure 2A) using ANT and CTvol software (Skyscan). The assessment of the bone volume density was measured by the fraction of the VOI (i.e. the Total Volume TV) that is occupied by mineralized bone (Bone Volume BV) (BV/TV) expressed as a percentage (%).

Histology analysis

Harvested calvarias were fixed in 4% buffered formaldehyde and decalcified with 4.13% EDTA and 0.2% paraformaldehyde in phosphate buffered saline (PBS) for 96 hrs. using the KOS microwave histostation (Milestone, Kalamazoo, MI, http://www.milestonemed.com) before embedding in paraffin. 6 coronal 4-mm-thick sections were obtained from 3 levels of middle calvaria (each one separated by 300 μm). All slides were stained for tartrate-resistant acid phosphatase (TRAP) to identify osteoclasts by 1-hour incubation in a 1 mg/mL naphthol AS-TR phosphate, 60 mmol/L N,Ndimethylformamide, 100 mmol/L sodium tartrate, and 1 mg/ mL Fast red TR salt solution (all from Sigma Chemical Co.) and counterstained with haematoxylin.

For immunohistochemistry detection, histological sections were treated with citrate buffer at pH=6 for antigen unmasking and with goat serum 5%, BSA 1% diluted in 1XTBST pH=7.6 for blocking of non-antibody-specific sites. The immunostaining for F4-80 was realized using rabbit monoclonal anti-F4-80

antibody (1/150 overnight at 4°C; Abcam, Cambridge, MA, http://www.abcam.com) and goat anti-rabbit biotinylated (Dako, Glostrup, Denmark) as a secondary antibody. The immunostaining for Alkaline Phosphatase (ALP) was performed using rabbit monoclonal anti-ALP antibody and goat anti-rabbit biotinylated (Dako, Glostrup, Denmark) as a secondary antibody. Following incubation with a Streptavidine/Peroxidase kit (1/200, Dako), antibody detection was made with a liquid DAB-Substrate Chromogen system (Dako).

Histological images were acquired by the digital slide scanner NanoZoomer 2.0-RS (Hamamatsu, Japan) and then exported as a 10X field by viewing software NDP.view2 (Hamamatsu, Japan). The region of interest (ROI) corresponds to a rectangular area (1.7 mm^2, 1.74 mm wide and 980 mm high, 1913 x 582 pixels) centred in the middle sagittal suture and comprising the full thickness of the parietal bones. Quantification of relative osteoclast surface (TRAP-positive area) in the defined ROI was assessed by a macro of ImageJ software (NIH, Bethesda, MD).

RNA extraction from calvaria tissue and quantitative real-time polymerase chain reaction

Total RNA was extracted from implanted calvaria in one sample of each group using homogenizer Ika Ultra-Thurax T 25 (Janke and Kunkel) and TRIzol reagent (Invitrogen). Synthesis of the first strand of complementary DNA and the polymerase chain reaction were carried out in triplicate using the same protocol as described above. The listed oligonucleotides were used to amplify *Mus musculus* Cathepsin K (*CathK*, 5'-GGAGGCGGCTATATGACCA-3' and 5'-GATCTATGTCCTCACCGAACG-3'), Interleukin-1 (*Il-1b*, 5'-TTGACGGACCCCAAAAGAT-3' and 5'-GATGTGCTGCTGCGAGATT-3'), Interleukin-6 (*Il-6,* 5'-TAGTCCTTCCTACCCCAATTTCC-3' and 5'-TTGGTCCTTAGCCACTCCTTC-3') and Tumour necrosis factor alpha (*Tnf-α*, 5'-GGGTGATCGGTCCCCAAAGGGA-3' and 5'-TGGTTTGCTACGACGTGGGCTAC-3').

Statistical analysis

All analyses were performed using GraphPad InStat Version 3.02 software (GraphPad Software, La Jolla, CA, USA). *In vitro* experimentation and micro-CT results were analyzed with the unpaired non-parametric Mann-Whitney U test using two-tailed p values. The histological results were analyzed with ANOVA and an unpaired two-tailed t-test. Results are given as mean ± SD, considering a p value < 0.05.

STUDY 3

Cell culture

The $CD14^+$ human monocyte/macrophage were purified from peripheral blood mononuclear cells (PBMCs) obtained from healthy donors (EFS, Etablissement Français du Sang) by positive selection using the MACS system (Miltenyi Biotech, Bergisch Gladbach, Germany) and then seeded in 6-well plate and cultured for 3 days in 2 ml of minimum essential medium alpha (MEM-α, Lonza, Belgium) supplemented with 10% Fetal Bovine Serum (FBS, Ozyme, France) and 1% of antibiotics (conditioned media). Adherent monocytes were differentiated into M0 macrophages by culturing them for 7 days in conditioned media supplemented with 25 ng/mL of human macrophage colony stimulating factor (hM-CSF, R&D systems, Minneapolis, MN, USA),

Fluorescent nanoparticles of polyethylene:

Fluorescent nanoparticles of polyethylene (fPE) were synthetized according the protocol of Faucon A., *et al*. (2013) (154) and kindly provided by Pr. Elena Ishow (CEISAM, Faculty of Science, University of Nantes).

Name:

(E)-icosyl 3-(4-(bis(4'-(tert-butyl)-[1,1'-biphenyl]-4-yl)amino)phenyl)-2-cyanoacrylate (X)

Chemical structure (Figure 32**):**

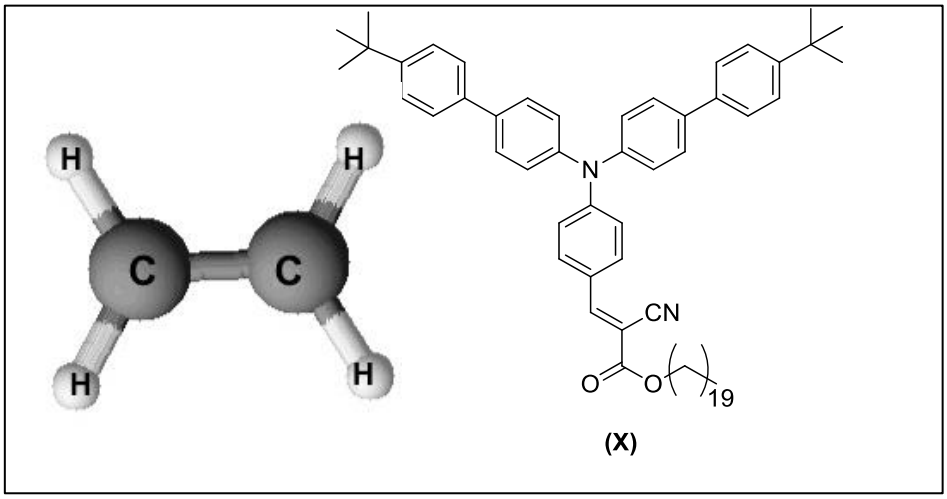

Figure 32. Chemical structure of fluorescent PE (fPE).

Transmission electron microscopy (TEM):

Nanoparticle morphology was investigated by transmission electron microscopy (TEM, Hitachi HF2000-FEG (100 kV)). Solutions of nanoparticles were deposited onto holey carbon-coated copper grids (300 mesh).

Size distribution by dynamic light scattering (DLS):

The hydrodynamic diameter and dispersivity of the nanoparticles were determined by dynamic light scattering (DLS) by means of a nanoparticle size analyzer Zetasizer Nano ZS ZEN 3600 (Malvern Instruments) equipped with a 4 mW He-Ne laser, operating at 633 nm, and a photomultiplier detector collecting backscattered light at an angle of 175°. Measurements were carried out at 20 °C on aqueous solutions of NPs. For each sample, intensity measurements were carried out in a multi-acquisition mode implying automatically adjusted correlograms, and averaged measurements on 3 acquisitions. Nanoparticle mean sizes and distribution widths were obtained by fitting each correlogram with a Cumulants algorithm.

Spectral measurement of nanoparticles:

UV-visible absorption spectra were recorded using a Varian Model Cary 5E spectrophotometer, using an integrating sphere DRA 2500. Emission spectra were obtained using Jobin-Yvon. Inc spectrofluorimeter (Fluorolog 2).

Fixed-cell imaging semi-quantification - flow cytometry

The detection of mean fluorescence intensity (MFI) of polyethylene nanoparticles uptake by $CD14^+$ monocyte/macrophages using flow cytometer (FC500 Beckman Coulter, Inc. Brea, CA, US) after fixation (Paraformaldehide 4%). The results were expressed as the relative MFI fold-change, corresponding to the ratio: MFI of the polyethylene fluorescent nanoparticles uptake by the macrophages of each condition / MFI of the control isotype.

Live-cell imaging - Confocal microscopy

The acquisitions were performed using a confocal microscopy (Nikon A1 RSi, Nikon, France). Images were obtained from the fluorescence emitted by nanoparticles (ex: 488 nm; em: 580 nm), AlexaFluor546 and Hoechst 33258. The analysis of images was performed using the software Fiji (NIH, USA).

Time-lapse video microscopy:

Cells were cultured in 8 well culture plate (u-Slide 8 well, Ibidi, Germany) and then transferred and maintained into the culture chamber of confocal microscope (Leica DMI 6000B) by 72 hrs. The images were acquired using light background and fluorescence by 40x lens.

RESULTS

STUDY 1: Cellular profilling of human retrieved pseudomembranes

Introduction

Periprosthetic osteolysis has been associated with the accumulation of wear debris at the implant-bone interface, leading to implant loosening (3). Analysis of the periprosthetic membranes removed during revision surgery has led to the characterisation of the particulate and cellular infiltrate observed once the disease is initiated (155). Histological analysis has documented a fibrous granulomatous reaction that is consistent with a foreign-body inflammatory response (35). Many studies have confirmed the predominance of wear debris from UHMWPE in periprosthetic tissues (156,157). (157)(156) Cellular profiling has highlighted the role played by macrophages in the inflammatory response (79). Cytokine profiling has confirmed the elevated expression of IL-1, IL-6 and TNF-α, RANK, RANK ligand (RANKL) and osteoprotegerin (OPG) in human pseudomembranes (155,158,159). Furthermore, the involvement of specific matrix MMPs and tissue-inhibitors of MMPs (TIMPs), which are endogenous inhibitors of MMP activity, have been associated with aseptic loosening (121,160,161).

Moreover, the periprosthetic niche may include heterogeneous cell types, including fibroblasts, stromal cells, mast cells and endothelial cells, which could play a little-known role in the mechanisms of periprosthetic osteolysis (162). Beginning a few years ago, a new component was proposed as a relevant actor in the periprosthetic niche: the immune system (9). The balance among pro- and anti-inflammatory chemokines, cytokines and cells modulated the local microenvironment, leading to catabolic or anabolic features (79). Additionally, the persistence of a chronic inflammatory state can activate the acquired immune response mediated by the specific molecular interactions between macrophages and lymphocytes (9). Characterising the inflammatory cells in human retrieved pseudomembranes constitutes an interesting opportunity to deepen our knowledge of the pathophysiology of periprosthetic osteolysis to propose potential targets for preventive therapy. The aim of this study is to describe the inflammatory cell types present in human retrieved tissues from patients who have undergone surgical revision of loosened prostheses due to periprosthetic osteolysis.

Results

Clinical data

Epidemiological data of patients underwent a revision of implants are summarized in Table 5. Imaging features of selected patients are presented in Figure 33, Figure 34 and Figure 35.

Age	Sex	Survival (months)	Implant revised
48	M	94	Hip revised with chrome cobalt head and polyethylene cup
66	M	90	Hip revised for metal on polyethylene wear
72	F	29	Hip revised with modular system and ceramic on ceramic couple
49	F	162	Hip revised for metal on polyethylene wear
83	M	96	Hip revised by pseudotumour associated with loose of metal on metal couple
75	F	216	Hip revised with loose of femoral cemented stem
84	F	98	Knee revised with loose of femoro-tibial components

Table 5. Information of patients who received a revision surgery.

Figure 33. Right metal-on-polyethylene THA revised by acetabular and femoral osteolysis (black arrows) after 94 months of survival in 48-years-old male patient.

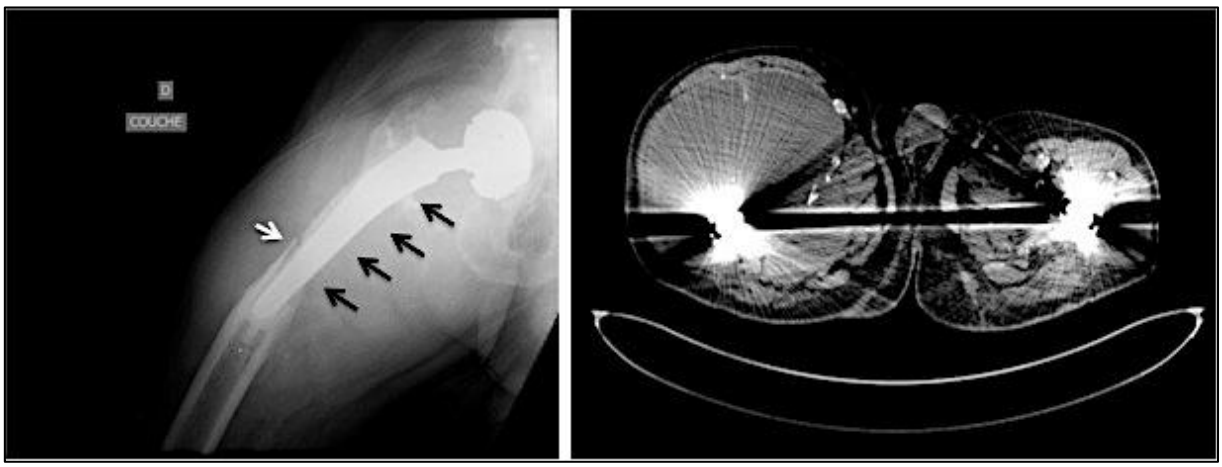

Figure 34. Antero-posterior view of X-Ray (left side) and axial view of computed tomography (right side) of right metal-on-metal THA revised by pseudotumour with extensive osteolysis in medial cortical femora (black arrows) after 96 months of survival in 83-year-old male patient. Pathological fracture was observed in lateral cortical femora (white arrow).

Figure 35. Left metal-on-polyethylene TKA revised by tibial osteolysis (black arrows) after 98 months of survival in 84-years-old female patient.

Immunohistochemistry

Histological examination showed that the pseudomembranes exhibit a peripheral fibrous layer surrounding a central stroma compared with primary synovium (Figure 36). A highly vascularised and cell-infiltrated fibrous tissue comprised this central stroma. Multinucleated giant cells engulfing polyethylene (PE) and metallic particles constituted the predominant cell infiltrate. Lymphoid cells were recognised in perivascular sites throughout the pseudomembranes. T ($CD3^+$, $CD4^+$ and $CD8^+$) and B ($CD20^+$) cells were identified forming a perivascular syncytium. Mast cells ($CD117^+$) were also detected scattered in some of the pseudomembranes. In the case of a pseudotumour lesion associated with a pair of metal-on-metal implants, we observed an extensive necrosis of the pseudomembrane with few recognisable cellular elements (Figure 37).

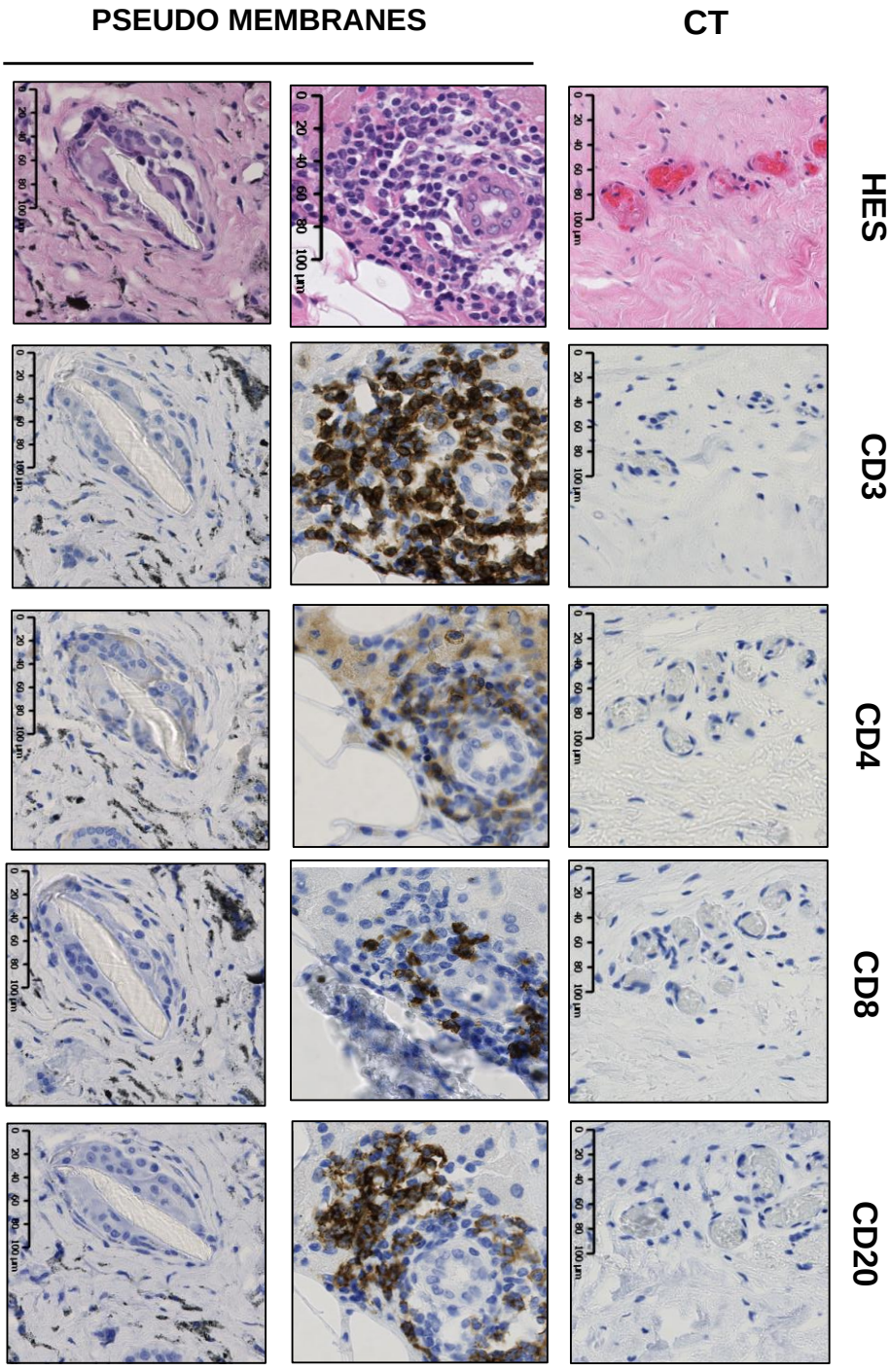

Figure 36. Selected images of cell response in retrieved pseudomembranes from loosed implants compared with controls.

A remarkably perivascular lymphocytic infiltrate was observed (middle). Furthermore, a less dense lymphocytic infiltrate was observed surrounding the multinucleated phagocytic cells (bottom). Some samples exhibited mast cells scattered in the fibrous tissue (CD117 - middle).

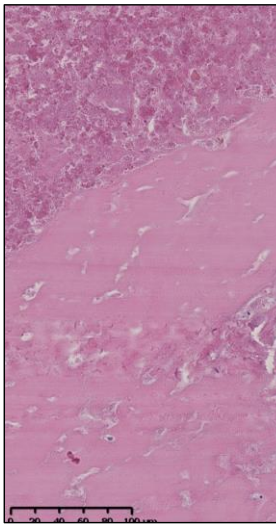

Figure 37. Extensive necrosis was observed in one sample of a retrieved pseudomembrane.

A heterogeneous particulate morphology was observed in the retrieved pseudomembranes compared with the control tissues. This particulate was

composed of PE exclusively in the knee-revised tissue or both PE and metallic debris in the remaining samples. Moreover, the PE debris exhibited a wide range of sizes and shapes. While some of the particles were 100 to 200 μm, others were approximately 6 μm or less (Figure 38A and Figure 38B). Concerning the shape of the PE particulates, some were polyhedral, and others were elongated. In contrast, the metallic particulate exhibited a more homogenous morphology (in size and rounded shape) than did the former, and they were scattered in the fibrous stroma and or localised to the adventitia of blood vessels (Figure 38D).

Multinucleated giants cells had engulfed the PE and metallic particulate (Figure 38C). These cells were recognised as a $CD68^{+}$ and $TRAP^{-}$ (Figure 39), confirming their monocyte/macrophage phenotype. Moreover, we observed T lymphocytes ($CD3^{+}$, $CD4^{+}$ and $CD8^{+}$) in close contact with multinucleated monocyte/macrophage cells surrounding large PE particles (Figure 39). However, lymphocytes were not observed around the multinucleated cells that phagocytised metallic debris.

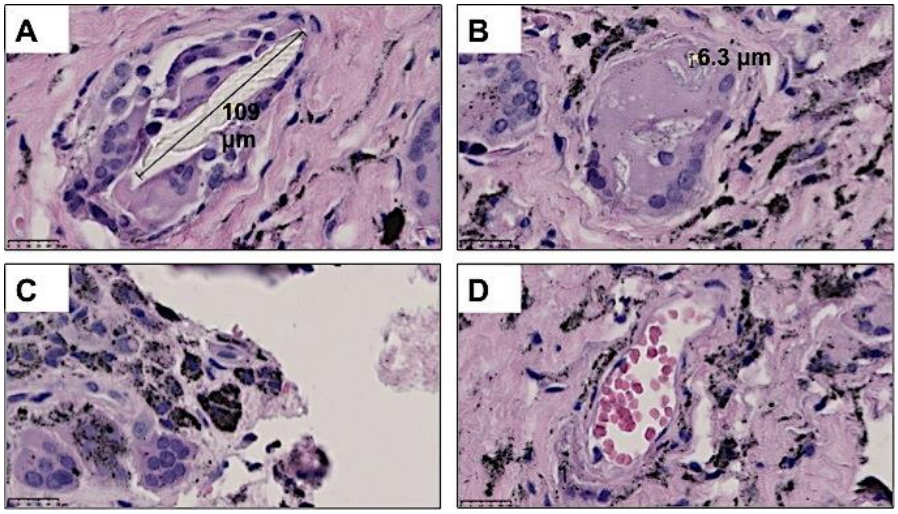

Figure 38. Wear debris in periprosthetic tissues.

Multinucleated cells phagocytize large (A) and small PE (B) particles. Metallic debris were internalized by multinuclear cells (C) and they are also detected in perivascular site, surrounding the adventitia (D). Haematoxylin & Eosin staining.

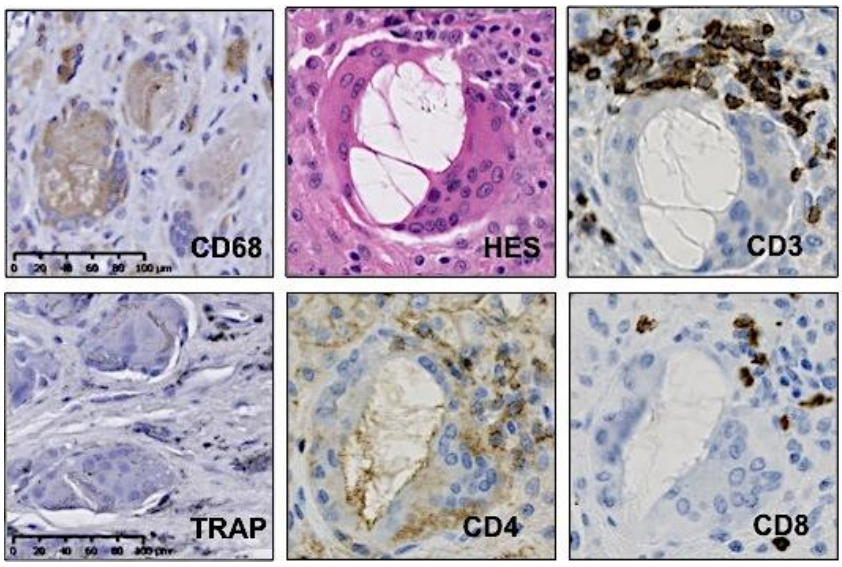

Figure 39. Immunohistochemistry and TRAP staining in multinucleated and T cells.

$CD68^+$ and $TRAP^-$ monocyte/macrophage cells surround a particle of polyethylene. T lymphocytes were recognized in close contact with them.

Discussion

The mean implant survival time of 112.1±59.8 months is a short lifespan for a prosthetic device. However, this finding could be explained by the interindividual variability: first, some data come from patients who had undergone a second surgical revision, and moreover, the cause of their revision was variable (i.e., pseudotumour with associated fracture, dislocation of the prosthetic femoral head or pain). Furthermore, the morphological heterogeneity (nature, size and shape) of the wear particulates observed in retrieved pseudomembranes could be explained by their origin in the prosthetic device. Thus, while PE (and metallic) particles were released from the articular (bearing surfaces), metallic particles could be released from the non-articular components by impingement (e.g.: cam-effect) in dislocated prosthesis (163) or fretting phenomenon in modular designs (e.g., the head-neck or neck-body tapers) (164).

Our biological findings confirm the cause-and-effect relationship between the release of wear particulates from loosed orthopaedic implants and the triggering of the cellular response in human periprosthetic tissues. In our study, this relationship was well characterised by the detection of an extensive number of cell-surface antigens demonstrating two main cell populations: myeloid (monocytes/macrophages and mast cells using anti-CD68 and anti-CD117 antibodies, respectively) and lymphoid cells (T lymphocytes using anti-CD3, -4, -8 antibodies and B lymphocytes using anti-CD20 monoclonal antibodies).

The immunodetection of $CD68^+$ and $TRAP^-$ multinucleated cells engulfing large and/or small particles of PE and/or metal, classically named "foreign body cells", confirms the involvement of the first-line cell effectors of innate immunity: macrophages. These cells are classically described as phagocytes that protect the host from external pathogens (165). The presence of monocytes/macrophages in periprosthetic pseudomembranes has also been confirmed by other studies (79,166).

Another important role attributed to the monocyte/macrophages lineage is to act as an antigen presenting cell (APC), linking the non-specific inflammatory response to specific adaptive immune responses (165). In our study, we showed morphological evidence of the close contact between $CD68^+$ monocytes/macrophages and T cells, suggesting cross-talk between the lineages. Indeed, we recognised stronger staining for CD3 and CD4 than for CD8, suggesting the activation of a T helper-mediated response over a cytotoxic response. In a similar manner, we recognised a perivascular lymphocytic infiltrate with more $CD3^+$ and $CD4^+$ cells than $CD8^+$ cells. Interestingly, strong immunostaining for B perivascular cells was also observed at the same site. These findings suggest the triggering of an adaptive cellular and humoral response triggered by macrophages engulfing large PE particles. However, the presence of B cells in periprosthetic tissues has been reported in pseudotumuoral and lymphocyte-dominated lesions associated with metal-on-metal implants (46,167) without any associated PE debris. Further studies will be necessary to confirm these findings.

A role for mast cells in the inflammatory response to particulate debris has also been proposed (167). However, we did not observe specific activation of mast cells in the retrieved tissues. We instead observed exceptional immunostaining for CD117 without a specific location.

The extensive necrosis observed in a pseudomembrane retrieved from a patient with a hip pseudotumour associated with a metal-on-metal implant pair is in agreement with other reports, suggesting an adverse reaction to metal debris (ARMD) (168) or possibly an aseptic lymphocyte-dominated vasculitis-associated lesion (ALVAL) (46,167). However, we could not identify any of the cell types due to the necrosis in the retrieved tissues.

STUDY 2: Local administration of siRNA-targeting *RANK* in a polyethylene–particle-induced osteolysis mouse model

Introduction

During the periprosthetic osteolysis process, wear particles released from bearing surfaces result in a local inflammatory response challenged by proinflammatory macrophages (M1) which produce IL-1 and TNF-α (169). The largest particles (>20 µm) act as damage-associated molecular pattern molecules (DAMPs) and are sensed by macrophagic Toll-Like-Receptors (TLRs) (88,170), leading to the activation of an innate inflammatory immune response like a 'foreign body reaction" (9,115). The smallest particles (<20 µm), however, and released ions are uptaken, activating the NALP3 inflammasome leading to the adaptive immune response (9,94,115,170). Both immune pathways activate the transcription factors (NF-KB and NF-IL6), increasing synthesis of the Receptor Activator of Nuclear factor Kappa-B Ligand (RANKL) and pro-

inflammatory cytokines (IL-1β, IL-6, TNF-α) (90,162). These cytokines have been recognized as the main molecules responsible for maintaining the periprosthetic inflammatory environment and for increased osteoclastogenesis (162).

Inhibition of the RANKL-RANK axis was an efficient therapeutic approach for decreasing osteoclast differentiation/activation. The anti-osteoclastogenic drug-based therapies such as bisphosphonates and the anti-RANKL monoclonal antibody (Denosumab™), have evolved from experimental models of osteolytic bone diseases (171–174) to clinical uses (175–177). Furthermore, new inhibitors, such as the small peptide designed to target a specific region of the RANK membrane (148), are currently in pre-clinical development. The prevention of bone loss by blocking the RANK-RANKL axis was reported in two experimental models of particle-induced osteolysis using: a) a recombinant protein of RANK (RANK:Fc) (178) and b) zoledronic acid (179). Despite these encouraging pre-clinical results, they have still not been transferred to clinical use (180).

Small interference ribonucleic acid (siRNA) regulates the synthesis of proteins by means of a specific gene silencing mechanism (181–183). The use of siRNA-based therapy is a specific and biocompatible approach that has led to significant advances in cancer, age-related macular degeneration and viral diseases (184). Two key aspects need to be considered in this strategy: the identification of clinically relevant targets and the use of efficient delivery vectors. Targeting of the key RANKL-RANK axis was first reported *in vitro* in murine cells by Wang *et al* (2010 and 2012) and Ma *et al* (2012) with effective inhibition of *Rank* expression, osteoclast differentiation and osteolysis using *Rank*-siRNAs and *Rank*-shRNAs, respectively, which target the mouse *Rank* transcript (185–187). The systemic delivery of therapeutic siRNAs using biological and synthetic vectors was reported in bone disease-experimental models, including: bone-metastatic cancer (targeting Luciferase and delivered by atelocollagen) (188) and rheumatoid arthritis (targeting *Tnf-α*, *Il-1β*, *Il-6* and *Il-18* and delivered by the cationic liposome DMAPAP/DOPE (189,190). In the field of particle-induced osteolysis, siRNA targeting of the type I bone morphogenetic protein receptor transcript (*BMPR-IB*) systemically delivered by a recombinant adenoviral vector (191) was reported. However, the nature of aseptic loosening by wear debris seems to be a confined condition that requires a local intervention. In this sense, the local delivery of siRNA is a logical strategy for bypassing the anatomical barriers and optimizing its biotransformation during its

trafficking. In this sense, the local delivery of *Rankl*-siRNA by the cationic liposome DMAPAP/DOPE in a murine model of osteosarcoma (147) and a local lentiviral delivery of *β110*-siRNA, targeting a subunit of the PI3K/AKT pathway in a particle-induced osteolysis model, have been reported (192). Despite the current state of the art in experimental therapy of particle-osteolysis with siRNA-based technology, there are no scientific reports targeting the key RANKL-RANK axis by local delivery using a synthetic vector in an *in vivo* model. We hypothesized that siRNA targeting *RANK*, locally delivered by a cationic liposome might be an effective approach for locally inhibiting osteoclastogenesis *in vivo*. The aim of our study was to unveil the therapeutic effect of three doses of siRNA targeting both human *RANK* and mouse *Rank* transcripts (*RANK*-811 siRNA) in a mouse model of polyethylene (PE) particle-induced osteolysis.

Results

Design and *in vitro* validation of formulated siRNAs targeting *RANK*

We first evaluated the *in vitro* gene-silencing efficacy of three custom designed siRNAs whose sense strand presented a perfect identity with both human and mouse receptor activators of nuclear factor kappa-B transcripts (designated *RANK* and *Rank,* respectively). These siRNAs were transfected into HEK 293 cells which over-express *RANK* (RANK-HEK cells) and in a murine RAW 264.7 cell line which expresses *Rank* constitutively. *RANK* expression was assessed at the proteomic level by flow cytometry (Figure 40A), while *Rank* expression was measured at the transcriptional level by qRT-PCR (Figure 40C). Of the three siRNA, *RANK*-811 *and* -1661 siRNAs significantly decreased the fluorescence intensity due to RANK detection at the membrane of the RANK-HEK cells compared to cells transfected with control siRNA (Figure 40A et Figure 40B; 48.7 % and 38 % RANK inhibition, respectively). In contrast, the transfection of *RANK*-1622 siRNAs in RANK-HEK cells did not decrease RANK detection. The two efficient siRNAs were transfected in murine pre-osteoclasts derived from RAW 264.7 cells and both *RANK*-811 *and* -1661 siRNAs made possible a significant decrease of *Rank* mRNA relative expression compared to the control siRNA (Figure 40C).

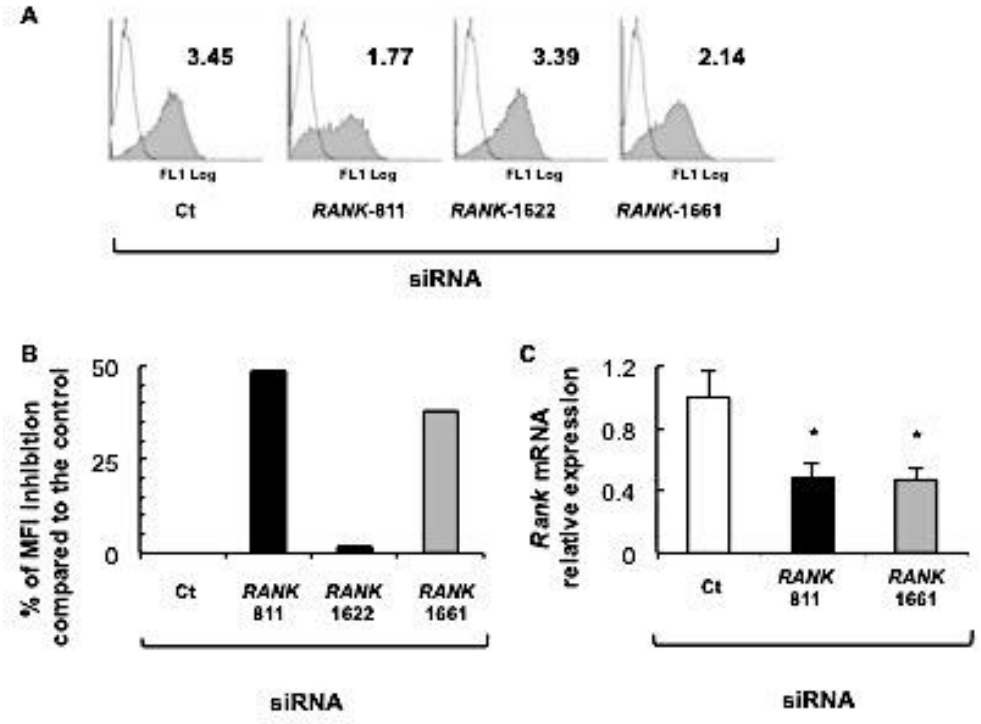

Figure 40. *In vitro* validation of siRNAs against *RANK* expression in *RANK*-expressing 293 HEK cells and in murine RAW 264.7 cells.

(A) RANK detection was analyzed by flow cytometry (shaded peaks) at the *RANK*-expressing 293 HEK cell surface following transfection with indicated siRNAs. Median fluorescence intensity is indicated. Fluorescence of the isotype control is shown as unshaded peaks. (**B**) Flow cytometry results are expressed as a % of RANK inhibition with 0% corresponding to the median fluorescence intensity of cells transfected with Ct-siRNA. (**C**) *Rank* mRNA relative expression in murine RAW cell line following transfection of *RANK*-811 and -1661 siRNAs. Significant decrease compared to cells transfected with control siRNAs is indicated (*p<0.05).

Mouse model of inflammation and osteolysis induced by wear particles

In our modified mouse model of wear-induced osteolysis, PE particles induced bone lesions that were detected by micro-CT at day 7 (PE-NaCl group in Figure 41A). The quantification of bone parameters revealed a significant decrease in calvaria bone volume density for the PE-implanted group compared to the non-implanted group (Sham group) (Figure 41C). Histological analysis demonstrated the presence of PE particles (black arrow in zoomed window of Figure 41B) and osteoclast activation ($TRAP^+$ cells in PE-NaCl group in Figure 41B) after 7 days of particle implantation. As well as the osteolytic changes, the increased inflammatory signs around the implanted particles were greater at day 7 than those detected at days 14 and 21 (data not shown), as shown by the thickness of the inflammatory membrane in PE-implanted group compared to Sham

group (black asterisks in left and right panels in Figure 41B above). Similarly, at day 14 and even more at day 21, reparative changes had led to a significant decrease in $TRAP^+$ cells and to a thinning of the inflammatory layer over PE-implanted calvaria (data not shown). These findings were concordant with other studies (132,193).

As expected and demonstrating the relevance of this model, a treatment with two doses of 50 µg/kg of zoledronic acid (ZOL), one of the most potent nitrogen bisphosphonates, markedly reduced the bone loss induced by PE particles (group PE-ZOL in Figure 41A, Figure 41B). This inhibitory effect was associated with a strong and significant increases in calvaria bone volume density (group PE-ZOL in Figure 41A and Figure 41C) and decrease in $TRAP^+$ osteoclast numbers at day 7 (group PE-ZOL and histogram in Figure 41B).

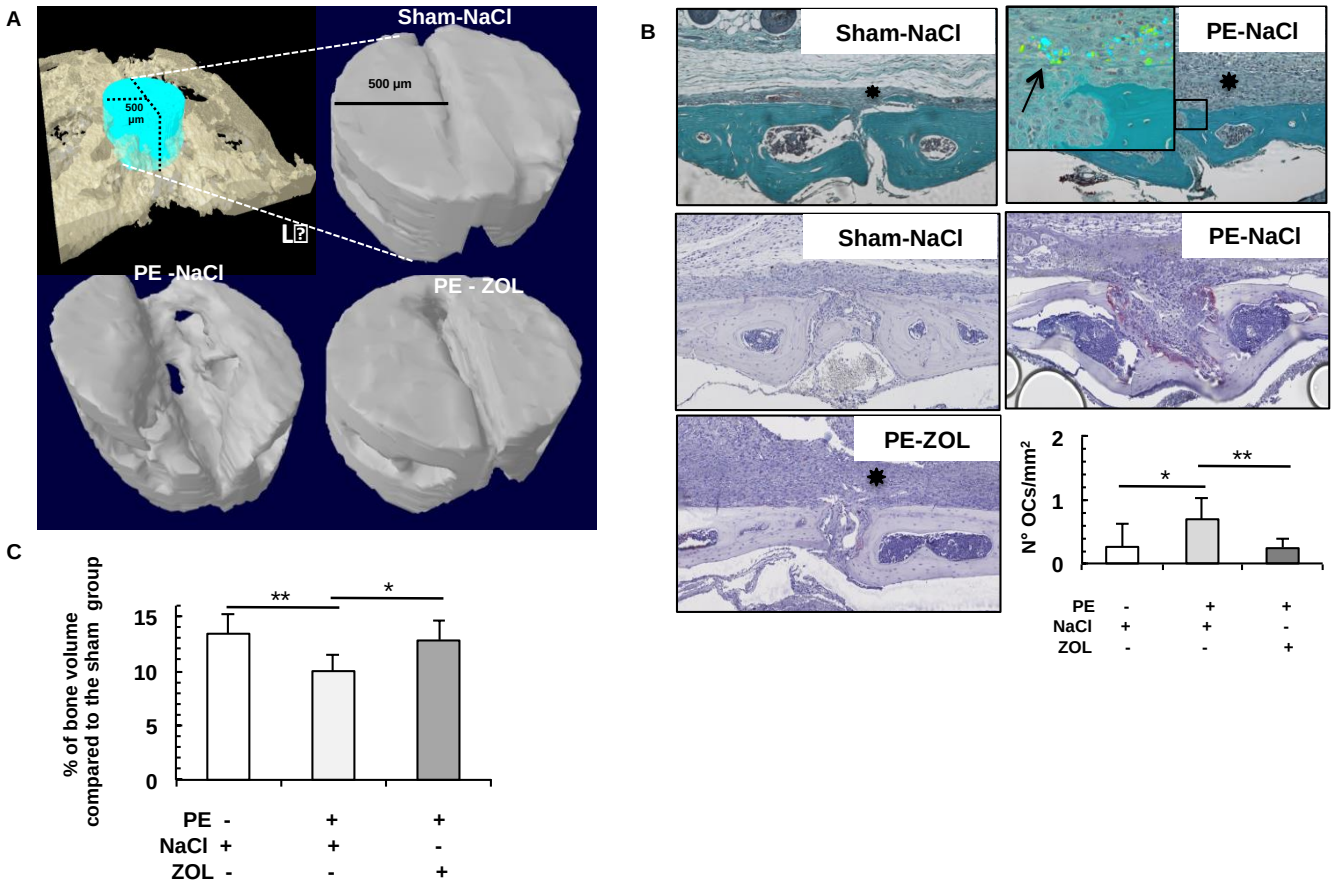

Figure 41. Zoledronic acid showed a protective effect on the PE particle - induced osteolysis *in vivo*.

Implanted PE particles over the periosteum of calvaria for 7 days induced middle sagittal osteolysis and thickening of the inflammatory membrane (black arrow polarized light in zoomed window and black asterisk in group PE-NaCl of **B** above) compared with the Sham group (black asterisk). 50 µg/Kg of **Z**oledronic acid decreased the number of activated osteoclasts (group PE-ZOL and histogram of **B**), preventing the bone loss assessed by micro-CT (group PE-ZOL of **A**) and maintaining the inflammatory changes (asterisk in group PE-ZOL of **B**). VOI, volume of interest; PE, polyethylene; ZOL, zoledronic acid; BV/TV, bone volume/tissue volume. (**p*<0.05) and (***p*<0.01).

RANK-811 siRNA prevents the bone loss induced by implanted PE particles by inhibiting osteoclastogenesis and osteoclast activation

In the light of the unveiled potent *in vitro* efficacy of *RANK-811* siRNA on human and murine *RANK/Rank* expression, we next assessed the effect of this siRNA *in vivo* at day 9 in our modified mouse model of PE-induced osteolysis as inflammatory and osteolytic lesions were maximal at this time. Micro-computed tomography of the calvaria showed that the inner cortical of the calvaria was preserved from osteolysis in the groups treated with 5 or 10 µg of *RANK*-811 siRNAs, while bone loss of the inner cortical was observed for groups treated with control siRNAs or with 2.5 µg of *RANK*-811 siRNAs (Figure 42A). However,

bone quantification revealed a significant reduction in the bone loss only for the PE-implanted group that received 10 µg of *RANK*-811 siRNAs per injection (Figure 42B) ($p<0.05$). Indeed a similar bone loss induced by PE particles was observed for the mouse groups that were treated with 2.5 µg of *LucF*-siRNAs, or with 2.5 µg and 5 µg of *RANK*-811 siRNAs compared to the Sham group (Figure 42B).

Interestingly, TRAP staining on histological sections revealed that *RANK*-811 siRNAs induced dose-dependent inhibitory activity on osteoclast differentiation. The TRAP-positive cell area was effectively reduced by 70% for 2.5 µg *RANK*-811 siRNA injections ($p<0.01$) and by 90% for 5 and 10 µg *RANK-811* siRNA injections ($p<0.001$) (Figure 43B). Moreover, the osteoclasts detected in the groups injected with 5 or 10 µg of RANK-811 siRNAs seem to be smaller than those of the group injected with 2.5 µg *LucF*- or *RANK*-811 siRNAs (Figure 43A).

The inhibitory effect of *RANK*-811 siRNAs on osteoclastogenesis and osteoclast activity was also suggested by the down expression of *Rank* (Right panel in Figure 43B middle). In addition to the inhibition of osteoclastogenesis, *RANK*-811 siRNAs also decreased *Cathepsin K* expression (Right panel in Figure 43B below), suggesting inhibition of the osteoclast activity. Overall, these data demonstrated that *RANK*-811 siRNA represents an effective candidate for the treatment of wear debris-associated osteolysis.

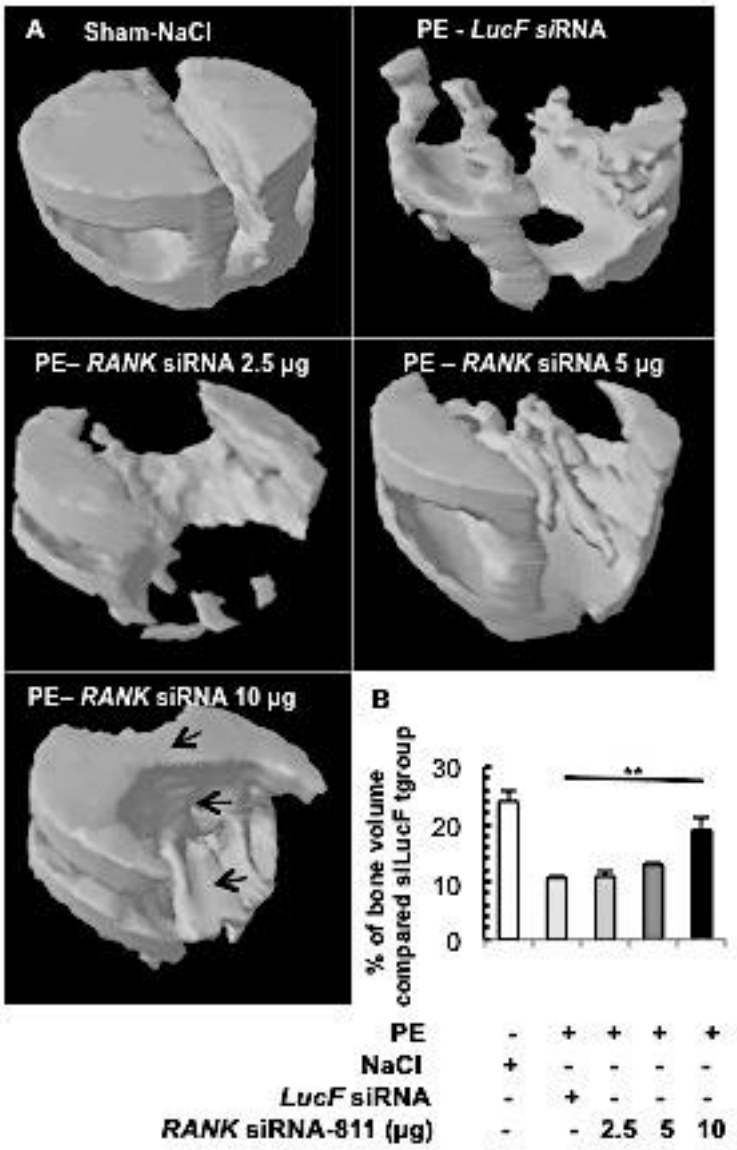

Figure 42. *RANK* siRNA-811 exhibits a significant protective effect against PE particle-induced osteolysis *in vivo.*

PE particles were implanted or not (Sham-NaCl) over the periosteum of calvaria for 9 days. Increasing doses (2.5, 5 and 10 µg) of *RANK* siRNA-811 were injected locally and bone loss intensity was followed compared to the control *LucF* siRNA. PE particles induced osteolysis and the efficacy of *RANK* siRNA-811 was followed qualitatively by micro-CT scan (**A**) and quantitatively determined by the measure of the BV/TV (**B**). Bone preserved areas were recognized in spongy bone as well as in external and inner corticals (black arrows). PE, polyethylene; BV/TV, bone volume/tissue volume. (*p<0.05).

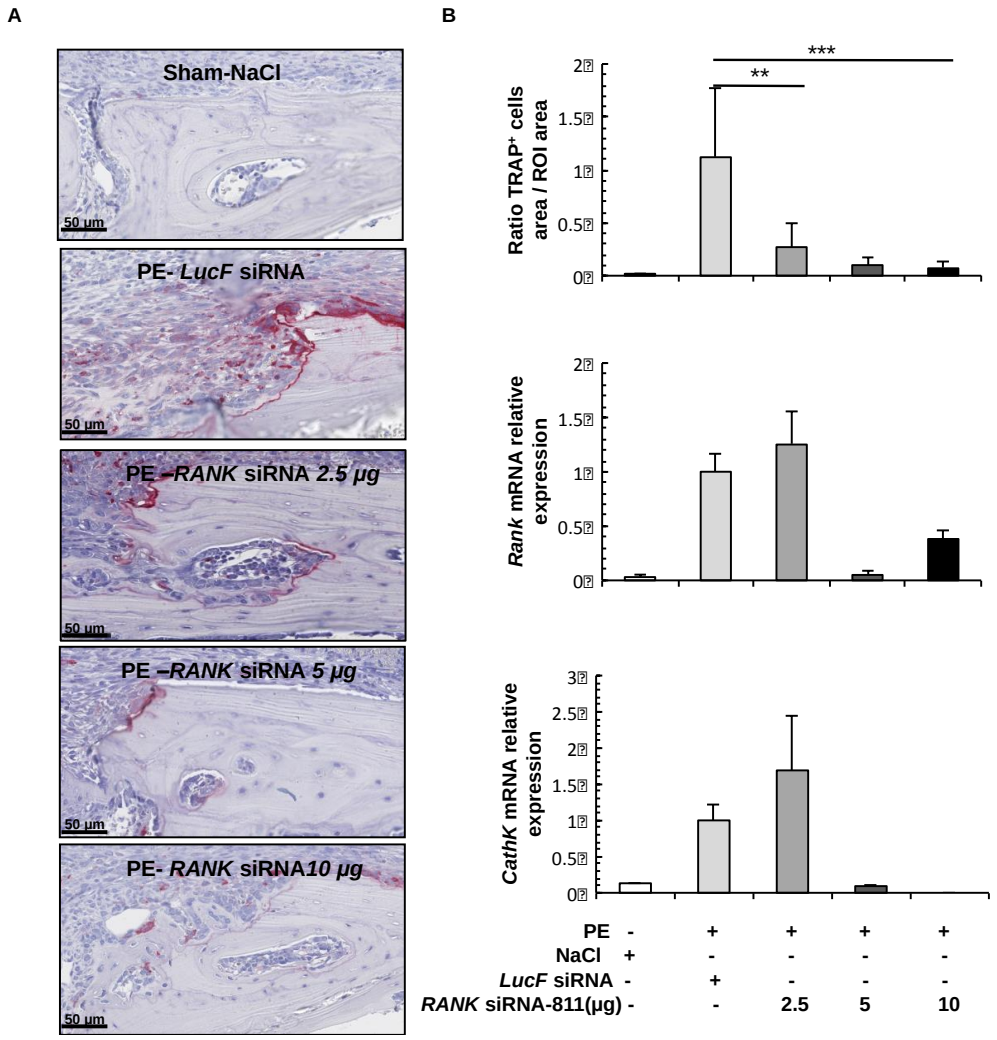

Figure 43.*RANK* siRNA-811 inhibits *in vivo* the number of osteoclasts in a dose dependent manner.

PE particles were implanted or not (Sham-NaCl) over the periosteum site of calvaria for 9 days. Increasing doses (2.5, 5 and 10 µg) of *RANK* siRNA-811 were injected locally and bone loss intensity was followed compared to the control *LucF* siRNA. Osteoclasts were detected by TRAP staining (**A**) and their number was quantified by the $TRAP^+$ area/ROI area ratio (**B above**). *Rank* (**B middle**) and *cathepsin K* (**B below**) expression was determined by qRT-PCR from calvaria tissue explants compared to the *LucF* siRNA. PE, polyethylene; ROI: Region of Interest; qRT-PCR, quantitative *reverse transcriptase PCR;* (**p<0.01); (***p*<0.001).

Local treatment with the formulated siRNA induces an anabolic bone response characterized by the total renewal of osteoblastic cell lineage

PE-implanted mice exhibit a strong osteonecrotic and osteolytic lesions compared with non-implanted mice (Sham group). In this study we confirmed the presence of numerous empty lacunae, without osteocytes inside in the external cortex of the calvaria of PE-implanted mice (Figure 44A, zoomed window, above), suggesting osteocyte death. On the contrary, we observed osteocytes in the cavities in the inner cortex of the

calvaria of all groups (Figure 44A, zoomed window, bottom). Moreover, we were surprised to recognize osteoformative changes characterized by the formation of new trabeculas in the PE implanted and siRNA-treated mice, suggesting a reparative response (Figure 44A and Figure 44B). We also detected an increase in alkaline phosphatase (Figure 44A, zoomed window, bottom) and osterix (Figure 44B) immunostaining in the area of interest in mice injected with *RANK* 811-siRNA compared with the Sham group.

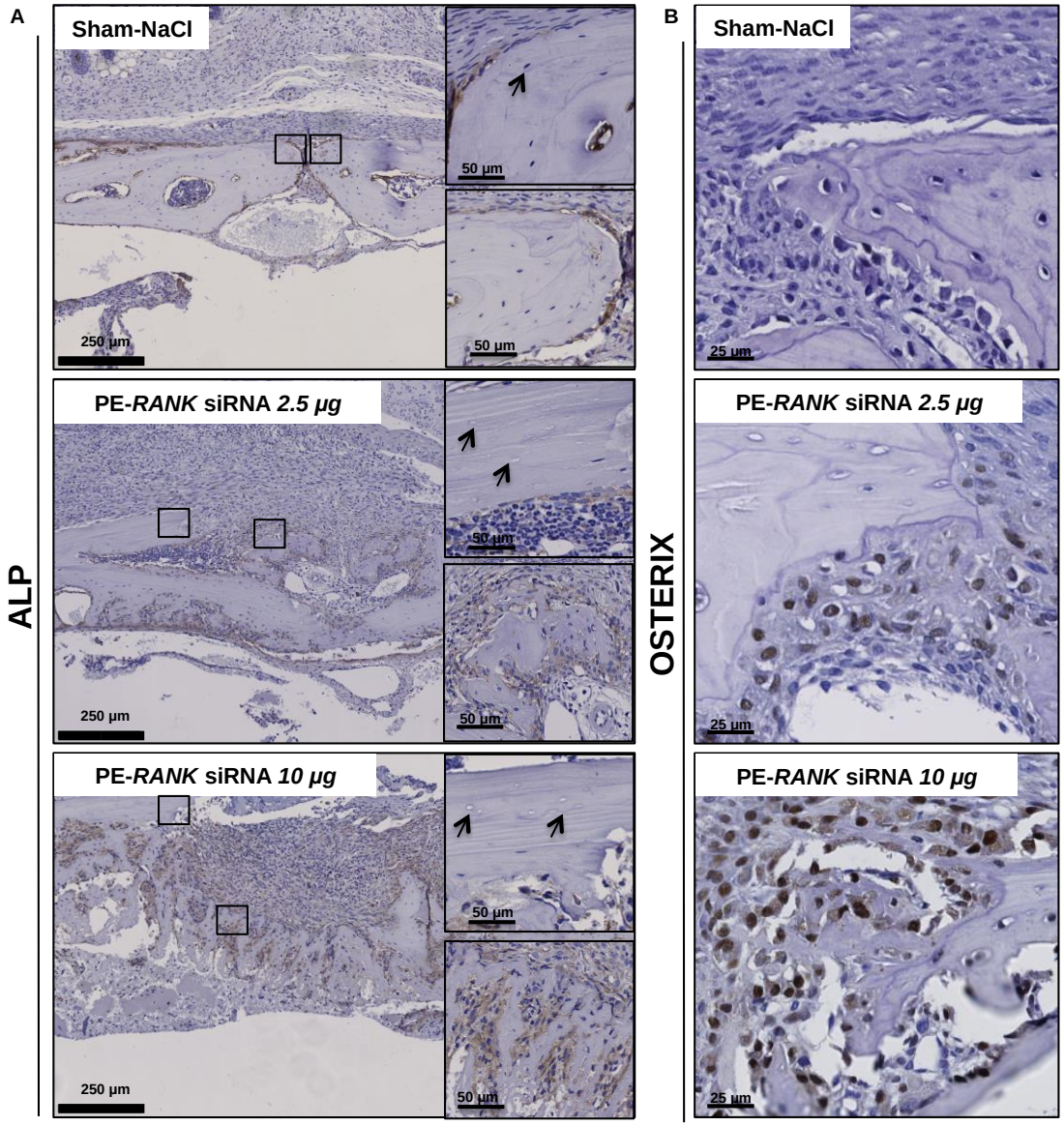

Figure 44.*RANK* siRNA-811 induces the renewal of osteoblastic cell lineage after osteolytic/osteonecrotic stimulus induced by PE.

PE particles were implanted or not (Sham-NaCl) over the periosteum of calvaria for 9 days. Increasing doses (2.5; 5 and 10 µg) of *RANK* siRNA-811 were injected locally and bone formation was followed compared to the Sham group. ALP (A) and Osterix (B) immunostaining was used to detect mature osteoblasts and pre-osteoblasts, respectively. Empty lacunaes were recognized in external cortical of calvaria (black arrows in A, zoomed window, above). PE, polyethylene; ALP, alkaline phosphatase.

RANK-811 siRNA reduced the inflammatory environment without depletion of macrophages

Because it is admitted that wear debris induces an inflammatory reaction (79,94), we assessed the consequence of a *Rank* blockade on the inflammatory process. Histological analysis showed that the implantation of PE particles resulted in a reaction characterized by the thickening of an inflammatory membrane more invaded by cells compared with the non-implanted group. Of these infiltrating cells, $F4/80^{+}$ macrophages were detected either in the Sham group (loosely distributed in the subcutaneous connective tissue) as well as in the implanted groups (highly localized within the inflammatory membrane and surrounding the implanted particles) (Figure 45A). Similarly, we observed the proinflammatory effect of PE particles by the increased expression of proinflammatory cytokines genes (*Tnf-α*, *Il-6* and *Il-1β*) from the PE-*LucF*-siRNA group compared with the Sham-NaCl group Figure 45B). We observed that the injections of 2.5 µg *RANK*-811 siRNAs decreased *Tnf-α* expression and slightly increased the expression of *Il-1β* compared to the *LucF* siRNA injections. In contrast, the injections of 5 and 10 µg of *RANK*-811 siRNAs decreased the expression of *Tnf-α, Il-6 and Il-1β* (Figure 45B). Interestingly and despite the down-regulation of proinflammatory genes associated with the injection of the three doses of *RANK*-811 siRNA, they did not suppress the infiltration of macrophages (Figure 45A).

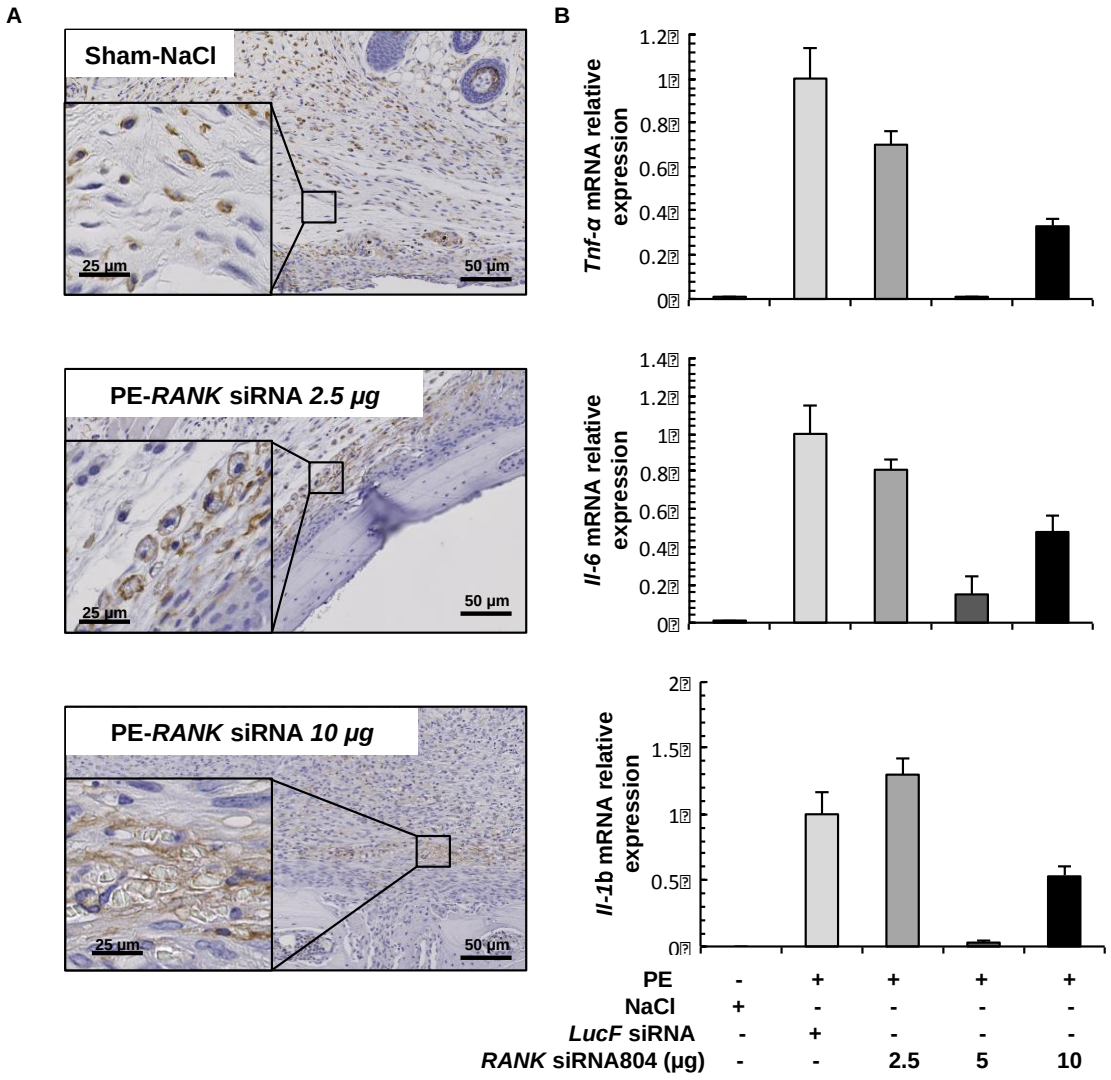

Figure 45.*RANK* siRNA-811 does not modulate the invading macrophages.

PE particles were implanted or not (Sham-NaCl) over the periosteum of calvaria for 9 days. Increasing doses (2.5, 5 and 10 µg) of *RANK* siRNA-811 were injected locally and inflammatory *status* was followed compared to the control *LucF* siRNA. Macrophages were identified by 4-80 in all groups (implanted and sham) mice (**A**). *RANK* siRNA-811 decreases the expression of pro-inflammatory *Tnf-α, Il-6* and *Il-1β* cytokines (**B**). The relative expression of *Tnf-α, Il-6* and *Il-β* was determined in explanted tissues by qRT-PCR. PE, polyethylene; qRT-PCR, quantitative *reverse transcriptase PCR; Tnf-α,* tumour necrosis factor alpha*; Il, interleukine.*

Discussion

Targeting the components of the triad OPG/RANKL/RANK by interference of RNA seems to be a promising approach. Experimental studies blocking RANKL-RANK signalling by siRNAs targeting *Mus musculus Rank* have already been reported in *in vitro* systems with an effective inhibition of *Rank* expression, osteoclast differentiation and osteolysis (185–187). Furthermore, the effectiveness of siRNAs targeting of *Rankl* to decrease the targeted transcript in *in vitro* culture of *RANKL*-expressing HEK 293 cells and in a murine model of osteosarcoma has been reported (147,153). Our study provides strong evidence of the efficiency in *RANK* in knock-down using three formulated cross-species sequences of siRNAs in both human *RANK*-expressing HEK 293 cells and in murine RAW 264.7 cells *in vitro*. Then, once the down-regulation of *RANK* and *Rank* was confirmed, we selected the most efficient sequence among the three evaluated (*RANK*-811 siRNA with 48.7% of inhibition) to assess its effect on osteolysis in the animal model.

We first confirmed the pertinence of the calvaria mouse model used in our experiments with the assessment of formulated siRNA. The challenge of calvaria with PE particles is the current standard for the early assessment of particle-host tissue interactions and its response under new therapeutic agents in an orthotopic bone site (93,129,179). We used commercial particles with a mean size of 7 µm (data not shown), considered phagocytables according the "particle critical size" concept (194). Furthermore, we confirmed the internal validity of the model by the significant differences observed in all osteolytic parameters between the implanted group (PE-siLucF) and the Sham group. Our study shows for the first time an effective inhibition of particle-induced osteolysis in an *in vivo* model using a *RANK*-directed siRNA sequence. We observed a large reduction in the number of $TRAP^+$ activated cells (presumably osteoclasts) in the parasagittal area on implanted calvarias using three different doses of *RANK*-811 siRNAs. Thus, we were able to propose a high sensitivity of osteoclast precursors in the uptake of the injected lipoplex. The synthetic vector used in our experiments (cationic liposome DMAPAP/DOPE + plasmid) has also shown considerable efficacy in the local delivery of formulated *Rankl*-directed siRNA by intra-tumour injection in previous reports (147,153). Moreover, Khoury *et al*. (2006 and 2008), reported a successful systemic delivery of siRNAs targeting proinflammatory cytokines

(*Tnf-α, Il- 1β, Il-6* and *Il-18*) in a mouse model of rheumatoid arthritis using the same siRNA formulation (189,190).

While the doses of 5 and 10 µg of *RANK*-811 siRNAs significantly decreased the expression of *Rank* and *Cathepsin K*, confirming the inhibition of osteoclastogenesis and osteolysis, we observed a contradictory response with the dose of 2.5 µg: significant inhibition in the number of $TRAP^+$ cells with high expression of *Rank* and *Cathepsin K*. To explain this finding, we propose an imbalance between the amount of *Rank* transcript and the weak dose of siRNA (2.5 µg). The volumetric assessment by micro-CT showed that 10 µg of *RANK*-811 siRNA was capable of preventing bone loss compared with the implanted control (PE- *LucF*-siRNA). We also observed a major effectiveness of lipoplex in the external cortical rather than in the inner cortical of the calvaria. Thus, the diffusion of the injected volume to the inner cortical may be a difficulty from the modified local anatomy (eroded surface of bone and trabecular spaces in the diploe), the inflammatory reaction and/or the viscosity of the lipoplex.

Our findings were consistent with a direct anti-resorptive effect of *RANK*-811 siRNA demonstrated by conclusive signs of inhibition of osteoclastogenesis, decrease in osteoclast activation and osteolysis. Moreover, an observed similar bone protective effect using Zoledronic acid, a compound that targets pre-osteoclasts and activated osteoclasts, supports our hypothesis. The findings observed in our study may be related to the internalization of carboxyfluorescein-labeled siRNAs (FAM-siRNAs) delivered by the same cationic liposome by monocyte/macrophages in a murine model of rheumatoid arthritis (190). The utility of FAM sequences to detect its trafficking in bone tissue was also showed by Zhang *et al.* (2014) using siRNA targeting osteogenic lineages delivered by cationic liposomes attached to six repetitive sequences of amino acids, reporting the colocalization with osteoblastic cells (195). Otherwise, the cationic liposome used in our study does not have an inherent affinity for bone tissue, making this a limitation for it. However, we can suppose specific delivery of our formulated *RANK*-siRNA in bone tissue using biomaterials for bone regeneration (187), peptides (196) or a modified cationic liposome (195). Further studies are in progress to unveil the specific cell(s) that uptake *RANK* 811-siRNA and its intracellular sites of interaction.

We observed the persistence of macrophages both in non-implanted (Sham) and in all *RANK*-811 siRNA-treated groups. While those observed in the Sham group exhibited a heterogeneous distribution in connective tissue and could be associated with the inflammatory process after a surgical approach, those observed in the *RANK*-811 siRNA treated groups were always closely related to the PE particles (presumably phagocytosed by them). The potential immunoactivatory role of the lipoplex (197,198) (or some of its components [cationic liposome or nucleic acids]) could explain this fact. Controversially, we did not observe any qualitative differences (cellular infiltrate) in the fibro-inflammatory membrane of all implanted and siRNA-treated groups in our current study compared with previous implanted and saline-treated groups (i.e.: experiment of Zoledronic acid *versus* saline therapy as shown in Figure 2). Similarly, in a previous study, we showed that the same construct used in an intra-osseous site did not activate the systemic immune response (147). These contradictory data reinforce our hypothesis for the existence of non-identified cellular sources for pro-inflammatory mediators (i.e.: osteoclast precursors, dendritic cells, lymphoid cells and/or stromal cells).

Interestingly, the unexpected bone formation observed in siRNA treated mice, suggests the establishment of a local anabolic microenvironment. Thus, we propose a complete renewal of osteoblastic cell lineage characterized by a sequence of localized osteolysis/osteonecrosis induced by PE particles, followed by a bone formation pulse induced by the lipoplex.

STUDY 3: Interaction of macrophages and PE particles at the periprosthetic interface: an *in vitro* study

Introduction

Macrophages are phagocytes that internalize and kill dangerous agents, thereby activating the innate and adaptive immune responses via inflammatory responses and antigen presentation, respectively. Additionally, they contribute to tissue homeostasis during catabolic processes by clearing apoptotic cells, cell bodies and debris during the inflammatory response, tissue development or bone resorption. Phagocytes constitute an attractive target to understand or treat human diseases mediated by an overactive immune response (199).

The plasma membrane is a dynamic structure to segregate and coordinate the homoeostasis of the intra- and extracellular milieus through the entry or exit of molecules. While small molecules (amino acids, sugars and ions) traverse the membrane through pumps or channels, macromolecules must be carried into the intracellular space by membrane-bound vesicles derived by endocytosis (the invagination of the plasma membrane). Endocytosis includes the uptake of solid and large particles (phagocytosis) or fluid compounds (pinocytosis). Four different mechanisms have been recognised in the pinocytosis process: macropinocytosis, clathrin- or caveolae-mediated endocytosis (CME) and clathrin- and caveolae-independent endocytosis (Figure 46). These endocytic pathways are implicated in many physiological processes such as hormone-mediated signal transduction, immune surveillance, antigen presentation and cellular homeostasis (165).

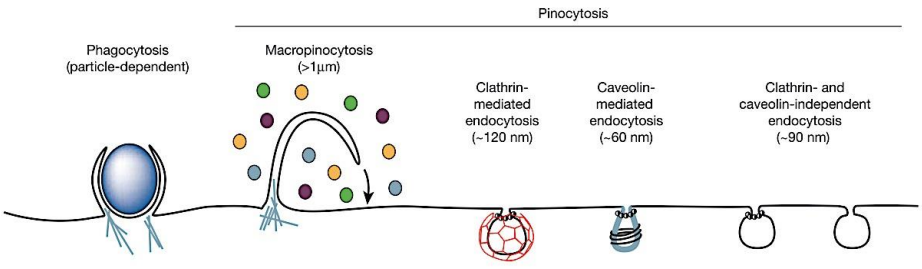

Figure 46. Fourth mechanisms to explain the internalization process. (165)

Wear particles released from metal-on-UHMWPE low-friction arthroplasties constitute a key factor in the inflammatory and osteolytic response at the periprosthetic interface that leads to the formation of periprosthetic chronic inflammatory tissue and consequent osteolysis (4). After 13 years of the clinical use of

highly cross-linked re-melted PE, an optimised PE, in bearing surfaces, the released wear debris and the wear rates appear to have significantly diminished, thus improving the lifespan of the implants and the prognosis of the patients after a total arthroplasty (8). Despite this encouraging report, the number of retrospective studies concerning the long-term assessment of such implants is still low, and the level of clinical evidence is poor.

Classically, the size of debris has been correlated with the internalization capacity of macrophages (4,75). While large particles (> 20 μm) induce macrophage fusion and multinucleation, smaller particles (ranging from 1 to 20 μm) induce internalization by phagocytosis (70). However, 90% of the wear particles generated in joint replacements are submicrometric (on the nanometric scale). Because they are too small to be phagocytosed, the effect of PE nanoparticles remains unknown. Furthermore, the release of short-chain alkane polymers from the breakdown of PE has been reported as an additional challenge for periprosthetic tissues (200). Thus, PE nanoparticles appear to be relevant actors in the pathophysiology of the aseptic loosening of the currently available bearing surfaces.

Recently, the nexus between the immune and osseous systems activated by products released from bearing surfaces has been proposed to play a role in aseptic loosening, opening a new era in this field (9,75). Our knowledge of the macrophage-particle interactions in the field of periprosthetic osteolysis has been considerably improved in recent years by the optimisation of *in vitro* cellular models (79,200). The vast majority of reports have focused on the relationship between the nature and size of the released particles and the type of biological response induced; however, few reports have described the internalization, intracellular trafficking and impact on cellular activation and survival of PE nanoparticles in human macrophages. The aim of this report is to assess the internalization of formulated PE fluorescent nanoparticles by human $CD14^+$ monocyte cells.

Results

Characterization of polyethylene fluorescent nanoparticles

Transmission electron microscopy (TEM) (Figure 47):

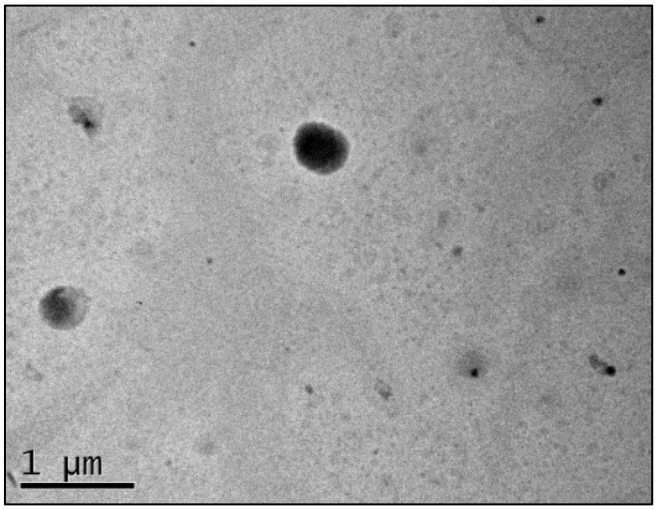

Figure 47. TEM showed regular solid spheres of less than 200 nm in size.

Size distribution (DLS) (Figure 48):

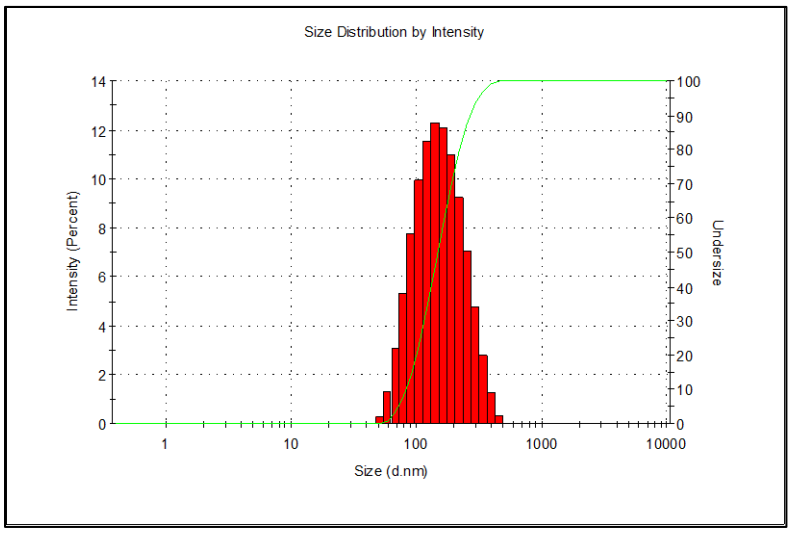

Figure 48. Mean diameter: 169 ±77 nm.

Spectral measurement of nanoparticles (Figure 49 **and** Figure 50**):**

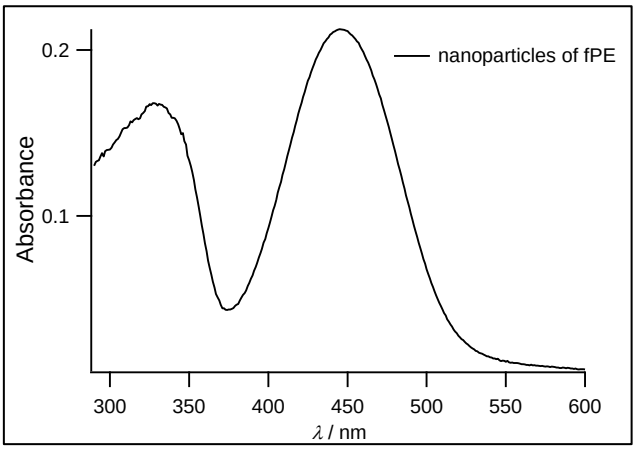

Figure 49. Absorption spectrum in water of fPE nanoparticles (max : 445 nm).

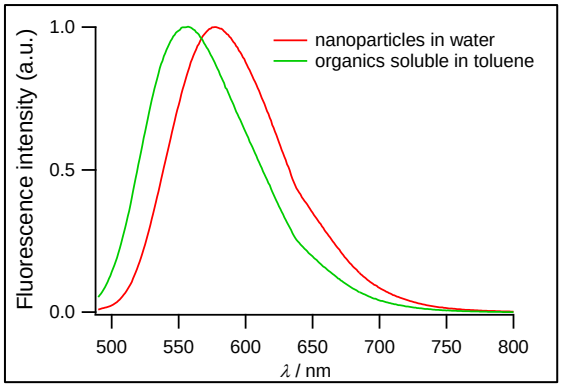

Figure 50. Emission spectra of nanoparticles in water and free molecules in toluene (max : 580 and 555 nm).

CD14^{+} monocytes/macrophages take up PE fluorescent nanoparticles in a dose- and time-dependent manner.

To examine the uptake of PE fluorescent nanoparticles by cultured monocytes/macrophages, we compared the effects of two ratios (2000 and 4000 nanoparticles per cell) after 24, 48 and 72 hrs. of stimulation (Figure 51.A). No significant changes in the uptake of nanoparticles at a ratio of 2000 nanoparticles per cell were observed after 24 hrs (2.3-fold), 48 hrs (2.2-fold) or 72 hrs (2.3-fold). Although the uptake at a ratio of 4000 nanoparticles per cell exhibited an increase in the relative mean fluorescent intensity (MFI) values

compared with the uptake for the ratio of 2000 nanoparticles per cell, it maintained a similar pattern of uptake at 24 hrs (3.2-fold), 48 hrs (3.4-fold) and 72 hrs. (3.7-fold) (Figure 51A).

We next assessed the effect of the PE fluorescent nanoparticles using a ratio of 4000 nanoparticles per cell during the first 12 hrs. using the same methods. Interestingly, we observed a time-dependent response with a progressive increase in the relative MFI compared with the first hour. We observed increasing uptake at 1 hr (1.5-fold), 4 hrs (2.3-fold), 8 hrs (3.3-fold) and 12 hrs (5.1-fold) (Figure 51B).

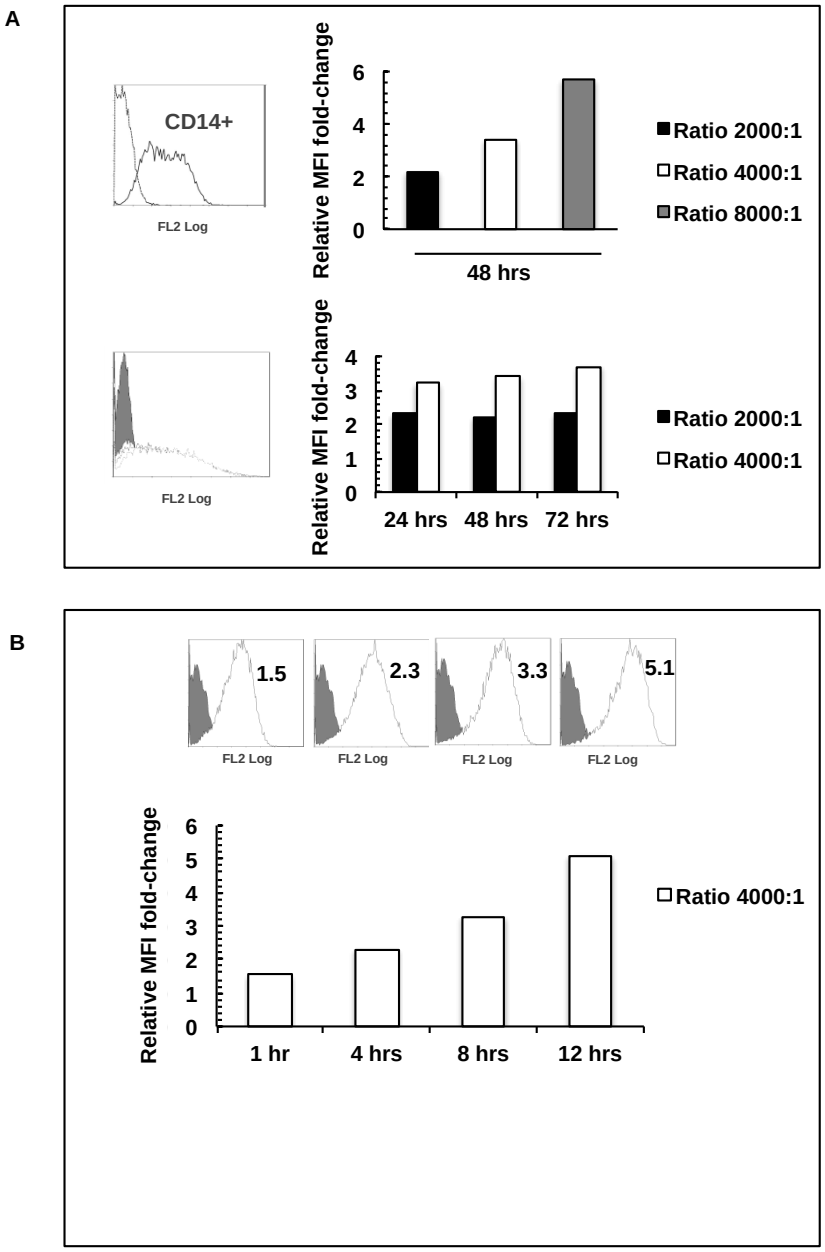

Figure 51. ***In vitro*** **cultured CD14^{+} monocyte/macrophages uptake the PE fluorescent nanoparticles in a dose and time-dependent manner at 48 hrs and within the first 12 hrs, respectively.**

The macrophagic capacity of uptake the polyethylene fluorescent nanoparticles was assessed by the measure of relative mean fluorescent intensity (MFI) from 1 to 72 hrs of stimulation using flow cytometry. A dose dependent response was observed at 48 hrs. No differences in relative MFI was observed in the CD14^{+} monocyte/macrophages between 24-48-72 hrs **(A).** Conversely, at 1, 4, 8 and 12 hrs following to the polyethylene fluorescent nanoparticles stimulation, a 1.5, 2.3, 3.3 and 5.1 fold increase in the relative MFI of the polyethylene fluorescent nanoparticles were observed in the CD14^{+} monocyte/macrophages, respectively **(B).**

PE fluorescent nanoparticles were effectively internalized by CD14$^+$ monocytes/macrophages

While the increase in the MFI confirmed the uptake of PE fluorescent nanoparticles by CD14$^+$ monocytes/macrophages under *in vitro* conditions, we were unable to differentiate between internalized and adherent nanoparticles. In this regard, we assessed the internalization of nanoparticles at a ratio of 4000 nanoparticles per cell by CD14$^+$ monocytes/macrophages using stacked sections acquired by confocal microscopy after 48 hrs of stimulation. We recognised two cell morphology patterns: a) adherent cells, which were characterised by an elongated shape, and b) non-adherent cells, which were characterised by a rounded shape and an empty cytosol (Figure 52A). We also observed that the PE fluorescent nanoparticles were detected both inside and outside the cells. The internalized nanoparticles were organised in rounded bodies that were heterogeneously distributed within the cell (cytoplasmic distribution) (Figure 52A, Figure 52B and Figure 52C). Additionally, other nanoparticles were detected crossing the cell membrane (Figure 52B and Figure 52C). Otherwise, the nanoparticles located outside the cells were recognised as having either compact and small or large and rounded bodies (Figure 52D).

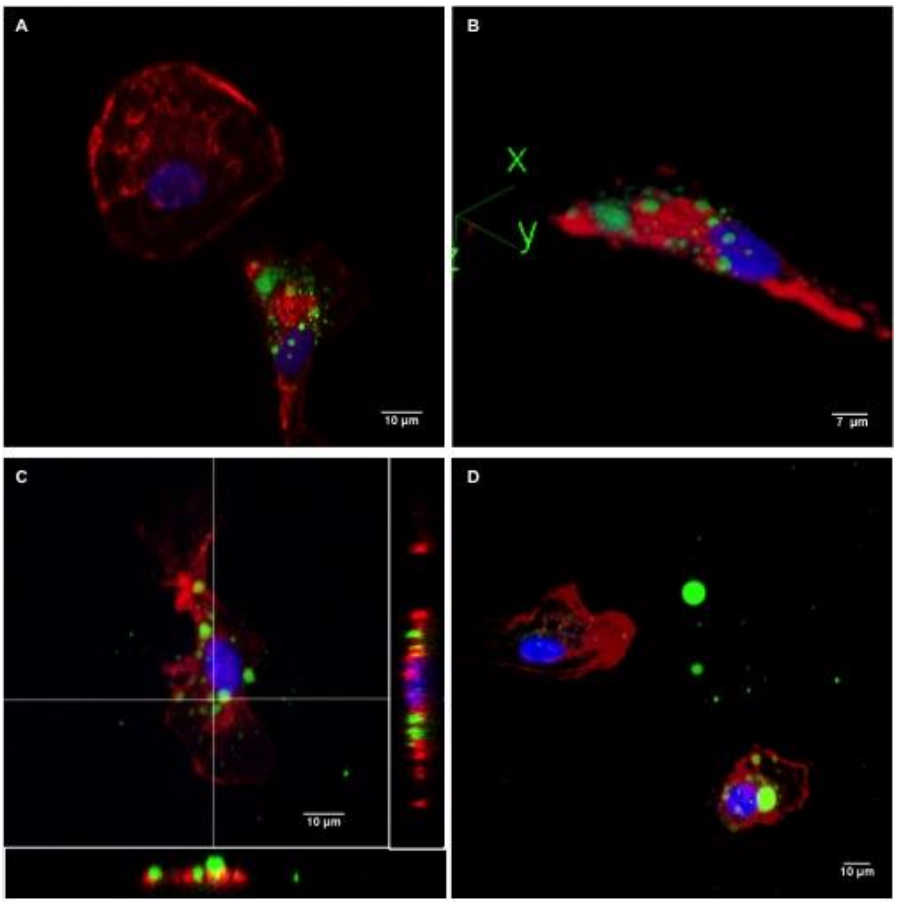

Figure 52. The fluorescence of internalized polyethylene nanoparticle was detected in CD14$^+$ human monocytes/macrophages by confocal microscopy after 48 hrs of stimulation.

Polyethylene fluorescent nanoparticles were detected as green round bodies heterogeneously distributed in the surface of adherent cells (A and B) and also outside the cells (C and D). Some dead cells with a rounded shape and without fluorescent signal were recognized (A and D). Orthogonal views confirm that polyethylene fluorescent nanoparticles were a cytoplasmic location. Also, some others fluorescent nanoparticles cross the boundary of the cell, suggesting their expulsion. Interestingly, both the big round and small compact fluorescent bodies were detected outside the cell (D).

Green, polyethylene nanoparticles fluorescence; Red, actine cellular cytoskeleton stained by Phaloydine and Blue, nuclear stained by Hoechst.

CD14$^+$ monocytes/macrophages died after releasing the PE fluorescent nanoparticles

To assess the dynamic behaviour of CD14$^+$ monocytes/macrophages after stimulation with PE fluorescent nanoparticles, we performed time-lapse video-microscopy over 72 hrs (Figure 52 and video 1, 2 3 and 4). We confirmed the presence of the nanoparticles in the cytoplasm after 4 hrs of stimulation. Then, after 4.5 to 5.5 hrs of stimulation, we observed the intracellular trafficking and release of the particles into the extracellular medium at 6 hrs. (Video 1). Later, we observed that some of the cells became rounded and non-adherent, suggesting that they had died by 10 hrs after stimulation (Figure 52A and Video 2). Other cells

remained alive and formed intracellular and extracellular vesicles, which was followed by the violent release of the vesicles at 20 hrs. (Figure 52B and Video 3). Furthermore, between 48 and 72 hrs. we observed some active cells that attacked some of the living cells and other cells that were carrying cellular debris (Video 4).

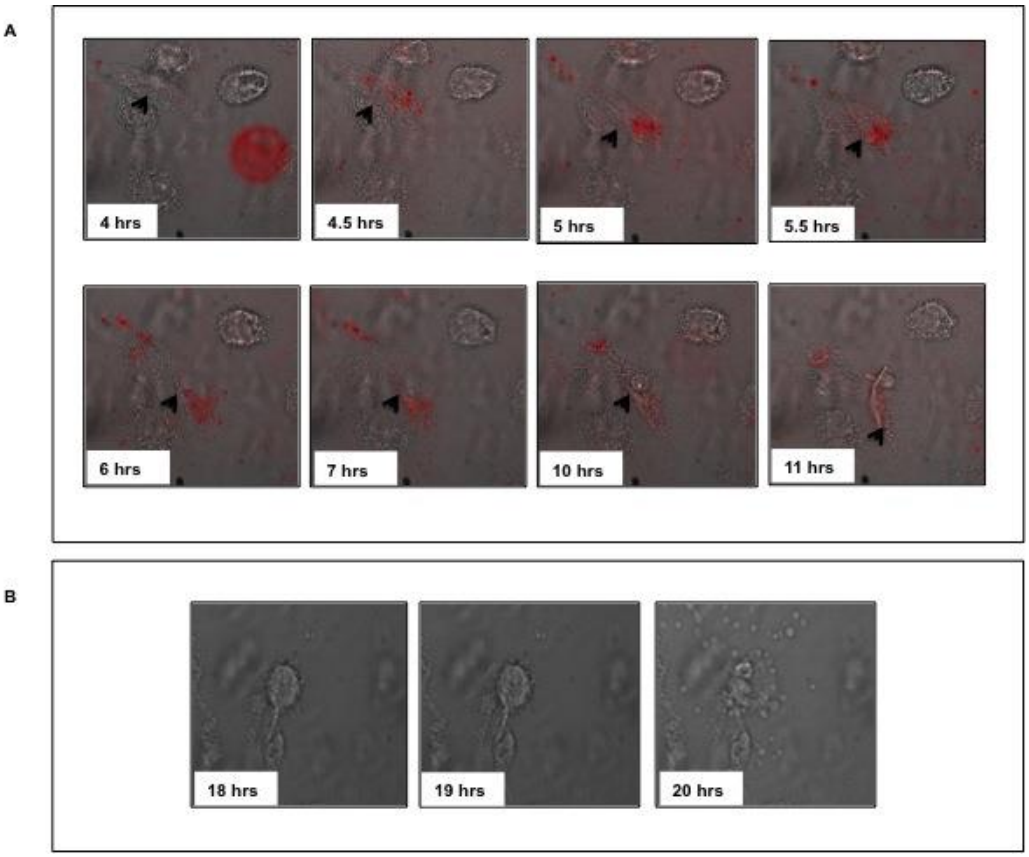

Figure 52. Some CD14^{+} human monocytes/macrophages die after to internalize, traffic and to release polyethylene nanoparticles, becoming cellular debris that perpetuate inflammatory vicious cycle in periprosthetic tissues.

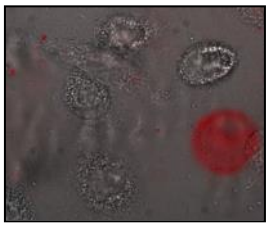

Video 1

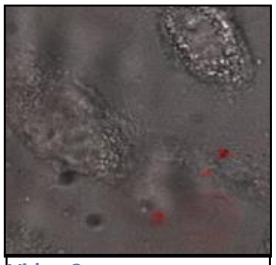

Video 2

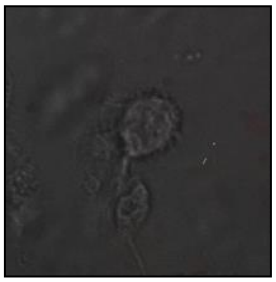

Video 3

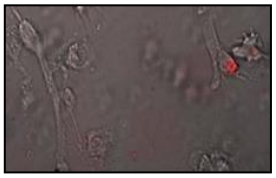

Video 4

Discussion

We confirmed that the PE fluorescent nanoparticles were taken up and internalized by $CD14^+$ monocytes/macrophages in a time-dependent manner until 24 hrs after stimulation. No changes in the uptake were observed at 24, 48 and 72 hrs, suggesting a depletion of the maximum cellular capture volume. Once internalized, the nanoparticles appeared to be dissociated, packaged and then released into the extracellular medium by 48 hrs, inducing dramatic changes in the cellular shape and inducing cell death.

The MFI method used to assess the particle uptake by flow cytometry has the benefit of simplicity and reliability; however, it does not discriminate between adherent and internalized nanoparticles (201). To overcome this drawback, we detected the fluorescent signal from internalized nanoparticles using confocal microscopy. We confirmed their presence and organisation into heterogeneous rounded cytosolic bodies. We also observed these structures crossing the cellular limits and even more structures outside the cells, suggesting an active process of foreign body release by exocytosis. While some reports have not differentiated between adherent and internalized nanoparticles (202,203), others have tried to elucidate this difference using right angle scatter (RAS) correlated with cell granulometry (204), quenching (205,206) and physico-chemical elimination of adherent nanoparticles (207). Otherwise, confirmation by optical methods has also been reported as the only way to confirm the intracellular location of nanoparticles; however, this method does not allow for quantification (207). We assessed the internalization of nanoparticles by combining quantitative and qualitative approaches.

Macrophages constitute the first cellular barrier to recognise exogenous pathogen-associated-molecular-patterns (PAMPs) and activate the innate and/or adaptive immune responses. Furthermore, the released particles from orthopaedic surfaces can act as damage-associated molecular patterns (DAMPS), activating both the macrophage Toll-like receptor (TLR) pathway and the nucleotide binding and oligomerisation domain (NOD)-like receptor family (NLR), pyrin domain containing 3 (NALP3) inflammasome, an intracellular danger signal (53,200). The activation of these intracellular pathways induces the activation of NF-κB and the cleavage of immature forms of IL-1β and IL-18 into mature IL-1β and IL-18 by caspase-1. New insights into alternatives

forms of programmed cell dead have been reported (208). Among them, pyroptosis, a caspase-1-dependent cell death programme, constitutes an interesting phenomenon to explain the behaviour of phagocytes under pathophysiological challenges and to compare with the better-known concept of apoptosis (208).

Our findings were consistent with the internalization and subsequent release of dissociated nanoparticles into the extracellular medium by macrophages. Additionally, we observed morphological changes that suggested cell death, including cellular fragmentation and detachment. However, we do not know the true nature of this process or its molecular basis. Interestingly, both clinical and experimental *in vitro* and *in vivo* evidence has confirmed the presence of caspase-1 and the release of IL-1β in the particle-macrophage interaction model (53,200).

GENERAL DISCUSSION

MOUSE MODEL AND TRANSLATIONAL RESEARCH IN ASEPTIC LOOSENING

Despite the preclinical progress made, new insights gained using mouse models have not yet been successfully translated to clinical practice. We analyse this failure with a critical view on the performance of the models, the benefits gained from the emerging knowledge and the future challenges for mouse models in particle-induced osteolysis.

Benefit-cost analysis.

The use of mouse models for the study of the pathophysiology of periprosthetic osteolysis has produced vastly more benefits than costs. Benefits include their biological fidelity, effectiveness, reproducibility, dynamism and the diversity of the genetic and molecular tools available. The biological fidelity of mouse models is based upon their resemblance with the human periprosthetic environment, sharing the bone tissue organization and physiological control of bone remodelling. Furthermore, this species has a reduced life cycle, giving the advantage of a rapid development of pathological features. The effectiveness and reproducibility of mouse models has been demonstrated repeatedly, predicting bone behaviour under different conditions (e.g. drug therapy or surgical procedures). Furthermore, mouse models have proven to be dynamic, evolving from air pouches to intra-medullary devices and proving useful for the assessment of the oldest as well as the latest generation of biomaterials (*i.e.* wear from cross-linked polyethylene). The availability of genetically modified or immunodeficient strains and the abundance of specific molecular tools have made possible the identification of genes, pathways, cells or tissues involved in the pathology, improving our understanding of the mechanisms of this disease.

Limitations include the bias of a partial reproduction of the real human condition. Given that mice are small quadrupeds, mouse models cannot reproduce the "load bearing effect" of the implant, as there are no devices available that mimic a total joint replacement in mice. Other disadvantages of mouse models are the small animal size and the low amount of cancellous bone, making their surgical manipulation difficult.

Relevance of mice models

We believe that there is no one animal model useful for all stages of research in this field. Periprosthetic osteolysis is a multifactorial condition, with a close interplay between biomechanical and biological aspects. Mouse models are the first step in *in vivo* research, indispensable for confirming previous *in vitro* findings; however, we believe that they do not have the necessary performance to translate their advances directly into clinical trials. There are still controversial issues, such as the genetic predisposition, immune and endocrinological regulation of periprosthetic bone loss, pharmacological considerations in drug delivery as well as the biomechanical aspects involved in loaded endochondral bone. These heterogeneous topics need to be confirmed and tested in complementary larger and loaded models (e.g.: sheep or horse).

Achievements and future challenges

The use of mice has been useful for understanding the pathophysiology of particle-induced osteolysis, testing therapeutic strategies and, recently, improving early diagnosis. First, there was the confirmation of a "multifactorial condition" that depends on interplay between wear production, bone niche homeostasis and host susceptibility. Concerning the wear aspects, it has been widely accepted that polymeric and metallic micrometric particles within a critical size range are bioactive materials capable of triggering a biological response. Moreover, the local chemo-cytokine-mediated homeostasis of periprosthetic bone has been better-understood using mouse models. The central role of macrophages in primary inflammatory response has been confirmed in mice, highlighting the role of chemokines (MCP-1 and S1P), PRRs (TLR pathway) sensing danger signals, pro-inflammatory cytokines how mediators in the initiation of innate immune response. Furthermore, the role of NALP3 inflammasome has recently been confirmed as a critical mediator for orthopaedic wear-induced osteolysis in a mouse model. The uncovering of a key role for osteoclastogenesis and osteoclast-mediated osteolysis has created a link between recent and general concepts of bone biology, such as the role of the RANK/RANKL/OPG axis or the pro-osteolytic effect of cytokines TNF-α or IL-1 or, inversely, the osteoprotective role of IL-10. The cross-talk established between osteoclasts, macrophages and osteoblasts/stromal cells has progressively become a consensus in the field of periprosthetic osteolysis. In the same vein, a systemic control of periprosthetic bone response, especially by the endocrine system, has been

proposed. The involvement of calcitonin or estrogenic control of periprosthetic bone is an emergent and interesting topic to explore.

Second, therapeutic progress made in mice includes the feasibility of systemic drug administration and delivery. Third, an innovative and useful application for mice has been validated, making possible the early diagnosis of inflammatory changes using a systemic nanovector.

Future challenges (Figure 53) for mouse models include improving understanding of the bioactivity of nanometric particles derived from improved polyethylene, as well as the potential cytotoxic response to metallic nanoparticles and ions. Furthermore, the endocrine regulation of the periprosthetic environment (by calcitonin, estrogens or others) needs to be clarified. Genetic susceptibility may have high value and open up the path for the development of new inter-individual prognostic markers. However, in order to exploit this knowledge, a human genetic profile first needs to be established and then mimicked in mice.

The role of the immune response in periprosthetic tissues seems to be an extremely relevant chapter for future research, considering the strong evidence that supports the involvement of macrophages and probably lymphocytes. Understanding of the cellular and molecular mechanisms involved in the recruitment, differentiation and activation of monocyte/macrophage cells seem to be a central axis of research in the immunomodulation of bone response. Furthermore, pharmacological aspects related to drug delivery will make it possible to clarify the equivalence of animal doses, frequency and route of administration by taking into account human requirements. In this regard, nanotechnology may be a potentially useful tool for this field. Finally, the current models of loaded intra-medullary implants developed in mice need to be tested under controlled, preventive or curative protocols, using the same markers established in the calvaria model. This aspect would give more validity to the results, considering the human-mouse homology of the intra-medullary site.

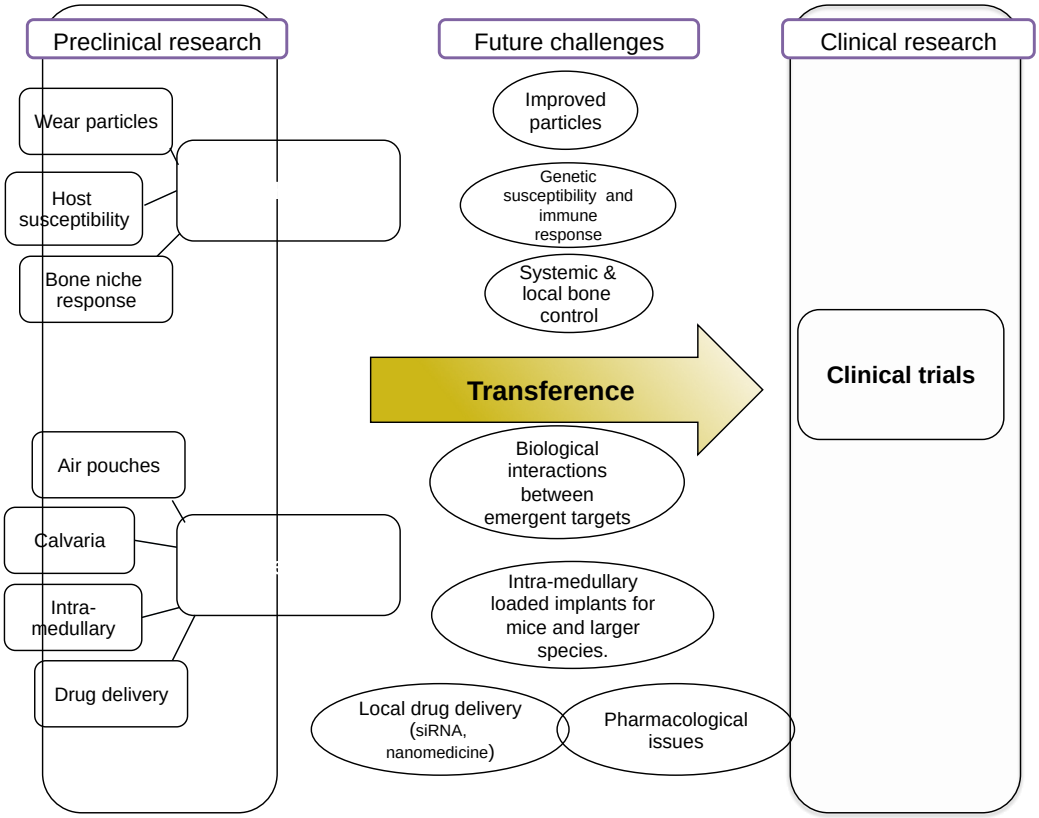

Figure 53. Translational challenges in orthopaedic aseptic loosening. (134)

RANK-811 siRNA: A NEW THERAPY FOR ASEPTIC LOOSENING?

Once the primary and direct anti osteolytic effect of RANK-811 siRNA has been well described in our study, we discuss another potential beneficial effect of this sequence. Considering that the dramatic inhibition in the expression of proinflammatory cytokine in harvested tissues from mice treated with 5 and 10 µg of *RANK*-811 siRNA, suggest that its primary targeted cells (probably $RANK^+$ pre-osteoclasts and osteoclasts) modulate those inflammatory cell sources (probably including $RANK^-$ macrophages). Therefore, we propose a second and indirect effect of *RANK*-811 siRNA, modulating the NF-KB and NF-IL6 pathways in inflammatory

cells (monocyte/macrophages and may be lymphocytes). The central role of these transcription factors in the orchestration of the vicious cycle inflammation-osteolysis in particle-challenged periprosthetic tissues has been well documented (90). *RANK*-811 siRNA interrupts this influence, generating an anabolic periprosthetic niche, propicious to the phenotypic re-polarization of macrophages, from a proinflammatory (M1) to an anti-inflammatory (M2) and/or similarly to lymphocytes (Figure 54). This asseveration may be supported by the immunomodulatory effect of IL-4 observed in *in vitro* activated macrophages harvested from periprosthetic membranes and then confirmed in the PE-induced osteolysis calvaria mouse model (79,129).

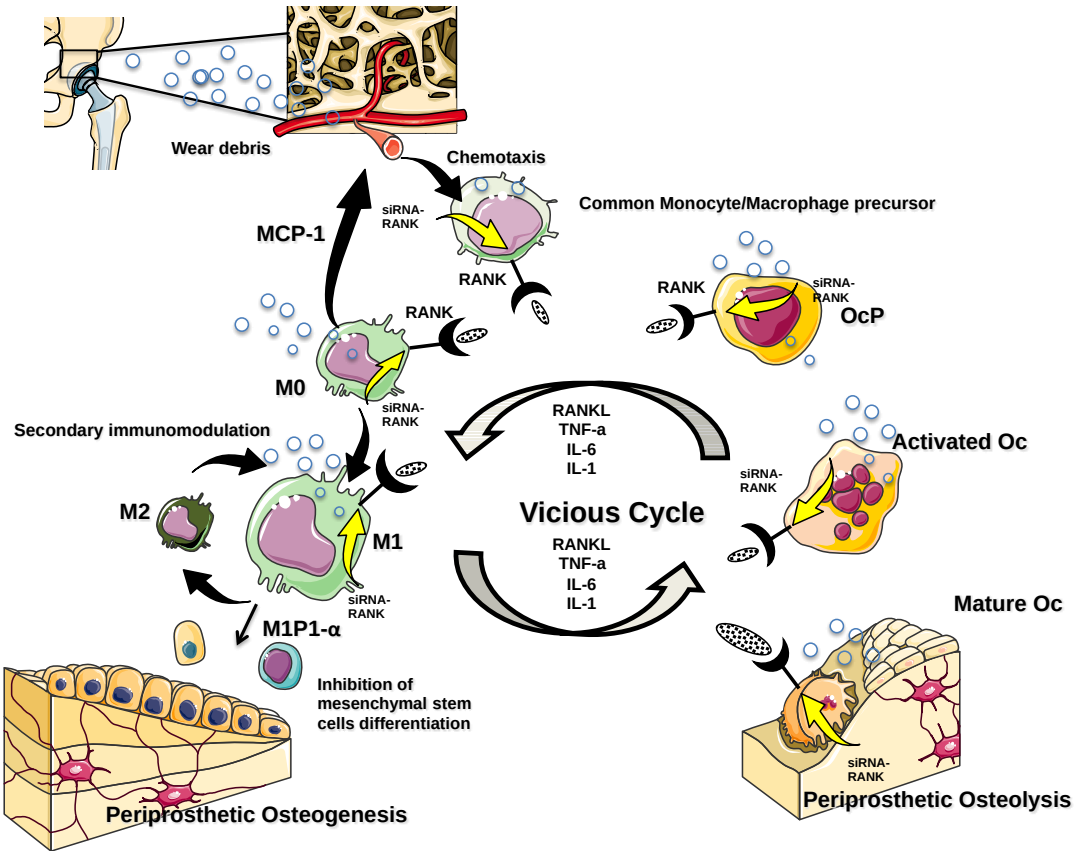

Figure 54. Proposed mechanism of action of formulated *RANK*-811 siRNA in the periprosthetic bone niche.

siRNA targeting *RANK* may inhibit reciprocally the cytokine signalling process induced by PE particle activation (RANKL, TNF and IL-6 and IL-1β siRNAs are internalized in early myeloid cells (macrophage precursors) and osteoclast precursors degrading mRNA encoding RANK. Secondarily, a down regulation of intracellular pathways related to proinflammatory, pro-osteoclastogenic gene expression and cytokine synthesis (regulated by the transcription factors Nf-KB and Nf-IL6) is also inhibited. Thus, the vicious cycle generated by paracrine signalling between macrophages and osteoclasts is interrupted by intracellular control, leading to the creation of an anabolic periprosthetic bone niche. An indirect immunomodulator effect was also proposed, with a macrophagic re-polarization from M1 to M2 macrophages that promoted bone repair (209).

MCP-1, Monocyte chemoattractant protein-1; MIP1- α, Macrophage inflammatory protein-1α.

GENERAL COMMENTS

We want to highlight the identification of RANK as a relevant target in periprosthetic osteolysis. While RANK's ligand RANKL has classically been the most targeted cytokine in osteolytic diseases, we propose strong evidence of the critical role that RANK plays in the orchestration of bone loss in periprosthetic tissues. The fact of that RANK is expressed by both bone and immune cells may be an advantage in the particular case of aseptic loosening due to the inflammatory nature of osteolysis. Another relevant aspect was the control of bone loss through the local administration of short interfering RNA (siRNA). Clinical and preclinical data support the idea that aseptic loosening remains a local disease. Thus, it would appear logical to propose a "local therapy", avoiding systemic distribution and the biotransformation of a siRNA. In this regard, the use of a cationic liposome with an adjuvant plasmid appears to be a well-adapted method that allows for optimal delivery and stability. The benefits of local administration and optimal local delivery need to be confirmed in our current studies using 6-carboxyfluorescein (FAM) RANK-811 siRNA in the same model.

Though our study has shown an innovative approach in an animal model, we have also found matching data between histologic and *in vitro* studies. The central role of monocytes/macrophages in the aseptic loosening of implants was shown by the histology data from human pseudomembranes and by *in vitro* findings from human cells cultured with PE particles. Both studies were similar in the detection of internalized particles by human macrophages. While human retrieved tissues showed the presence of different morphologies of $CD68^+$ cells (giant multinucleated cells) surrounding large and small wear particles, $CD14^+$ cells were capable of internalizing nanoscale particles under *in vitro* conditions. Taken together, these findings confirm the capacity of macrophages to internalize a wide range of particles. The detection of multinucleated giant cells surrounding large particles (approximately 200 μm) in the case of a knee revision support the concept of "frustrated phagocytosis". In contrast, we observed the internalization, intracellular trafficking and expulsion to the extracellular space of nanoparticles, suggesting a high clearance of particles beginning at least 1 hour after particle stimulation. These findings suggest a high adaptability of macrophages to the challenge with particles

of heterogeneous composition and morphology. Further studies are in progress to elucidate the different mechanisms of internalization, cell activation and cell survival stimulated with different sizes of PE particles under experimental conditions.

Finally, we provided morphologic evidence of the nexus between the cells of the innate and acquired immune responses. The close contact between macrophages and T or B lymphocytes support suspicions of the triggering of histocompatibility mechanisms by the products released from prosthetic devices. These aspects need to be confirmed by increasing the collection of human retrieved samples and correlating their findings with clinical data to eventually establish behavioural patterns for the different types of prostheses.

CONCLUSIONS AND PERSPECTIVES

STUDY 1

We provide evidence that pseudomembranes retrieved from patients with loosened prostheses exhibit different cellular features compared with the synovium retrieved from osteoarthritic patients. These differences include histologic elements of the innate immune response such as an inflammatory reaction to wear particles that is characterised by a highly vascularised stroma, a dense cell infiltrate including $CD68^+$ and $TRAP^-$ monocytes/macrophages and, exceptionally, $CD117^+$ mast cells. Furthermore, we observed the activation of T and B cells in perivascular sites, suggesting the activation of the acquired immune response.

The perspective of this study consists of increasing the number of subjects in the database by including prospective clinical and histologic records to allow for the creation of a cohort of patients. Thus, it could be possible to confirm the existence of specific cellular patterns in revised patients. Additionally, this prospective study would allow us to correlate the clinical and cellular data to identify potential risk factors and inter-individual risk factors that predispose patients to loosening of their articular implants.

STUDY 2

The local treatment with three doses of *RANK*-811 siRNA delivered by the cationic lipid DMAPAP/DOPE in a PE particle-induced osteolytic mouse model preserved the bone volume with the dose of 10 µg. While 5 µg of *RANK*-811 siRNA dramatically decreased the osteoclastogenesis, osteolysis and inflammation, the dose of 2.5 µg revealed contradictory effects, may be by immunoactivation of the lipoplex. We have consistent micro-architectural, histological and molecular findings to support the effectiveness of a siRNA-based approach locally delivered targeting *RANK* in the prevention of experimental osteolysis induced by PE particles. Further studies will be necessary to specify the optimal conditions for siRNA administration, the site of interaction and potential side effects. This study strengthens the concept for the usefulness of siRNA-based therapy targeting *RANK*, an innovative and relevant actor in the pathophysiology of particle-induced osteolysis. This approach could be potentially transferred to clinical uses.

The perspectives of this study include:

- The detection of the cells that effectively uptake the *RANK* -811 siRNA using FAM sequences in the same in vivo model.
- To optimize the internalization of siRNA sequence by the target cells, assessing alternatives adjuvants molecules to plasmid. (i.e.: pegylated or similar molecules)
- To analyse de pharmacologic issues of *RANK* -811 siRNA in a small animal, such as the stability, toxicity and biodistribution of the lipoplex.
- To evaluate this preclinical protocol in a large animal model, which involve the load bearing effect.

STUDY 3

We conclude that PE fluorescent nanoparticles were internalized by macrophages within the first 24 hrs. until a maximal depletion of their internalization capacity. The internalized nanoparticles induced the activation of a macrophage death-signal that generated cellular debris and perpetuated the vicious cycle of inflammation. These findings support the cellular basis of the inflammatory response observed in periprosthetic tissues.

Among the perspectives of this study, we include the following:

- Assessment of the viability of the macrophages at short (1-24 hrs) and middle intervals (48 hrs).
- To study the mechanism of internalization
- To study the effect of nanoparticle stimulus on the activation and phenotypic polarisation of macrophages
- To compare the particle internalization, viability, activation and phenotypic polarisation of macrophages stimulated with PE nano- and microparticles under *in vitro* conditions.

REFERENCES

1. Affatato S, Spinelli M, Zavalloni M, Mazzega-Fabbro C, Viceconti M. Tribology and total hip joint replacement: Current concepts in mechanical simulation. Med Eng Phys. déc 2008;30(10):1305‑1317.

2. Bozic KJ, Kurtz S, Lau E, Ong K, Chiu V, Vail TP, et al. The epidemiology of bearing surface usage in total hip arthroplasty in the United States. J Bone Joint Surg Am. juill 2009;91(7):1614‑1620.

3. Marshall A, Ries MD, Paprosky W. How prevalent are implant wear and osteolysis, and how has the scope of osteolysis changed since 2000? J Am Acad Orthop Surg. 1 juill 2008;16(suppl 1):S1‑S6.

4. Purdue PE, Koulouvaris P, Nestor BJ, Sculco TP. The central role of wear debris in periprosthetic osteolysis. HSS J Musculoskelet J Hosp Spec Surg. sept 2006;2(2):102‑113.

5. Zhu YH, Chiu KY, Tang WM. Review Article: Polyethylene wear and osteolysis in total hip arthroplasty. J Orthop Surg Hong Kong. juin 2001;9(1):91‑99.

6. Kurtz SM, Lau E, Ong K, Zhao K, Kelly M, Bozic KJ. Future young patient demand for primary and revision joint replacement: national projections from 2010 to 2030. Clin Orthop. oct 2009;467(10):2606‑2612.

7. Shetty N, Hamer AJ, Stockley I, Eastell R, Willkinson JM. Clinical and radiological outcome of total hip replacement five years after pamidronate therapy: A TRIAL EXTENSION. J Bone Jt Surg Br. 1 oct 2006;88-B(10):1309‑1315.

8. Bragdon CR, Doerner M, Martell J, Jarrett B, Palm H, Malchau H. The 2012 John Charnley Award: Clinical multicenter studies of the wear performance of highly crosslinked remelted polyethylene in THA. Clin Orthop. févr 2013;471(2):393‑402.

9. Goodman SB. Wear particles, periprosthetic osteolysis and the immune system. Biomaterials. déc 2007;28(34):5044‑5048.

10. Coathup MJ, Blackburn J, Goodship AE, Cunningham JL, Smith T, Blunn GW. Role of hydroxyapatite coating in resisting wear particle migration and osteolysis around acetabular components. Biomaterials. juill 2005;26(19):4161‑4169.

11. Goodman SB, Song Y, Yoo JY, Fox N, Trindade MCD, Kajiyama G, et al. Local infusion of FGF-2 enhances bone ingrowth in rabbit chambers in the presence of polyethylene particles. J Biomed Mater Res A. 15 juin 2003;65(4):454‑461.

12. Bragg B, Epstein NJ, Ma T, Goodman S, Smith RL. Histomorphometric analysis of the intramedullary bone response to titanium particles in wild-type and IL-1R1 knock-out mice: a preliminary study. J Biomed Mater Res B Appl Biomater. févr 2008;84(2):559‑570.

13. Ma T, Huang Z, Ren P-G, McCally R, Lindsey D, Smith RL, et al. An in vivo murine model of continuous intramedullary infusion of polyethylene particles. Biomaterials. sept 2008;29(27):3738‑3742.

14. Seeman E. Principles of Bone Biology. Third edition, Elsevier Inc. United States of America: Bilezikian J.P.,RaiszL.G.,V T.J.; 2008. 3-28 p.

15. Morrison SJ, Scadden DT. The bone marrow niche for haematopoietic stem cells. Nature. 16 janv 2014;505(7483):327‑334.

16. Guihard P. ROLE DES MONOCYTES / MACROPHAGES DANS LES PROCESSUS D'OSSIFICATION PHYSIOPATHOLOGIQUE. [Nantes]: Universite de Nantes; 2013.

17. Hodgson SF, Clarke CL, Wermers R, Hefferan T, Yaszemski M. Bone Histology and Histopathology for Clinicians. United States of America; 2007.

18. Genetos DC, Kephart CJ, Zhang Y, Yellowley CE, Donahue HJ. Oscillating fluid flow activation of gap junction hemichannels induces atp release from MLO-Y4 osteocytes. J Cell Physiol. 1 juill 2007;212(1):207‑214.

19. Winkler DG, Sutherland MK, Geoghegan JC, Yu C, Hayes T, Skonier JE, et al. Osteocyte control of bone formation via sclerostin, a novel BMP antagonist. EMBO J. 1 déc 2003;22(23):6267‑6276.

20. Suda T, Takahashi N, Udagawa N, Jimi E, Gillespie MT, Martin TJ. Modulation of osteoclast differentiation and function by the new members of the tumor necrosis factor receptor and ligand families. Endocr Rev. juin 1999;20(3):345‑357.

21. Sørensen MG, Henriksen K, Schaller S, Henriksen DB, Nielsen FC, Dziegiel MH, et al. Characterization of osteoclasts derived from CD14+ monocytes isolated from peripheral blood. J Bone Miner Metab. 1 janv 2007;25(1):36‑45.

22. Lakkakorpi PT, Väänänen HK. Cytoskeletal changes in osteoclasts during the resorption cycle. Microsc Res Tech. 1 févr 1996;33(2):171‑181.

23. Georges S, Ruiz Velasco C, Trichet V, Fortun Y, Heymann D, Padrines M. Proteases and bone remodelling. Cytokine Growth Factor Rev. févr 2009;20(1):29‑41.

24. Rousselle A-V, Heymann D. Osteoclastic acidification pathways during bone resorption. Bone. avr 2002;30(4):533‑540.

25. Theoleyre S, Wittrant Y, Tat SK, Fortun Y, Redini F, Heymann D. The molecular triad OPG/RANK/RANKL: involvement in the orchestration of pathophysiological bone remodeling. Cytokine Growth Factor Rev. déc 2004;15(6):457‑475.

26. Bucay N, Sarosi I, Dunstan CR, Morony S, Tarpley J, Capparelli C, et al. osteoprotegerin-deficient mice develop early onset osteoporosis and arterial calcification. Genes Dev. 1 mai 1998;12(9):1260‑1268.

27. Min H, Morony S, Sarosi I, Dunstan CR, Capparelli C, Scully S, et al. Osteoprotegerin reverses osteoporosis by inhibiting endosteal osteoclasts and prevents vascular calcification by blocking a process resembling osteoclastogenesis. J Exp Med. 21 août 2000;192(4):463‑474.

28. Boyle WJ, Simonet WS, Lacey DL. Osteoclast differentiation and activation. Nature. 15 mai 2003;423(6937):337‑342.

29. Lee S-K, Lorenzo JA. Regulation of receptor activator of nuclear factor-kappa B ligand and osteoprotegerin mRNA expression by parathyroid hormone is predominantly mediated by the protein kinase a pathway in murine bone marrow cultures. Bone. juill 2002;31(1):252‑259.

30. Andersen TL, Sondergaard TE, Skorzynska KE, Dagnaes-Hansen F, Plesner TL, Hauge EM, et al. A physical mechanism for coupling bone resorption and formation in adult human bone. Am J Pathol. janv 2009;174(1):239‑247.

31. Byrne D, Mulhall K, Baker J. Anatomy and biomechanics of the hip. Open Sports Med J. 2010;4:51‑57.

32. Odri G-A. Les Moyens d'Union de l'Articulation Coxo-Fémorale. [Nantes, France]: Université de Nantes; 2006.

33. Judman KP, Reinisch G. Tribological aspects of total hip arthroplasty. European Cells and Materials. Vol. 1. Suppl. 2, 2001. 46.

34. Konttinen YT, Pajarinen J. Surgery: Adverse reactions to metal-on-metal implants. Nat Rev Rheumatol. janv 2013;9(1):5‑6.

35. Ingham E, Fisher J. The role of macrophages in osteolysis of total joint replacement. Biomaterials. Abril 2005;26(11):1271‑1286.

36. Saikko V, Ahlroos T, Calonius O, Keränen J. Wear simulation of total hip prostheses with polyethylene against CoCr, alumina and diamond-like carbon. Biomaterials. 15 juin 2001;22(12):1507‑1514.

37. Charnley J. The long-term results of low-friction arthroplasty of the hip performed as a primary intervention. J Bone Joint Surg Br. févr 1972;54(1):61‑76.

38. Gomez-Barrena E, Puertolas J-A, Munuera L, Konttinen YT. Update on UHMWPE research From the bench to the bedside. Acta Orthop. janv 2008;79(6):832‑840.

39. Atkins GJ, Haynes DR, Howie DW, Findlay DM. Role of polyethylene particles in peri-prosthetic osteolysis: A review. World J Orthop. 18 oct 2011;2(10):93‑101.

40. Thomas GER, Simpson DJ, Mehmood S, Taylor A, McLardy-Smith P, Gill HS, et al. The seven-year wear of highly cross-linked polyethylene in total hip arthroplasty: a double-blind, randomized controlled trial using radiostereometric analysis. J Bone Joint Surg Am. 20 avr 2011;93(8):716‑722.

41. Kuzyk PRT, Saccone M, Sprague S, Simunovic N, Bhandari M, Schemitsch EH. Cross-linked versus conventional polyethylene for total hip replacement: a meta-analysis of randomised controlled trials. J Bone Joint Surg Br. mai 2011;93(5):593‑600.

42. Wroblewski BM, Siney PD, Fleming PA. Charnley low-friction arthroplasty SURVIVAL PATTERNS TO 38 YEARS. J Bone Joint Surg Br. 8 janv 2007;89-B(8):1015‑1018.

43. Jacobs JJ, Roebuck KA, Archibeck M, Hallab NJ, Glant TT. Osteolysis: basic science. Clin Orthop. déc 2001;(393):71‑77.

44. Keegan GM, Learmonth ID, Case CP. A systematic comparison of the actual, potential, and theoretical health effects of cobalt and chromium exposures from industry and surgical implants. Crit Rev Toxicol. 2008;38(8):645‑674.

45. Helm CS, Greenwald AS. The rationale and performance of modularity in total hip arthroplasty. Orthopedics. sept 2005;28(9 Suppl):s1113‑1115.

46. Hasegawa M, Yoshida K, Wakabayashi H, Sudo A. Prevalence of adverse reactions to metal debris following metal-on-metal THA. Orthopedics. mai 2013;36(5):e606‑612.

47. Cuckler JM. The rationale for metal-on-metal total hip arthroplasty. Clin Orthop. déc 2005;441:132‑136.

48. Hartmann A, Hannemann F, Lützner J, Seidler A, Drexler H, Günther K-P, et al. Metal Ion Concentrations in Body Fluids after Implantation of Hip Replacements with Metal-on-Metal Bearing - Systematic Review of Clinical and Epidemiological Studies. PloS One. 2013;8(8):e70359.

49. Hart AJ, Satchithananda K, Liddle AD, Sabah SA, McRobbie D, Henckel J, et al. Pseudotumors in association with well-functioning metal-on-metal hip prostheses: a case-control study using three-dimensional computed tomography and magnetic resonance imaging. J Bone Joint Surg Am. 15 févr 2012;94(4):317‑325.

50. Whitehouse MR, Endo M, Masri BA. Adverse Local Tissue Reaction Associated With a Modular Hip Hemiarthroplasty. Clin Orthop. 29 juin 2013;

51. Langton DJ, Sidaginamale RP, Joyce TJ, Natu S, Blain P, Jefferson RD, et al. The clinical implications of elevated blood metal ion concentrations in asymptomatic patients with MoM hip resurfacings: a cohort study. BMJ Open. 1 janv 2013;3(3):e001541.

52. Billi F, Campbell P. Nanotoxicology of metal wear particles in total joint arthroplasty: a review of current concepts. J Appl Biomater Biomech JABB. avr 2010;8(1):1‑6.

53. Caicedo MS, Desai R, McAllister K, Reddy A, Jacobs JJ, Hallab NJ. Soluble and particulate Co-Cr-Mo alloy implant metals activate the inflammasome danger signaling pathway in human macrophages: a novel mechanism for implant debris reactivity. J Orthop Res Off Publ Orthop Res Soc. juill 2009;27(7):847‑854.

54. Solarino G, Piazzolla A, Notarnicola A, Moretti L, Tafuri S, De Giorgi S, et al. Long-term results of 32-mm alumina-on-alumina THA for avascular necrosis of the femoral head. J Orthop Traumatol Off J Ital Soc Orthop Traumatol. mars 2012;13(1):21‑27.

55. Sugano N, Takao M, Sakai T, Nishii T, Miki H, Ohzono K. Eleven- to 14-year follow-up results of cementless total hip arthroplasty using a third-generation alumina ceramic-on-ceramic bearing. J Arthroplasty. mai 2012;27(5):736‑741.

56. Kim YH, Kim JS, Cho SH. A comparison of polyethylene wear in hips with cobalt-chrome or zirconia heads. A prospective, randomised study. J Bone Joint Surg Br. juill 2001;83(5):742‑750.

57. Wang S, Zhang S, Zhao Y. A comparison of polyethylene wear between cobalt-chrome ball heads and alumina ball heads after total hip arthroplasty: a 10-year follow-up. J Orthop Surg. 2013;8:20.

58. Dahl J, Snorrason F, Nordsletten L, Röhrl SM. More than 50% reduction of wear in polyethylene liners with alumina heads compared to cobalt-chrome heads in hip replacements. Acta Orthop. août 2013;84(4):360‑364.

59. Bozic K. Modes of Failure in Revision Hip and Knee Replacement. 2004.

60. Van der Veen HC, van Jonbergen H-PW, Poolman RW, Bulstra SK, van Raay JJAM. Is there evidence for accelerated polyethylene wear in uncemented compared to cemented acetabular components? A systematic review of the literature. Int Orthop. janv 2013;37(1):9‑14.

61. Toossi N, Adeli B, Timperley AJ, Haddad FS, Maltenfort M, Parvizi J. Acetabular components in total hip arthroplasty: is there evidence that cementless fixation is better? J Bone Joint Surg Am. 16 janv 2013;95(2):168‑174.

62. Zhang H-Y, Blunt L, Jiang X-Q, Brown L, Barrans S, Zhao Y. Femoral stem wear in cemented total hip replacement. Proc Inst Mech Eng [H]. juill 2008;222(5):583‑592.

63. Zhang HY, Brown L, Barrans S, Blunt L, Jiang XQ. Investigation of relative micromotion at the stem-cement interface in total hip replacement. Proc Inst Mech Eng [H]. nov 2009;223(8):955‑964.

64. Shearwood-Porter N, Browne M, Sinclair I. Micromechanical characterisation of failure in acrylic bone cement: The effect of barium sulphate agglomerates. J Mech Behav Biomed Mater. sept 2012;13:85‑92.

65. Stoffel KA, Yang DT, Arola D. The influence of surface topography on wear debris generation at the cement/bone interface under cyclic loading. J Mater Sci Mater Med. mai 2008;19(5):1935‑1943.

66. Bourne RB, Corten K. Cemented versus cementless stems: a verdict is in. Orthopedics. sept 2010;33(9):638.

67. Corten K, Bourne RB, Charron KD, Au K, Rorabeck CH. What works best, a cemented or cementless primary total hip arthroplasty?: minimum 17-year followup of a randomized controlled trial. Clin Orthop. janv 2011;469(1):209‑217.

68. Geissmann F, Jung S, Littman DR. Blood monocytes consist of two principal subsets with distinct migratory properties. Immunity. juill 2003;19(1):71‑82.

69. Antonios JK, Yao Z, Li C, Rao AJ, Goodman SB. Macrophage polarization in response to wear particles in vitro. Cell Mol Immunol. nov 2013;10(6):471‑482.

70. Cobelli N, Scharf B, Crisi GM, Hardin J, Santambrogio L. Mediators of the inflammatory response to joint replacement devices. Nat Rev Rheumatol. oct 2011;7(10):600‑608.

71. Yao Z, Keeney M, Lin T-H, Pajarinen J, Barcay K, Waters H, et al. Mutant MCP-1 protein attenuates migration of and inflammatory cytokine release by macrophages exposed to orthopaedic implant wear particles. J Biomed Mater Res A. 7 oct 2013;

72. Yagil-Kelmer E, Kazmier P, Rahaman MN, Bal BS, Tessman RK, Estes DM. Comparison of the response of primary human blood monocytes and the U937 human monocytic cell line to two different sizes of alumina ceramic particles. J Orthop Res Off Publ Orthop Res Soc. juill 2004;22(4):832‑838.

73. Yang S-Y, Ren W, Park Y, Sieving A, Hsu S, Nasser S, et al. Diverse cellular and apoptotic responses to variant shapes of UHMWPE particles in a murine model of inflammation. Biomaterials. sept 2002;23(17):3535‑3543.

74. Shanbhag AS, Jacobs JJ, Black J, Galante JO, Glant TT. Macrophage/particle interactions: effect of size, composition and surface area. J Biomed Mater Res. janv 1994;28(1):81‑90.

75. Pal N, Quah B, Smith PN, Gladkis LL, Timmers H, Li RW. Nano-osteoimmunology as an important consideration in the design of future implants. Acta Biomater. juill 2011;7(7):2926‑2934.

76. Gordon S, Taylor PR. Monocyte and macrophage heterogeneity. Nat Rev Immunol. déc 2005;5(12):953‑964.

77. Mosser DM, Edwards JP. Exploring the full spectrum of macrophage activation. Nat Rev Immunol. déc 2008;8(12):958‑969.

78. Broz P, Monack DM. Newly described pattern recognition receptors team up against intracellular pathogens. Nat Rev Immunol. août 2013;13(8):551‑565.

79. Rao AJ, Gibon E, Ma T, Yao Z, Smith RL, Goodman SB. Revision joint replacement, wear particles, and macrophage polarization. Acta Biomater. juill 2012;8(7):2815‑2823.

80. Hoenders CSM, Harmsen MC, van Luyn MJA. The local inflammatory environment and microorganisms in « aseptic » loosening of hip prostheses. J Biomed Mater Res B Appl Biomater. 2008;86B(1):291‑301.

81. Bi Y, Collier TO, Goldberg VM, Anderson JM, Greenfield EM. Adherent endotoxin mediates biological responses of titanium particles without stimulating their phagocytosis. J Orthop Res Off Publ Orthop Res Soc. juill 2002;20(4):696‑703.

82. Greenfield EM, Bi Y, Ragab AA, Goldberg VM, Nalepka JL, Seabold JM. Does endotoxin contribute to aseptic loosening of orthopedic implants? J Biomed Mater Res B Appl Biomater. 15 janv 2005;72(1):179‑185.

83. Cho DR, Shanbhag AS, Hong C-Y, Baran GR, Goldring SR. The role of adsorbed endotoxin in particle-induced stimulation of cytokine release. J Orthop Res Off Publ Orthop Res Soc. juill 2002;20(4):704‑713.

84. Xing Z, Pabst MJ, Hasty KA, Smith RA. Accumulation of LPS by polyethylene particles decreases bone attachment to implants. J Orthop Res Off Publ Orthop Res Soc. mai 2006;24(5):959‑966.

85. Smith RA, Maghsoodpour A, Hallab NJ. In vivo response to cross-linked polyethylene and polycarbonate-urethane particles. J Biomed Mater Res A. avr 2010;93(1):227‑234.

86. Hansen JD, Vojtech LN, Laing KJ. Sensing disease and danger: a survey of vertebrate PRRs and their origins. Dev Comp Immunol. sept 2011;35(9):886‑897.

87. Blander JM, Sander LE. Beyond pattern recognition: five immune checkpoints for scaling the microbial threat. Nat Rev Immunol. mars 2012;12(3):215‑225.

88. Fukata M, Vamadevan AS, Abreu MT. Toll-like receptors (TLRs) and Nod-like receptors (NLRs) in inflammatory disorders. Semin Immunol. août 2009;21(4):242‑253.

89. Doyle SL, O'Neill LAJ. Toll-like receptors: from the discovery of NFkappaB to new insights into transcriptional regulations in innate immunity. Biochem Pharmacol. 30 oct 2006;72(9):1102‑1113.

90. Lin T, Tamaki Y, Pajarinen J, Waters HA, Woo DK, Yao Z, et al. Chronic inflammation in biomaterial-induced periprosthetic osteolysis: NF-κB as a therapeutic target. Acta Biomater. janv 2014;10(1):1‑10.

91. Tyson-Capper AJ, Lawrence H, Holland JP, Deehan DJ, Kirby JA. Metal-on-metal hips: cobalt can induce an endotoxin-like response. Ann Rheum Dis. 3 janv 2013;72(3):460‑461.

92. Zhao D-S, Ma G-F, Selenius M, Salo J, Pikkarainen T, Konttinen YT. Ectopic expression of macrophage scavenger receptor MARCO in synovial membrane-like interface tissue in aseptic loosening of total hip replacement implants. J Biomed Mater Res A. févr 2010;92(2):641‑649.

93. Nich C, Rao AJ, Valladares RD, Li C, Christman JE, Antonios JK, et al. Role of direct estrogen receptor signaling in wear particle-induced osteolysis. Biomaterials. janv 2013;34(3):641‑650.

94. Burton L, Paget D, Binder NB, Bohnert K, Nestor BJ, Sculco TP, et al. Orthopedic wear debris mediated inflammatory osteolysis is mediated in part by NALP3 inflammasome activation. J Orthop Res Off Publ Orthop Res Soc. janv 2013;31(1):73‑80.

95. Sabokbar A, Kudo O, Athanasou NA. Two distinct cellular mechanisms of osteoclast formation and bone resorption in periprosthetic osteolysis. J Orthop Res Off Publ Orthop Res Soc. janv 2003;21(1):73‑80.

96. Mandelin J, Li TF, Liljeström M, Kroon ME, Hanemaaijer R, Santavirta S, et al. Imbalance of RANKL/RANK/OPG system in interface tissue in loosening of total hip replacement. J Bone Joint Surg Br. nov 2003;85(8):1196‑1201.

97. Granchi D, Ciapetti G, Amato I, Pagani S, Cenni E, Savarino L, et al. The influence of alumina and ultra-high molecular weight polyethylene particles on osteoblast–osteoclast cooperation. Biomaterials. Agosto 2004;25(18):4037‑4045.

98. Lee HG, Minematsu H, Kim KO, Celil Aydemir AB, Shin MJ, Nizami SA, et al. Actin and ERK1/2-CEBPβ signaling mediates phagocytosis-induced innate immune response of osteoprogenitor cells. Biomaterials. déc 2011;32(35):9197‑9206.

99. Lochner K, Fritsche A, Jonitz A, Hansmann D, Mueller P, Mueller-Hilke B, et al. The potential role of human osteoblasts for periprosthetic osteolysis following exposure to wear particles. Int J Mol Med. déc 2011;28(6):1055‑1063.

100. Kwon SY, Lin T, Takei H, Ma Q, Wood DJ, O'Connor D, et al. Alterations in the adhesion behavior of osteoblasts by titanium particle loading: inhibition of cell function and gene expression. Biorheology. 2001;38(2-3):161‑183.

101. Lenz R, Mittelmeier W, Hansmann D, Brem R, Diehl P, Fritsche A, et al. Response of human osteoblasts exposed to wear particles generated at the interface of total hip stems and bone cement. J Biomed Mater Res A. mai 2009;89(2):370‑378.

102. Bostrom M, O'Keefe R. What experimental approaches (eg, in vivo, in vitro, tissue retrieval) are effective in investigating the biologic effects of particles? J Am Acad Orthop Surg. 2008;16 Suppl 1:S63‑67.

103. Shanbhag AS, Hasselman CT, Rubash HE. The John Charnley Award. Inhibition of wear debris mediated osteolysis in a canine total hip arthroplasty model. Clin Orthop. nov 1997;(344):33‑43.

104. Millett PJ, Allen MJ, Bostrom MPG. Effects of alendronate on particle-induced osteolysis in a rat model. J Bone Joint Surg Am. févr 2002;84-A(2):236‑249.

105. Ren W, Yang S, Wooley P. A novel murine model of orthopaedic wear- debris associated osteolysis. Scand J Rheumatol. janv 2004;33(5):349‑357.

106. Yang S, Yu H, Gong W, Wu B, Mayton L, Costello R, et al. Murine model of prosthesis failure for the long- term study of aseptic loosening. J Orthop Res. 1 mai 2007;25(5):603‑611.

107. Wooley PH, Morren R, Andary J, Sud S, Yang S-Y, Mayton L, et al. Inflammatory responses to orthopaedic biomaterials in the murine air pouch. Biomaterials. janv 2002;23(2):517‑526.

108. Goodman SB, Chin RC, Magee FP. Prostaglandin E2 production by the membrane surrounding loose and fixated cemented tibial hemiarthroplasties in the rabbit knee. Clin Orthop. nov 1992;(284):283‑287.

109. Spector M, Shortkroff S, Hsu HP, Lane N, Sledge CB, Thornhill TS. Tissue changes around loose prostheses. A canine model to investigate the effects of an antiinflammatory agent. Clin Orthop. déc 1990;(261):140‑152.

110. Gelb H, Schumacher HR, Cuckler J, Ducheyne P, Baker DG. In vivo inflammatory response to polymethylmethacrylate particulate debris: effect of size, morphology, and surface area. J Orthop Res Off Publ Orthop Res Soc. janv 1994;12(1):83‑92.

111. Gibon E, Ma T, Ren P-G, Fritton K, Biswal S, Yao Z, et al. Selective inhibition of the MCP-1-CCR2 ligand-receptor axis decreases systemic trafficking of macrophages in the presence of UHMWPE particles. J Orthop Res. 2012;30(4):547‑53.

112. Takahashi K, Onodera S, Tohyama H, Kwon HJ, Honma K, Yasuda K. In Vivo Imaging of Particle-Induced Inflammation and Osteolysis in the Calvariae of NFκB/Luciferase Transgenic Mice. J Biomed Biotechnol. 2011;2011.

113. Lai W-Q, Irwan AW, Goh HH, Melendez AJ, McInnes IB, Leung BP. Distinct roles of sphingosine kinase 1 and 2 in murine collagen-induced arthritis. J Immunol Baltim Md 1950. 1 août 2009;183(3):2097‑2103.

114. Nich C, Langlois J, Marchadier A, Vidal C, Cohen-Solal M, Petite H, et al. Oestrogen deficiency modulates particle-induced osteolysis. Arthritis Res Ther. 2011;13(3):R100.

115. St. Pierre CA, Chan M, Iwakura Y, Ayers DC, Kurt-Jones EA, Finberg RW. Periprosthetic osteolysis: Characterizing the innate immune response to titanium wear-particles. J Orthop Res. 2010;28(11):1418‑24.

116. Taki N, Tatro JM, Nalepka JL, Togawa D, Goldberg VM, Rimnac CM, et al. Polyethylene and titanium particles induce osteolysis by similar, lymphocyte-independent, mechanisms. J Orthop Res Off Publ Orthop Res Soc. mars 2005;23(2):376‑383.

117. Ren P-G, Irani A, Huang Z, Ma T, Biswal S, Goodman SB. Continuous infusion of UHMWPE particles induces increased bone macrophages and osteolysis. Clin Orthop. janv 2011;469(1):113‑122.

118. Ren W, Wu B, Peng X, Hua J, Hao H-N, Wooley PH. Implant wear induces inflammation, but not osteoclastic bone resorption, in RANK(-/-) mice. J Orthop Res Off Publ Orthop Res Soc. août 2006;24(8):1575‑1586.

119. Nakashima Y, Sun DH, Maloney WJ, Goodman SB, Schurman DJ, Smith RL. Induction of matrix metalloproteinase expression in human macrophages by orthopaedic particulate debris in vitro. J Bone Joint Surg Br. juill 1998;80(4):694‑700.

120. Yao J, Glant TT, Lark MW, Mikecz K, Jacobs JJ, Hutchinson NI, et al. The potential role of fibroblasts in periprosthetic osteolysis: fibroblast response to titanium particles. J Bone Miner Res Off J Am Soc Bone Miner Res. sept 1995;10(9):1417‑1427.

121. Syggelos SA, Aletras AJ, Smirlaki I, Skandalis SS. Extracellular matrix degradation and tissue remodeling in periprosthetic loosening and osteolysis: focus on matrix metalloproteinases, their endogenous tissue inhibitors, and the proteasome. BioMed Res Int. 2013;2013:230805.

122. Kauther MD, Neuerburg C, Wefelnberg F, Bachmann HS, Schlepper R, Hilken G, et al. RANKL-associated suppression of particle-induced osteolysis in an aged model of Calcitonin and α-CGRP deficiency. Biomaterials. avr 2013;34(12):2911‑2919.

123. Ren W, Zhang R, Wu B, Wooley PH, Hawkins M, Markel DC. Effects of SU5416 and a vascular endothelial growth factor neutralizing antibody on wear debris-induced inflammatory osteolysis in a mouse model. J Inflamm Res. 2011;4:29‑38.

124. Wooley PH, Morren R, Andary J, Sud S, Yang S-Y, Mayton L, et al. Inflammatory responses to orthopaedic biomaterials in the murine air pouch. Biomaterials. janv 2002;23(2):517‑526.

125. Merkel KD, Erdmann JM, McHugh KP, Abu-Amer Y, Ross FP, Teitelbaum SL. Tumor Necrosis Factor-[alpha] Mediates Orthopedic Implant Osteolysis. Am J Pathol. janv 1999;154(1):203‑210.

126. Schwarz EM, Benz EB, Lu AP, Goater JJ, Mollano AV, Rosier RN, et al. Quantitative small‐animal surrogate to evaluate drug efficacy in preventing wear debris‐induced osteolysis. J Orthop Res. 1 nov 2000;18(6):849‑855.

127. Taki N, Tatro JM, Lowe R, Goldberg VM, Greenfield EM. Comparison of the roles of IL-1, IL-6, and TNFα in cell culture and murine models of aseptic loosening. Bone. mai 2007;40(5):1276‑1283.

128. Carmody EE, Schwarz EM, Puzas JE, Rosier RN, O'Keefe RJ. Viral interleukin-10 gene inhibition of inflammation, osteoclastogenesis, and bone resorption in response to titanium particles. Arthritis Rheum. mai 2002;46(5):1298‑1308.

129. Rao AJ, Nich C, Dhulipala LS, Gibon E, Valladares R, Zwingenberger S, et al. Local effect of IL-4 delivery on polyethylene particle induced osteolysis in the murine calvarium. J Biomed Mater Res A. juill 2013;101(7):1926‑1934.

130. Rao AJ, Zwingenberger S, Valladares R, Li C, Lane Smith R, Goodman SB, et al. Direct subcutaneous injection of polyethylene particles over the murine calvaria results in dramatic osteolysis. Int Orthop. juill 2013;37(7):1393‑1398.

131. Zhang X, Morham SG, Langenbach R, Young DA, Xing L, Boyce BF, et al. Evidence for a Direct Role of Cyclo-Oxygenase 2 in Implant Wear Debris‐Induced Osteolysis. J Bone Miner Res. 1 avr 2001;16(4):660‑670.

132. Valladares RD, Nich C, Zwingenberger S, Li C, Swank KR, Gibon E, et al. Toll-like receptors-2 and 4 are overexpressed in an experimental model of particle-induced osteolysis. J Biomed Mater Res A. 1 oct 2013;

133. Ren K, Purdue PE, Burton L, Quan L, Fehringer EV, Thiele GM, et al. Early detection and treatment of wear particle-induced inflammation and bone loss in a mouse calvarial osteolysis model using HPMA copolymer conjugates. Mol Pharm. 1 août 2011;8(4):1043‑1051.

134. Cordova LA, Stresing V, Gobin B, Rosset P, Passuti N, Gouin F, et al. Orthopaedic implant failure: aseptic implant loosening–the contribution and future challenges of mouse models in translational research. Clin Sci. 2014;127(Part. 5):277‑293.

135. Warme BA, Epstein NJ, Trindade MCD, Miyanishi K, Ma T, Saket RR, et al. Proinflammatory mediator expression in a novel murine model of titanium-particle-induced intramedullary inflammation. J Biomed Mater Res B Appl Biomater. 15 nov 2004;71(2):360‑366.

136. Epstein NJ, Warme BA, Spanogle J, Ma T, Bragg B, Smith RL, et al. Interleukin‐1 modulates periprosthetic tissue formation in an intramedullary model of particle‐induced inflammation. J Orthop Res. 1 mai 2005;23(3):501‑510.

137. Shi Y, Yang X, Nestor B, Bostrom M, Camacho N, Li G, et al. Histologic and FTIR studies on long term effect of PMMA particle in a murine intramedullary osteolysis model. - Recherche Google. Trans Orthop Res Soc. 2007;53:217.

138. Epstein NJ, Bragg WE, Ma T, Spanogle J, Smith RL, Goodman SB. UHMWPE wear debris upregulates mononuclear cell proinflammatory gene expression in a novel murine model of intramedullary particle disease. Acta Orthop. juin 2005;76(3):412‑420.

139. Ortiz SG, Ma T, Epstein NJ, Smith RL, Goodman SB. Validation and quantification of an in vitro model of continuous infusion of submicron-sized particles. J Biomed Mater Res B Appl Biomater. févr 2008;84(2):328‑333.

140. Ortiz SG, Ma T, Regula D, Smith RL, Goodman SB. Continuous intramedullary polymer particle infusion using a murine femoral explant model. J Biomed Mater Res B Appl Biomater. nov 2008;87(2):440‑446.

141. Jameson SS, Baker PN, Mason J, Rymaszewska M, Gregg PJ, Deehan DJ, et al. Independent predictors of failure up to 7.5 years after 35 386 single-brand cementless total hip replacements: a retrospective cohort study using National Joint Registry data. Bone Jt J. juin 2013;95-B(6):747‑ 757.

142. Onuora S. Osteoarthritis: Surgical options for hip OA: digging beneath the surface of implant survival. Nat Rev Rheumatol. nov 2012;8(11):631‑ 631.

143. Smith AJ, Dieppe P, Howard PW, Blom AW, National Joint Registry for England and Wales. Failure rates of metal-on-metal hip resurfacings: analysis of data from the National Joint Registry for England and Wales. Lancet. 17 nov 2012;380(9855):1759‑ 1766.

144. Fabbri N, Rustemi E, Masetti C, Kreshak J, Gambarotti M, Vanel D, et al. Severe osteolysis and soft tissue mass around total hip arthroplasty: description of four cases and review of the literature with respect to clinico-radiographic and pathologic differential diagnosis. Eur J Radiol. janv 2011;77(1):43‑ 50.

145. Gallo J, Goodman SB, Konttinen YT, Wimmer MA, Holinka M. Osteolysis around total knee arthroplasty: A review of pathogenetic mechanisms. Acta Biomater. sept 2013;9(9):8046‑ 8058.

146. Del Buono A, Denaro V, Maffulli N. Genetic susceptibility to aseptic loosening following total hip arthroplasty: a systematic review. Br Med Bull. 2012;101:39‑ 55.

147. Rousseau J, Escriou V, Lamoureux F, Brion R, Chesneau J, Battaglia S, et al. Formulated siRNAs targeting Rankl prevent osteolysis and enhance chemotherapeutic response in osteosarcoma models. J Bone Miner Res Off J Am Soc Bone Miner Res. oct 2011;26(10):2452‑ 2462.

148. Téletchéa S, Stresing V, Hervouet S, Baud'huin M, Heymann M-F, Bertho G, et al. Novel RANK Antagonists for the Treatment of Bone Resorptive Disease: Theoretical Predictions and Experimental Validation. J Bone Miner Res. 2014;n/a‑ n/a.

149. Duplomb L, Baud'huin M, Charrier C, Berreur M, Trichet V, Blanchard F, et al. Interleukin-6 inhibits receptor activator of nuclear factor kappaB ligand-induced osteoclastogenesis by diverting cells into the macrophage lineage: key role of Serine727 phosphorylation of signal transducer and activator of transcription 3. Endocrinology. juill 2008;149(7):3688‑ 3697.

150. Vandesompele J, De Preter K, Pattyn F, Poppe B, Van Roy N, De Paepe A, et al. Accurate normalization of real-time quantitative RT-PCR data by geometric averaging of multiple internal control genes. Genome Biol. 18 juin 2002;3(7):RESEARCH0034.

151. Nich C, Marchadier A, Sedel L, Petite H, Vidal C, Hamadouche M. Decrease in particle‑ induced osteolysis in ovariectomized mice. J Orthop Res. 1 févr 2010;28(2):178‑ 183.

152. Rhinn H, Largeau C, Bigey P, Kuen RL, Richard M, Scherman D, et al. How to make siRNA lipoplexes efficient? Add a DNA cargo. Biochim Biophys Acta. avr 2009;1790(4):219‑ 230.

153. Rousseau J, Escriou V, Perrot P, Picarda G, Charrier C, Scherman D, et al. Advantages of bioluminescence imaging to follow siRNA or chemotherapeutic treatments in osteosarcoma preclinical models. Cancer Gene Ther. juin 2010;17(6):387‑ 397.

154. Faucon A, Lenk R, Hémez J, Gautron E, Jacquemin D, Questel J-YL, et al. Fluorescent carboxylic and phosphonic acids: comparative photophysics from solution to organic nanoparticles. Phys Chem Chem Phys. 10 juill 2013;15(30):12748‑ 12756.

155. Zolotarevova E, Entlicher G, Pavlova E, Slouf M, Pokorny D, Vesely F, et al. Distribution of polyethylene wear particles and bone fragments in periprosthetic tissue around total hip joint replacements. Acta Biomater. sept 2010;6(9):3595‑ 3600.

156. Wang ML, Sharkey PF, Tuan RS. Particle bioreactivity and wear-mediated osteolysis. J Arthroplasty. déc 2004;19(8):1028‑ 1038.

157. Richards L, Brown C, Stone MH, Fisher J, Ingham E, Tipper JL. Identification of nanometre-sized ultra-high molecular weight polyethylene wear particles in samples retrieved in vivo. J Bone Joint Surg Br. août 2008;90(8):1106‑1113.

158. Mandelin J, Li T-F, Hukkanen M, Liljeström M, Salo J, Santavirta S, et al. Interface tissue fibroblasts from loose total hip replacement prosthesis produce receptor activator of nuclear factor-kappaB ligand, osteoprotegerin, and cathepsin K. J Rheumatol. avr 2005;32(4):713‑720.

159. Ritchlin CT, Schwarz EM, O'Keefe RJ, Looney RJ. RANK, RANKL and OPG in inflammatory arthritis and periprosthetic osteolysis. J Musculoskelet Neuronal Interact. sept 2004;4(3):276‑284.

160. Takei I, Takagi M, Santavirta S, Ida H, Ishii M, Ogino T, et al. Messenger ribonucleic acid expression of 16 matrix metalloproteinases in bone-implant interface tissues of loose artificial hip joints. J Biomed Mater Res. 15 déc 2000;52(4):613‑620.

161. Sasaki K, Takagi M, Mandelin J, Takei I, Santavirta S, Ida H, et al. Quantitative analysis of mRNA expression of TIMPs in the periprosthetic interface tissue of loose hips by real-time PCR system. J Biomed Mater Res. 2001;58(6):605‑612.

162. Purdue PE, Koulouvaris P, Nestor BJ, Sculco TP. The central role of wear debris in periprosthetic osteolysis. HSS J Musculoskelet J Hosp Spec Surg. sept 2006;2(2):102‑113.

163. Schiopu D, Girard J, Soenen M, Krantz N, Migaud H. Metal ions levels measurements for early total hip replacement malfunction diagnosis with « plasma-sprayed ceramic » bearings couple. Orthop Traumatol Surg Res. févr 2010;96(1):75‑79.

164. Higgs GB, Hanzlik JA, MacDonald DW, Gilbert JL, Rimnac CM, Kurtz SM, et al. Is increased modularity associated with increased fretting and corrosion damage in metal-on-metal total hip arthroplasty devices?: a retrieval study. J Arthroplasty. sept 2013;28(8 Suppl):2‑6.

165. Conner SD, Schmid SL. Regulated portals of entry into the cell. Nature. 6 mars 2003;422(6927):37‑44.

166. Goodman SB, Huie P, Song Y, Schurman D, Maloney W, Woolson S, et al. Cellular profile and cytokine production at prosthetic interfaces. Study of tissues retrieved from revised hip and knee replacements. J Bone Joint Surg Br. mai 1998;80(3):531‑539.

167. Willert H-G, Buchhorn GH, Dipl-Ing, Fayyazi A, Flury R, Windler M, et al. Metal-on-Metal Bearings and Hypersensitivity in Patients with Artificial Hip JointsA Clinical and Histomorphological Study. J Bone Jt Surg. 1 janv 2005;87(1):28‑36.

168. Langton DJ, Jameson SS, Joyce TJ, Hallab NJ, Natu S, Nargol AVF. Early failure of metal-on-metal bearings in hip resurfacing and large-diameter total hip replacement A CONSEQUENCE OF EXCESS WEAR. J Bone Joint Surg Br. 1 janv 2010;92-B(1):38‑46.

169. Ingham E, Fisher J. The role of macrophages in osteolysis of total joint replacement. Biomaterials. avr 2005;26(11):1271‑1286.

170. Caicedo MS, Desai R, McAllister K, Reddy A, Jacobs JJ, Hallab NJ. Soluble and particulate Co-Cr-Mo alloy implant metals activate the inflammasome danger signaling pathway in human macrophages: a novel mechanism for implant debris reactivity. J Orthop Res Off Publ Orthop Res Soc. juill 2009;27(7):847‑854.

171. Gasser JA, Ingold P, Venturiere A, Shen V, Green JR. Long-term protective effects of zoledronic acid on cancellous and cortical bone in the ovariectomized rat. J Bone Miner Res Off J Am Soc Bone Miner Res. avr 2008;23(4):544‑551.

172. Le Goff B, Soltner E, Charrier C, Maugars Y, Rédini F, Heymann D, et al. A combination of methotrexate and zoledronic acid prevents bone erosions and systemic bone mass loss in collagen induced arthritis. Arthritis Res Ther. 2009;11(6):R185.

173. Odri GA, Dumoucel S, Picarda G, Battaglia S, Lamoureux F, Corradini N, et al. Zoledronic acid as a new adjuvant therapeutic strategy for Ewing's sarcoma patients. Cancer Res. 1 oct 2010;70(19):7610‑7619.

174. Moriceau G, Ory B, Gobin B, Verrecchia F, Gouin F, Blanchard F, et al. Therapeutic approach of primary bone tumours by bisphosphonates. Curr Pharm Des. 2010;16(27):2981‑2987.

175. Lacey DL, Boyle WJ, Simonet WS, Kostenuik PJ, Dougall WC, Sullivan JK, et al. Bench to bedside: elucidation of the OPG-RANK-RANKL pathway and the development of denosumab. Nat Rev Drug Discov. mai 2012;11(5):401‑419.

176. Orwoll ES, Miller PD, Adachi JD, Brown J, Adler RA, Kendler D, et al. Efficacy and safety of a once-yearly i.v. Infusion of zoledronic acid 5 mg versus a once-weekly 70-mg oral alendronate in the treatment of male osteoporosis: a randomized, multicenter, double-blind, active-controlled study. J Bone Miner Res Off J Am Soc Bone Miner Res. oct 2010;25(10):2239‑2250.

177. Leder BZ, Tsai JN, Uihlein AV, Burnett-Bowie S-AM, Zhu Y, Foley K, et al. Two Years of Denosumab and Teriparatide Administration in Postmenopausal Women with Osteoporosis (The DATA Extension Study): a Randomized Controlled Trial. J Clin Endocrinol Metab. 11 févr 2014;jc20134440.

178. Childs LM, Paschalis EP, Xing L, Dougall WC, Anderson D, Boskey AL, et al. In vivo RANK signaling blockade using the receptor activator of NF-kappaB:Fc effectively prevents and ameliorates wear debris-induced osteolysis via osteoclast depletion without inhibiting osteogenesis. J Bone Miner Res Off J Am Soc Bone Miner Res. févr 2002;17(2):192‑199.

179. Von Knoch M, Wedemeyer C, Pingsmann A, von Knoch F, Hilken G, Sprecher C, et al. The decrease of particle-induced osteolysis after a single dose of bisphosphonate. Biomaterials. mai 2005;26(14):1803‑1808.

180. Zeng Y, Lai O, Shen B, Yang J, Zhou Z, Kang P, et al. A systematic review assessing the effectiveness of alendronate in reducing periprosthetic bone loss after cementless primary THA. Orthopedics [Internet]. avr 2011 [cité 23 nov 2011];34(4). Disponible sur: http://www.ncbi.nlm.nih.gov/pubmed/21469631

181. Elbashir SM, Harborth J, Lendeckel W, Yalcin A, Weber K, Tuschl T. Duplexes of 21-nucleotide RNAs mediate RNA interference in cultured mammalian cells. Nature. 24 mai 2001;411(6836):494‑498.

182. Sijen T, Fleenor J, Simmer F, Thijssen KL, Parrish S, Timmons L, et al. On the Role of RNA Amplification in dsRNA-Triggered Gene Silencing. Cell. 16 nov 2001;107(4):465‑476.

183. Gherardini L, Bardi G, Gennaro M, Pizzorusso T. Novel siRNA delivery strategy: a new « strand » in CNS translational medicine? Cell Mol Life Sci CMLS. 19 mars 2013;

184. Bora RS, Gupta D, Mukkur TKS, Saini KS. RNA interference therapeutics for cancer: challenges and opportunities (review). Mol Med Rep. juill 2012;6(1):9‑15.

185. Wang Y, Grainger DW. siRNA Knock-Down of RANK Signaling to Control Osteoclast-Mediated Bone Resorption. Pharm Res. 24 mars 2010;27(7):1273‑1284.

186. Ma R, Xu J, Dong B, Kauther MD, Jäger M, Wedemeyer C. Inhibition of osteoclastogenesis by RNA interference targeting RANK. BMC Musculoskelet Disord. 2012;13:154.

187. Wang Y, Tran KK, Shen H, Grainger DW. Selective local delivery of RANK siRNA to bone phagocytes using bone augmentation biomaterials. Biomaterials. nov 2012;33(33):8540‑8547.

188. Takeshita F. Efficient delivery of small interfering RNA to bone-metastatic tumors by using atelocollagen in vivo. Proc Natl Acad Sci. 11 août 2005;102(34):12177‑12182.

189. Khoury M, Louis-Plence P, Escriou V, Noel D, Largeau C, Cantos C, et al. Efficient new cationic liposome formulation for systemic delivery of small interfering RNA silencing tumor necrosis factor α in experimental arthritis. Arthritis Rheum. 2006;54(6):1867‑77.

190. Khoury M, Escriou V, Courties G, Galy A, Yao R, Largeau C, et al. Efficient suppression of murine arthritis by combined anticytokine small interfering RNA lipoplexes. Arthritis Rheum. 2008;58(8):2356‑67.

191. Wang Y, Wu N-N, Hu M, Mou Y-Q, Li R-D, Chen L, et al. Inhibitory effect of adenovirus-mediated siRNA-targeting BMPR-IB on UHMWPE-induced bone destruction in the murine air pouch model. Connect Tissue Res. 2012;53(6):528‑534.

192. Huang J-B, Ding Y, Huang D-S, Zeng W-K, Guan Z-P, Zhang M-L. RNA Interference Targeting p110β Reduces Tumor Necrosis Factor-Alpha Production in Cellular Response to Wear Particles In vitro and Osteolysis In vivo. Inflammation. 13 avr 2013;

193. Rao AJ, Nich C, Dhulipala LS, Gibon E, Valladares R, Zwingenberger S, et al. Local effect of IL-4 delivery on polyethylene particle induced osteolysis in the murine calvarium. J Biomed Mater Res A. 5 déc 2012;

194. Green TR, Fisher J, Stone M, Wroblewski BM, Ingham E. Polyethylene particles of a « critical size » are necessary for the induction of cytokines by macrophages in vitro. Biomaterials. déc 1998;19(24):2297‑2302.

195. Zhang G, Guo B, Wu H, Tang T, Zhang B-T, Zheng L, et al. A delivery system targeting bone formation surfaces to facilitate RNAi-based anabolic therapy. Nat Med. févr 2012;18(2):307‑314.

196. Ye C, Bhan A, Deshpande V, Shankar P, Manjunath N. Silencing TNF-α in macrophages and dendritic cells for arthritis treatment. Scand J Rheumatol. août 2013;42(4):266‑269.

197. Yoshida H, Nishikawa M, Yasuda S, Mizuno Y, Toyota H, Kiyota T, et al. TLR9-dependent systemic interferon-β production by intravenous injection of plasmid DNA/cationic liposome complex in mice. J Gene Med. 2009;11(8):708‑17.

198. Lonez C, Bessodes M, Scherman D, Vandenbranden M, Escriou V, Ruysschaert J-M. Cationic lipid nanocarriers activate Toll-like receptor 2 and NLRP3 inflammasome pathways. Nanomedicine Nanotechnol Biol Med [Internet]. [cité 7 mars 2014]; Disponible sur: http://www.sciencedirect.com/science/article/pii/S1549963413007144

199. Ravetch J, Aderem A. Phagocytic cells. Immunol Rev. 1 oct 2007;219(1):5‑7.

200. Maitra R, Clement CC, Scharf B, Crisi GM, Chitta S, Paget D, et al. Endosomal damage and TLR2 mediated inflammasome activation by alkane particles in the generation of aseptic osteolysis. Mol Immunol. déc 2009;47(2–3):175‑184.

201. Leclerc L, Boudard D, Pourchez J, Forest V, Sabido O, Bin V, et al. Quantification of microsized fluorescent particles phagocytosis to a better knowledge of toxicity mechanisms. Inhal Toxicol. nov 2010;22(13):1091‑1100.

202. Sant S, Poulin S, Hildgen P. Effect of polymer architecture on surface properties, plasma protein adsorption, and cellular interactions of pegylated nanoparticles. J Biomed Mater Res A. 15 déc 2008;87A(4):885‑895.

203. Yan F, Zhang C, Zheng Y, Mei L, Tang L, Song C, et al. The effect of poloxamer 188 on nanoparticle morphology, size, cancer cell uptake, and cytotoxicity. Nanomedicine Nanotechnol Biol Med. févr 2010;6(1):170‑178.

204. Haberzettl P, Duffin R, Krämer U, Höhr D, Schins RPF, Borm PJA, et al. Actin plays a crucial role in the phagocytosis and biological response to respirable quartz particles in macrophages. Arch Toxicol. 1 juill 2007;81(7):459‑470.

205. Clift MJD, Rothen-Rutishauser B, Brown DM, Duffin R, Donaldson K, Proudfoot L, et al. The impact of different nanoparticle surface chemistry and size on uptake and toxicity in a murine macrophage cell line. Toxicol Appl Pharmacol. 1 nov 2008;232(3):418‑427.

206. Gratton SEA, Ropp PA, Pohlhaus PD, Luft JC, Madden VJ, Napier ME, et al. The effect of particle design on cellular internalization pathways. Proc Natl Acad Sci. 19 août 2008;105(33):11613‑11618.

207. Cho EC, Xie J, Wurm PA, Xia Y. Understanding the Role of Surface Charges in Cellular Adsorption versus Internalization by Selectively Removing Gold Nanoparticles on the Cell Surface with a I2/KI Etchant. Nano Lett. 11 mars 2009;9(3):1080‑1084.

208. Bergsbaken T, Fink SL, Cookson BT. Pyroptosis: host cell death and inflammation. Nat Rev Microbiol. févr 2009;7(2):99‑109.

209. Guihard P, Danger Y, Brounais B, David E, Brion R, Delecrin J, et al. Induction of Osteogenesis in Mesenchymal Stem Cells by Activated Monocytes/Macrophages Depends on Oncostatin M Signaling. STEM CELLS. 2012;30(4):762‑72.

RESUMÉ et MOTS CLÉS

Microenvironnement et ostéolyse : application aux descellements aseptiques des implants orthopédiques

Le remplacement d'une articulation par une prothèse est l'une des procédures médicales les plus abouties réalisées aujourd'hui, dont l'indication est en perpétuelle croissance. Néanmoins, entre 10-20% des patients montrent des signes à long terme d'ostéolyse aseptique périprothétique induite par des particules d'usure relarguées des couples de frottement. Ce qui conduit à un descellement de l'implant et à la nécessité d'un changement de prothèse (révision chirurgicale). Pour cette raison, la survie des implants articulaires à long terme continue d'être un défi majeur en orthopédie. Ainsi, une meilleure compréhension de la physiopathologie de l'ostéolyse périprothétique induite par les particules est essentielle pour le développement des nouvelles stratégies thérapeutiques.

Le présent rapport donne une vision générale des concepts actuels d'ostéoimmunologie des descellements aseptiques d'implants orthopédiques. Dans la partie expérimentale, cette étude veut approfondir la compréhension des mécanismes de l'ostéolyse en a) identifiant les populations cellulaires des membranes périprothétiques humaines prélevées lors de révisions chirurgicales, b) reproduisant les changements inflammatoires et ostéolytiques chez un modèle de calvaria de souris, puis en évaluant l'interférence de l'ARN ciblant le récepteur activateur du facteur nucléaire Kappa B (RANK) comme une nouvelle approche thérapeutique pour cette maladie et, enfin, c) en étudiant les interactions précoces entre les nanoparticules de polyéthylène et les macrophages humains à un niveau cellulaire.

Mots Clés: Osteolysis, Polyéthylène, Orthopédique, Remplacement articulaire totale, Biologie cellulaire, RANK, Nanoparticules, Ostéoclastes.

NOM: CORDOVA JARA **PRENOM: Luis**

UMR S957, LPRO, 4 Rue Gaston Veil

44035 Nantes cedex, France